AMRIT TECHNOLOGY

Arsenic and Metal Removal by Indian Technology

Submitted to

Dr. R.A. Mashelkar Committee

MDWS

Submitted by

Professor T. Pradeep
DST Unit of Nanoscience, Department of Chemistry,
IIT Madras, Chennai 600 036
Telephone: 044-22574208 Fax: 044-22570545
Email: pradeep@iitm.ac.in

May 2018

AFFORDABLE WATER PURIFICATION TECHNOLOGY BASED ON ADVANCED MATERIALS

Technology Commercialized/Implemented

May 10, 2018

TECHNOLOGY RECOMMENDATION

1. Category* : Water

2. Title* : AFFORDABLE WATER PURIFICATION TECHNOLOGY BASED ON ADVANCED MATERIALS

3. Current Stage of the Technology* : Technology Commercialized/Implemented

4. Summary of the Product* :

Safe drinking water is a significant, but simple indicator of development. Its availability at point-of-use can save over 2 million human lives per year globally.

Drinking water contamination is a multi-faceted issue. There are many contaminants found in water; yet, all contaminants do not occur simultaneously. A tailored solution for each contaminant is the key to ensure that local water is made healthy for drinking, without affecting its qualities such as taste. This is possible affordably with the advent of nanotechnology. Each technology has region-dependent advantages. For example, membrane technology is most suited where dissolved salt concentration is high (typically near the coastal belt or deep wells).

Using nanomaterials, it is possible to effectively destroy microorganisms (incl. enteric viruses), adsorb arsenic/fluoride, remove heavy metals and degrade pesticides found in drinking water. A product aptly titled, AMRIT, has been developed by IIT Madras. AMRIT is the acronym for **A**rsenic and **M**etal **R**emoval by **I**ndian **T**echnology. The technology behind the product has been scientifically validated by the international research community through research articles and patents.

The technology has been applied in various forms for community water purifiers. The products based on these technologies are designed considering an appeal of Indian-ness in the products.

The products are very easy to operate and maintain. The technology does not require electrical power. Implementations, spread across arsenic affected belt of the country, are constantly monitored and local communities are also trained for its regular upkeep.

The cost of clean water using this technology in the arsenic affected areas is under 4 paise per litre. It can be implemented at any level - domestic, community, or municipal - levels.

5. Supporting Images:

All the files are uploaded at following weblink (please copy and paste the link as web URL. A download will begin. After the download is complete, you may uncompress the files):
http://www.dstuns.iitm.ac.in/AMRIT IITM Technology - Mashelkar Committee.zip

A copy of the supporting files is provided with this application.

Files relevant for this sub-section are as follows:
5.0 List of Scientific Articles.jpeg
5.0.1 List of Patents.jpeg
5.1 Domestic Model.jpeg
5.2 AMRIT Water Supply Scheme Model.png
5.2 Phulia Water Supply Scheme Model.jpeg
5.2.0 AMRIT Small Community Units.png
5.2.1 AMRIT Small Community Units.jpeg
5.3 AMRIT Small Community Unit.jpeg
5.4 Standalone Community Model.jpeg

Video link for AMRIT technology
https://www.youtube.com/watch?v=RsxIgPFCf3o
https://www.youtube.com/watch?v=YvDPPq8embU
https://www.youtube.com/watch?v=4DO_PAougZs

Web-link for AMRIT technology
http://www.dstuns.iitm.ac.in/pradeep-research-group.php

6. Contaminants that can be removed through this Technology* (Max 500 Char.):
Using this technology, we have demonstrated effective removal of nearly all of the groundwater based contaminants including arsenic, fluoride and heavy metals. The solution can be integrated with other technologies as well.

7. Design Capacity*:

From 300 LPH to 100000 LPH

8. Document/Files ("txt","doc","docx","pdf","odt","ppt","pptx")
All the files are uploaded at following weblink (please copy and paste the link as web URL. A download will begin. After the download is complete, you may uncompress the files):
http://www.dstuns.iitm.ac.in/AMRIT IITM Technology - Mashelkar Committee.zip

A copy of the supporting files is provided with this application.

Files relevant for this sub-section are as follows:
8. Design of Unit - AMRIT Model.pdf
8.1 AMRIT brochure.pdf
8.2 Iron brochure.pdf
8.3 Ferrihydrite Arsenic Research article.pdf
8.3 Udhaya - PNAS + SI Research Article.pdf

9. Estimated Capital Cost, if Quoted: (In Rs.)
Rs. 30 per LPD

10. Document/Files ("txt","doc","docx.","pdf","odt","ppt","pptx")

11. Cost of Water Per Litre*: (Paise per liter)

4

12. Pre-Treatment Protocol:

The product provided for retrofitting with water supply scheme, is a complete treatment unit. It is integrated with a pre-filter comprising of 5 micron membrane cloth for surface filtration of turbidity and suspended particles. Objective of providing this pre-filter is to ensure that subsequent treatment unit remains free of clogging and the need for regular backwash. Nevertheless, we have provided a mechanism for backwash of each of treatment units.

If the raw water contains dissolved iron, we provide an iron removal unit integrated with an oxidation unit.

There is no need for any further pre-treatment.

13. Document/Files ("txt","doc","docx","pdf","odt","ppt","pptx")
12. Pre-treatment protocol.pdf is uploaded in the application.

14. Post-Treatment Protocol:

There is no post treatment required for correction of pH or TDS. Our treatment unit doesn't alter water quality in terms of pH or TDS (though pH may become less acidic, post contact with our water purification material). We advise providing microbiological treatment in order to ensure sterility of water prior to consumption (as mandated by WHO). This is because water may have stayed inside the overhead tank for long period prior to passage through the treatment unit.

15. Document/Files ("txt","doc","docx","pdf","odt","ppt","pptx")

16. Operations and Maintenance Cost and Protocol*:

Operation and maintenance cost is already included in the cost of water per liter (i.e., less than 4 paisa per liter, exact cost depend on the size of water supply unit). It includes the cost of operator running the plant, necessary consumables and electricity used for pumping, considering rural India.

Protocol for running of the treatment unit is quite straightforward. Each of the treatment unit in our product comprises of a multiport valve, which enables single point operation for run, backwash and rinse.

Typically, our treatment unit doesn't require any backwash (considering the pre-filter unit handles turbidity and suspended particle removal). However, we do recommend backwashing the filter once a quarter.

16.1 Operation and Maintenance.pdf is uploaded in the application.

17. Document/Files ("txt","doc","docx","pdf","odt","ppt","pptx")

18. Reject Management Cost and Protocol

As per the design, adsorbent to be used for the removal of contaminant from water has a useful life of 2-5 years. It is expected that after the passage of design life, contaminant content on the spent adsorbent will be definitely over 5%.

Highlights of our spent adsorbent disposal program are as follows:

a. The adsorbent will be regularly characterized by advanced scientific techniques in our laboratory to know the content of the contaminant. Once the adsorbent is saturated, it will be again subjected to detailed analysis.

b. We have already done TCLP studies on the adsorbent and it doesn't release any contaminant. Hence, the spent adsorbent is safe for use as landfill.

d. If needed, we will use advanced stabilization/solidification technologies to permanently trap arsenic in the adsorbent. This adsorbent is most suitable for permanent stabilization/solidification as the granules are extremely hard and almost impenetrable for other ions. It contains negligible moisture (less than 3%) and hence will not interfere in solidification procedure.

19. Document/Files ("txt","doc","docx","pdf","odt","ppt","pptx")

19.1 TCLP Result.pdf is uploaded in the application.

20. Certification of Product:

This technology has been certified by various governmental agencies and researchers. Some of these are attached.

21. Document/Files ("txt","doc","docx","pdf","odt","ppt","pptx")

All the files are uploaded at following web link (please copy and paste the link as web URL. A download will begin. After the download is complete, you may uncompress the files):
http://www.dstuns.iitm.ac.in/AMRIT IITM Technology - Mashelkar Committee.zip
A copy of the supporting files is provided with this application.

Files relevant for this sub-section are as follows:
21.1 MDWS approval.pdf
21.2 Arsenic Task Force Approval.pdf
21.3 Indian Institute of Scientific Education & Research Approval.pdf

22. Ease of Operations and Management:

No regeneration: Treatment units used earlier for groundwater purification, required regeneration through use of toxic/strong chemicals and release of adsorbed contaminants. Advanced materials detailed in this report don't require regeneration due to extremely high adsorption capacity.

Minimum backwash: Similarly, removal of iron needs regular backwash. Our Iron removal units can remove 80% of iron through adsorption and can remove iron for a very long period, without requiring backwash.

23. Interference by other Contaminants:

Contaminant adsorption on material surface is usually hindered by the presence of competing ions such as bicarbonate, phosphate, etc. Development of nanotechnology has helped in understanding material surfaces better. Now, it is possible to tailor make the surfaces so that adsorption is selective. This is achieved through the use of specific organic moieties.

24. Test Trailed: Whether Test Trailed/Implemented?*

We have tested our products in the arsenic belt of India having raw arsenic concentrations in the range of 100-800 ppb. Treated water concentration is well below the permissible limit. Similarly, we have tested our products in the fluoride belt having raw water fluoride concentration up to 8 ppm. Treated water concentration is well below the permissible limit. These results are obtained from units which are continuously running in the field for several years.

24.1 Test report.pdf

25. Key Word (Max 20 Char)

Water, Materials

26. Patent Information: 1529/CHE/2010 and 200767

27. Competitors:

There are a number of technologies which are currently in pilot stage/use for the removal of groundwater contaminants. It has been understood that outdated technologies have to be phased out, owing to emerging needs of water purification (lower limits, higher kinetics, reduced cost, ease of maintenance). Permissible limit for arsenic was 50 ppb earlier which is now at 10 ppb. Technologies need to upgrade and nanostructured materials are essential for these.

28. Provide Video Link:
https://www.youtube.com/watch?v=4DO_PAougZs

29. Contributors: Prof. T. Pradeep

30. About Innovator and Contributors *:

Thalappil Pradeep is an Institute Professor at the Indian Institute of Technology Madras, Chennai, India. He is the Deepak Parekh Institute Chair Professor and is also a Professor of Chemistry. He studied at the University of Calicut, Indian Institute of Science, UC Berkeley and Purdue. His research interests are in molecular and nanoscale materials and he develops instrumentation for such studies. He is an author of over 400 scientific papers and is an inventor in over 90 patents or patent applications. In addition to the work on advanced materials, he is involved in the development of affordable technologies for drinking water purification and some of them have been commercialized. His pesticide removal technology is estimated to have reached about 7.5 million people. Along with his associates, he has incubated four companies and two of them have production units. His arsenic removal

technology, approved for national implementation, is delivering arsenic free water to about 600,000 people every day. He is a recipient of several awards including the Shanti Swaroop Bhatnagar Prize, BM Birla Science Prize, National Award for Nanoscience and Nanotechnology, India Nanotech Innovation Award and JC Bose National Fellowship. He is the winner of the 2018 TWAS (The World Academy of Sciences) prize in Chemistry. He is a Fellow of all the science and engineering academies of India and is a fellow of the Royal Society of Chemistry. He is a distinguished professor in a few institutions in India and is also on the graduate faculty of Purdue University. He is the author of the introductory textbook, Nano: The Essentials (McGraw-Hill) and is one of the authors of the monograph, Nanofluids (Wiley-Interscience) and an advanced textbook, A Textbook of Nanoscience and Nanotechnology (McGraw-Hill). He is on the editorial boards of journals such as ACS Nano, Chemistry of Materials, Chemistry – An Asian Journal, Nanoscale, Particle, Scientific Reports, etc., and is an associate editor of ACS Sustainable Chemistry & Engineering. He has authored popular science books in Malayalam, a regional language of India and is the recipient of Kerala Sahitya Academi Award for knowledge literature. In 2015, he received the Lifetime Achievement Research Award of IIT Madras. As part of his philanthropic activities, he supports a school in his village where 500 students are on rolls.

Others mentioned have been the co-workers involved in the project. Anshup and Amrita Chaudhary obtained their B. Tech degrees from IIT Madras. Anshup conducted his undergraduate research work with Professor Pradeep. Udhaya Sankar holds an M. Tech from Madras University and worked with Professor Pradeep for his masters project. Three of them have been associated with the development and deployment of these technologies. Among the others, A. Anil Kumar and J. R. Swathy are PhD students currently with Professor Pradeep. Shihabudeen M. Maliyekkal obtained his PhD from IIT Madras and had postdoctoral training in Professor Pradeep's group and is now on the faculty of IIT Tirupati. K. R. Antony and Sahaja Aigal worked with Professor Pradeep as project associates.

Visit http://www.dstuns.iitm.ac.in/pradeep-research-group.php for more information.

SUPPORTING DOCUMENTS

Video link for AMRIT technology

https://www.youtube.com/watch?v=RsxIgPFCf3o

https://www.youtube.com/watch?v=YvDPPq8embU

https://www.youtube.com/watch?v=4DO_PAougZs

Web-link for AMRIT technology

http://www.dstuns.iitm.ac.in/pradeep-research-group.php

"4. SUMMARY OF THE PRODUCT"

a. List of Scientific Articles

b. List of Patents

c. Domestic Model

d. AMRIT Water Supply Scheme Model

e. Phulia Water Supply Scheme Model

f. AMRIT Small Community Unit

g. AMRIT Small Community Unit

h. AMRIT Small Community Unit

i. Standalone Community Model

A. LIST OF SCIENTIFIC ARTICLES

01. Species-specific uptake of arsenic on confined metastable 2-line ferrihydrite: A combined Raman-XPS investigation of the adsorption mechanism, Chennu Sudhakar, Avula Anil Kumar, Radha Gobinda Bhuin, Soujit Sen Gupta, Ganapati Natarajan, and T. Pradeep, ACS Sustain. Chem. Eng., 2018 (DOI: 10.1021/acssuschemeng.8b01217)
02. Biopolymer-reinforced synthetic granular nanocomposites for affordable point-of-use water purification, Mohan Udhaya Sankar, Sahaja Aigal, Shihabudheen M. Maliyekkal, Amrita Chaudhary, Anshup, Avula Anil Kumar, Kamalesh Chaudhari, T. Pradeep*, Proc. Natl. Acad. Sci. U S A,* 110 (2013) 8459–8464.
03. Confined metastable 2-line ferrihydrite for affordable point-of-use arsenic free drinking water, Anil Kumar Avula, Anirban Som, Paolo Longo, Chennu Sudhakar, Radha Gobinda Bhuin, Soujit Sen Gupta, Anshup, Mohan Udhaya Sankar, Amrita Chaudhary, Ramesh Kumar, T. Pradeep, *Adv. Mater*., 29 (2016) 1604260
04. Metallic nanobrushes made using ambient droplet sprays, Depanjan Sarkar, M. K. Mahitha, Anirban Som, Anyin Li, Michael Wleklinski, R. G. Cooks, T. Pradeep, *Adv. Mater*., 28 (2016) 2223–2228.
05. Rapid dehalogenation of pesticides and organics at the interface of reduced graphene oxide-silver nanocomposite, Dibyashree Koushik, Soujit Sen Gupta, Shihabudheen M. Maliyekkal, T. Pradeep, *J. Haz. Mater.,* 308 (2016) 192-198.
06. Cellulose derived graphenic fibers for capacitive desalination of brackish water, Nalenthiran Pugazhenthiran, Soujit Sen Gupta, Anupama Prabhath, Muthu Manikandan, Jakka Ravindran Swathy, V. Kalyan Raman, T. Pradeep, *ACS Appl. Mater. Interfaces*, 7 (2015) 20156-20163.
07. Approaching sensitivity of tens of ions using atomically precise cluster-nanofiber composites, Atanu Ghosh, Vedhakkani Jeseentharani, Mohd Azhardin Ganayee, Rani Hemalatha, Kamalesh Chaudhari, Cherianath Vijayan, T. Pradeep, *Anal. Chem*., 86 (2014) 10996–11001.
08. Facile and rapid synthesis of dithiol-protected Ag_7 quantum cluster for selective adsorption of cationic dyes, M. S. Bootharaju, T. Pradeep*, Langmuir*, 29 (2013) 8125-8132.
09. Selective visual detection of TNT at the sub-zeptomole level, Ammu Mathew, P. R. Sajanlal, T. Pradeep, *Angew. Chem. Int. Ed*., 51 (2012) 9596-9600.
10. Extraction of chlorpyrifos and malatheon from water by metal nanoparticles, A. Sreekumaran Nair, T. Pradeep*, J. Nanoscience and Nanotechnology*, 7 (2007) 1-7.
11. Potential of silver nanoparticle-coated polyurethane foam as an antibacterial water filter, Prashant Jain, T. Pradeep, *Biotechnol Bioeng*., 90 (2005) 59-63.
12. Halocarbon mineralization and catalytic destruction by metal nanoparticles, A. Sreekumaran Nair, T. Pradeep, *Current Science*., 84 (2003) 1560-1564.
13. Detection and extraction of endosulfan by metal nanoparticles, A. Sreekumaran Nair, Renjis T. Tom, T. Pradeep, *J. Environ. Monitoring*, 5 (2003) 363-365.

B. LIST OF PATENTS

01. A method of preparing purified water from water containing pesticides (chlorpyrifos and malatheon) and purified water prepared by the said method, A. Sreekumaran Nair and T. Pradeep, Indian patent 200767.
02. Extraction of malatheon and chlorpyrifos from drinking water by nanoparticles adsorbent composition, a device and a method for decontaminating water containing pesticides, A. Sreekumaran Nair and T. Pradeep, PCT application, PCT/IN2005/000002. Granted as, Extraction of malatheon and chlorpyrifos from drinking water by nanoparticles, US Patent 7968493; A method for decontaminating water containing pesticides, EP 17,15,947.
03. Polyurethane foam coated with silver nanoparticles, Prashant Jain and T. Pradeep, Indian patent 219111.
04. A method to produce supported noble metal nanoparticles in commercial quantities for drinking water purification, A. Sreekumaran Nair and T. Pradeep, India patent 277112.
05. Organic polymer-inorganic fine particle antimicrobial composites and uses thereof, A. Sreekumaran Nair and T. Pradeep, PCT/IB2010/002016, Aug. 17, 2010. US Patent 8268359.
06. Multi element and multi property tagging, P. R. Sajanlal and T. Pradeep, PCT/IB2010/002006, August 13, 2010. Issued as, Coated mesoflowers for molecular detection and smart barcode materials, WO2014178006A2. Issued in Japan No. 5492301, on March 7, 2014. Issued in the US as, Multi element and multi property tagging, US Patent 8,659,391 B2, on February 25, 2014.
07. Gravity-fed axial flow filter block for domestic water purifiers and the method of making the same, T. Pradeep, M. Udhaya Sankar, Anshup, Amrita Chaudhary, Indian patent.
08. Gold and silver quantum clusters and methods for their preparation and use, T. Pradeep and E. S. Shibu, PCT/IB2011/000260, February 14, 2011. Issued in the US 8999717, on April 7, 2015. Issued also as Japanese patent - IN-811301-05-JP-NAT.
09. Single container gravity-fed storage water purifier, T. Pradeep, Amrita Chaudhary, M. Udhaya Sankar and Anshup, 3510/RQ-CHE/2011 filed on May 2, 2011. Issued in UAE for the application number 1161/2013, in Australia with patent number 2012251424, in China with patent number 2012800247893, in Israel with patent number 229223.
10. Organic templated nanometal oxyhydroxide, T. Pradeep, Shihabudheen M. Maliyekkal, Anshup, Udhaya Sankar, Amrita Chaudhary, PCT/IB2011/001551, June 2, 2011. Issued in UAE for application No. 1238/2012.
11. Multilayer organic-templated-boehmite-nanoarchitecture for fluoride removal, T. Pradeep, A. Leelavathi, Amrita Chaudhary, M. Udhaya Sankar and Anshup, Indian Patent 286929
12. Detection of quantity of water flow using quantum clusters, T. Pradeep, Leelavathi A, M. Udhaya Sankar, Amrita Chaudhary, Anshup, T. Udayabhaskararao, 1521/CHE/2012, April 17, 2012. Issued in China with patent number 201380025718X.
13. A composition for enhanced biocidal activity and a water purification device based on the same, T. Pradeep, M. Udhaya Sankar, Amrita Chaudhary, Sahaja Aigel, Swathy JR,

Anshup, Patent Application Nos.: WO 2015/059562 A1, US20160135468. Issued in UAE for the application number PCT/IB2014/002316, in Australia for the application number 2014338691, in Brazil for the application number BR11 2015 0323731, in Oman for the application number OM/P/2015/00340, in Qatar for the application number 2867CHE2013.

14. One container gravity fed storage water purifier, Indian patent application, T. Pradeep, Amrita Chaudhary, M. Udhaya Sankar and Anshup, PCT/IB2012/001237. Issued in the Japan for application 2014-508886.
15. Water purifier, Design patent number 254443
16. Anti-gravity water filter cartridge, Design patent number 260460
17. AMRIT drinking water purifier, Design patent number 257312
18. Domestic water purification unit, design patent number 288810

DOMESTIC MODEL

A DOMESTIC MODEL OF OUR TECHNOLOGY

D. AMRIT WATER SUPPLY SCHEME MODEL

5.2 AMRIT Water Supply Scheme Model

Inset shows a 70 litres per capita daily (LPCD) unit installed in the shed seen in the larger image. These units supply drinking water to villages, typically with a population of 1500.

E. PHULIA WATER SUPPLY SCHEME MODEL

5.2 Phulia Water Supply Scheme Model

F. AMRIT SMALL COMMUNITY UNIT

G. AMRIT SMALL COMMUNITY UNIT

H. AMRIT SMALL COMMUNITY UNIT

Gram Panchayat : Sankarpur - 1
Village : Sankarpur
Habitation : Bamunpara
Location : Sankarpur FP School
GPS Coordinates: 22.30100ºN 88.43375ºE

I. STAND ALONE COMMUNITY MODEL

5.4 Standalone Community Model

SUPPORTING DOCUMENTS

"7. DESIGN CAPACITY"

a. Design of Unit - AMRIT Model

b. AMRIT brochure

c. Iron brochure

d. Ferrihydrite Arsenic Research article

e. Metal Oxyhydroxide - biopolymer composite Research Article

f. Species-specific uptake of arsenic - Research Article

A. DESIGN OF UNIT - AMRIT MODEL

UNDERSTANDING THE DESIGN OF AIRP BASED ON NANOTECHNOLOGY

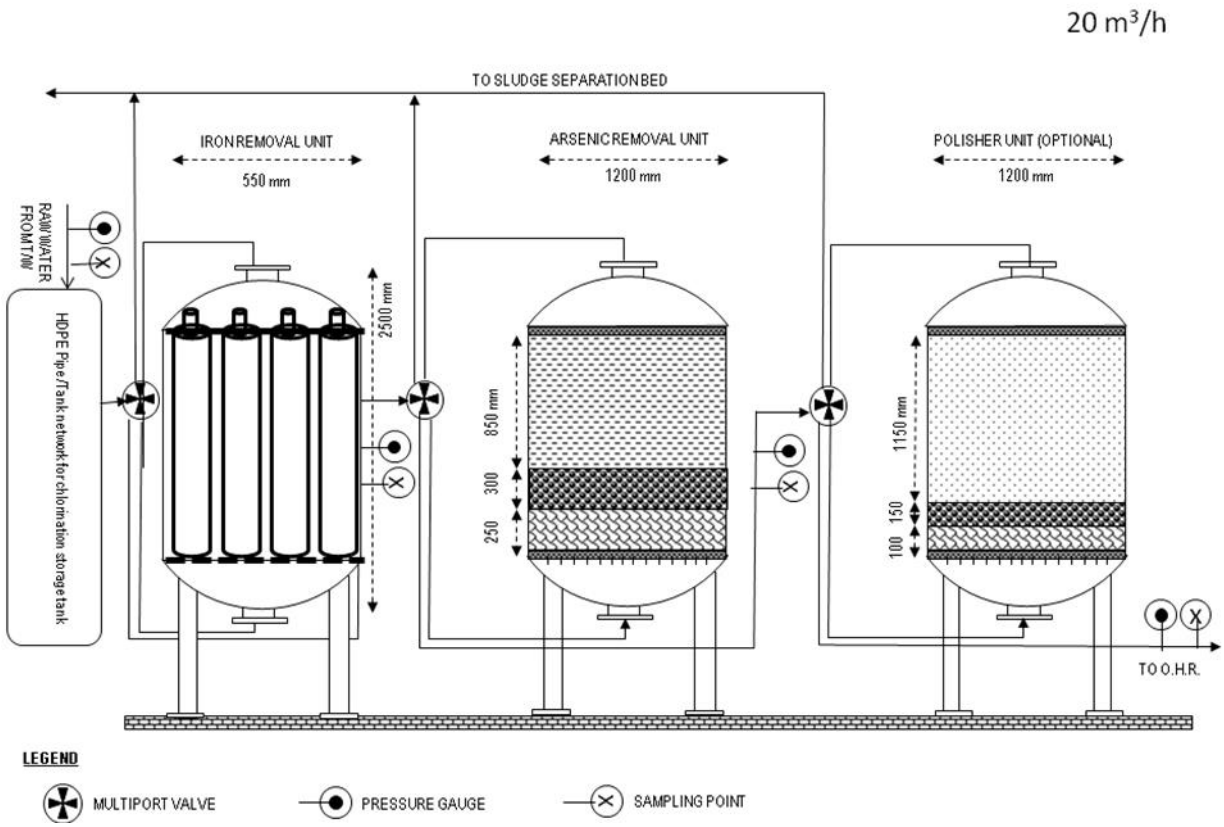

DESCRIPTION

Construction of Arsenic-cum-Iron Removal Plant (AIRP) to reduce arsenic concentration to 10 ppb and iron to 100 ppb from influent concentration up to 500 ppb and 3000 ppb respectively based on oxidation (chlorination or air compressor based aeration) followed by iron adsorption and arsenic adsorption.

Design to consist of inlet arrangement, oxidation chamber (chlorinator with water retention chamber or air compressor), iron adsorption unit with backwashing arrangement with water, arsenic adsorption unit with backwashing arrangement with clean water with all with pneumatic valves and control arrangements, clear water reservoir, sludge treatment unit, including the cost of all accessories all complete with trial run for a period of 3 (three) months after completion of the works and 3 months maintenance after successful trial run including the cost of chemicals showing all necessary arrangements.

COMMUNICATION

Confined Metastable 2-Line Ferrihydrite for Affordable Point-of-Use Arsenic-Free Drinking Water

*Avula Anil Kumar, Anirban Som, Paolo Longo, Chennu Sudhakar, Radha Gobinda Bhuin, Soujit Sen Gupta, Anshup, Mohan Udhaya Sankar, Amrita Chaudhary, Ramesh Kumar, and Thalappil Pradeep**

Nanomaterials with intrinsically high surface energy, prepared using naturally abundant ingredients can be helpful in creating green products.[1] Several nanoscale materials have been prepared recently for applications of water purification, which exhibit improved performance vis-à-vis existing compositions, thereby enhancing the effectiveness of point-of-use water purifiers. However, such materials cannot be used in the native form for water purification because of difficulties in particle separation, potential danger in view of their leaching into the purified water,[2] and poor hydraulic conductivity of the filtration device. Examples such as activated alumina,[3] activated carbon,[4,5] iron oxide,[5,6] silicon dioxide,[7] granular ferric hydroxide (GFH),[8] reduced graphene oxide (RGO)-metal/metal oxide composites,[9–11] and magnetite-reduced graphene oxide composite (M-RGO)[12] are well known in the literature. Important requirement in the context of arsenic (As) removal media is the simultaneous removal of both As(III) and As(V) species present in natural water with enhanced kinetics, enabling fast delivery of clean water.

Hydrous nanoscale metal oxides are available abundantly in nature,[13] they are formed in geological time scale by slow crystallization, often assisted by mild temperature and pressure variations. However, this leads to the destruction of adsorption sites. Researchers have looked at new methods to synthesize iron oxide/hydroxide/oxyhydroxide compositions in the laboratory and used them for water purification.[13] They exist in rich variety of structures and hydration states. They are commonly fine-grained (nanophase) and poorly crystalline. The competition between surface energies and energetics of phase transformation suggests that metastable micrometer-sized or larger polymorphs can often be stabilized at the nanoscale. Such size-driven crossovers in stability help to explain patterns of occurrence of different iron oxides in nature.[14] Many of them have been shown to be effective for the removal of As(III) and As(V) and such chemistry for arsenic remediation has been investigated.[15–17] Here, we present a simple method to maintain the metastable 2-line ferrihydrite phase at room temperature by confining it in biopolymeric cages. This material is termed as confined metastable 2-line ferrihydrite (CM2LF) having unprecedented adsorption capacity for both As(III) and As(V) in field conditions. We describe an affordable water purification device using such a composite, developed over several years, undergoing large scale field trials in India, as a potential solution for the eradication of arsenic from drinking water.[18] The material is green and causes no additional environmental impact for its production and in the course of use.

CM2LF appears to be largely amorphous in transmission electron microscopy (TEM) (**Figure 1**A). We believe that this is due to the small size of the crystalline domains of the material which might not be located under high resolution transmission electron microscopy (HRTEM). Nanoscale features are evident in the image, which are uniform throughout. Fast Fourier transform (FFT) diffraction pattern is shown in inset a_1. The phase continues to remain the same at ambient conditions, but gradually gets converted to more stable forms of hematite (α-Fe_2O_3, rhombohedral, JCPDS 89-8103) and goethite (α-FeOOH, orthorhombic, JCPDS 81-0464)[19] upon electron beam irradiation. FFT diffraction pattern (Figure 1Bb_1) of the irradiated material along with lattice resolved images of these phases (inset b_2, b_3, and b_4) are shown in Figure 1B. The phases were confirmed by the lattice planes of hematite (b_2, b_4) and goethite (b_3), which matches with the Cambridge crystallographic data (CCD). Electron beam induced time dependent HRTEM images of initial CM2LF, As(III) adsorbed and As(V) adsorbed samples show the conversion of amorphous to crystalline state. Lattice resolved images of these samples are shown in Figure S1 of the Supporting Information. Scanning electron microscope (SEM) image of the initial granular material is shown in Figure S2A (Supporting Information). The material was kept in water and was found to be stable even after six months without any leaching of Fe. Stability of the composition is attributed to abundant —O and —OH functional groups of chitosan, which help in the formation of metastable amorphous metal oxyhydroxide and also ensure strong covalent binding of the nanoparticle surface to the matrix. Iron oxyhydroxide nanoparticles bind to chitosan network, possibly through covalent sharing of oxygen, leading to metastable 2-line ferrihydrite phase similar to the formation of AlOOH nanoparticles in chitosan network, comparable to the mechanism reported by Sankar et al.[20] Figure 1C_1 shows the annular dark-field

A. A. Kumar, A. Som, C. Sudhakar, Dr. R. G. Bhuin, S. Sen Gupta, Anshup, M. U. Sankar, A. Chaudhary, R. Kumar, Prof. T. Pradeep
DST Unit of Nanoscience (DST UNS) and Thematic Unit of Excellence (TUE)
Department of Chemistry
Indian Institute of Technology Madras
Chennai 600036, India
E-mail: pradeep@iitm.ac.in
Dr. P. Longo
Gatan Inc.
5794 W Las Positas Blvd, Pleasanton, CA 94588, USA

DOI: 10.1002/adma.201604260

© 2016 WILEY-VCH Verlag GmbH & Co. KGaA, Weinheim

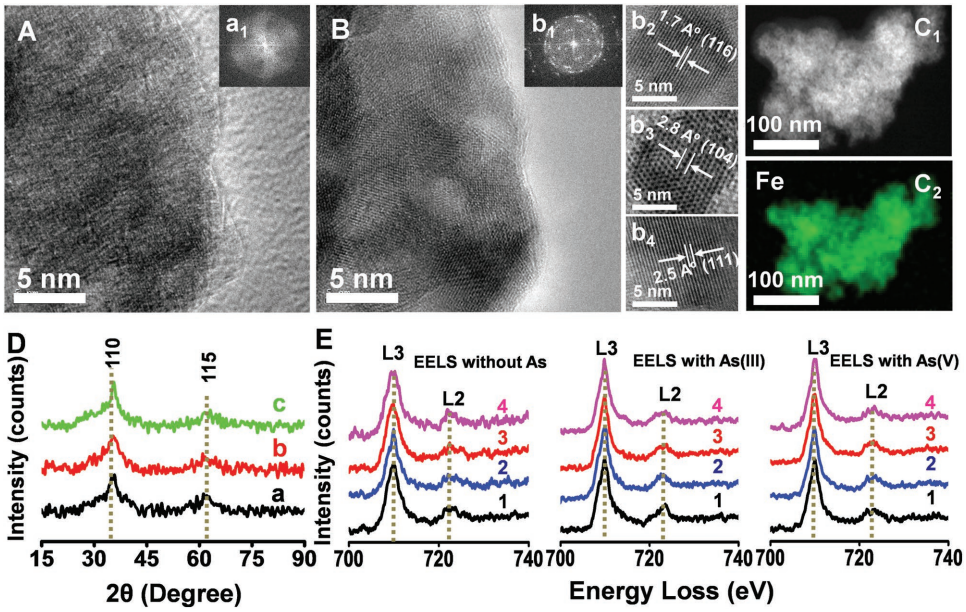

Figure 1. A) HRTEM amorphous feature of CM2LF along with dark field image (inset a_1). B) Beam induced crystallization of CM2LF along with dark field image and lattice resolved images (inset b_1, b_2, b_3, and b_4). C_1 and C_2) ADF-STEM image and Fe elemental mapping images of the initial material. D) XRD of CM2LF (a) before As adsorption (initial material), (b) after As(III), and (c) after As(V) adsorption. E) Dual EELS spectrum of iron L3, L2 region (Fe L3, L2) of CM2LF in four different locations (1, 2, 3, and 4) of the same sample.

scanning transmission electron microscopy (ADF-STEM) image of the initial composite (i.e., before arsenic adsorption) and elemental map (Figure 1C_2) of the image shows that Fe is uniformly distributed in the material. The ADF-STEM images along with the elemental maps of O, Fe, and As after the adsorption of As(III) and As(V) onto the composite are shown in Figure S2B and S2C (Supporting Information), respectively. Uniform distribution of As is seen in the material. Powder X-ray diffractogram (PXRD) pattern of the adsorbent shows the 2-line ferrihydrite phase (Figure 1D), which matches with the CCD (JCPDS, 46-1315). As(III) and As(V) adsorption does not change the PXRD profiles. No new phase was observed in PXRD of the used materials (Figure 1Db,c) which clearly shows the long-term stability of CM2LF nanocomposite in water.

Infrared spectroscopic investigation of CM2LF shows that the distinct chitosan features at 1662 cm^{-1} due to C=O of amide I, 1329 cm^{-1} due to N—H deformation and C—N stretching vibration and 1157 cm^{-1} corresponding to asymmetric C—O—C stretching[21,22] are shifted to 1636, 1375, and 1069 cm^{-1}, respectively indicating strong interaction with the ferrihydrite particles (Figure S3, Supporting Information). $NaHAsO_2$ shows As-O stretching peaks at 843 and 1210 cm^{-1} which are blueshifted to 808 and 1070 cm^{-1} after adsorption. Similarly, Na_2HAsO_4 shows peaks at 851 and 1175 cm^{-1} due to As-O stretching, which are blueshifted to 808 and 1070 cm^{-1} after interaction with CM2LF. These are shown in Figure S3 (Supporting Information).

Dual electron energy loss spectroscopy (Dual EELS) studies were performed to understand local effects in view of nanoscale nature of the materials (Figure 1E). However, no drastic changes were observed in the L2, L3 regions of Fe 2p edges upon As(III)/As(V) interaction, which may be correlated with the X-ray photoelectron spectroscopy (XPS). Fe 2p does not undergo a significant chemical shift upon As(III)/As(V) interaction (to be discussed later in the text). We believe that this is due to adsorption, which leads to no significant chemical changes.

CM2LF is stable in dry and wet conditions. Figure S4 (Supporting Information) shows the Young's moduli of the materials evaluated to be 2.42 and 2.64 MPa in dry and wet conditions, respectively and the values are comparable to standard Ennore sand used as reference.[23] The corresponding data of Mohr–Coulomb failure pattern are shown in Figure S5 (Supporting Information). The data show that CM2LF has higher shear strength in comparison to sand (friction angle, $\phi = 34.68°$). This stability, in loose and wet conditions, is important in device fabrication. Indirectly, this also suggests that the material does not leach out anything which is desirable for a material used for drinking water purification.

CM2LF due to its inherently porous structure and high surface area (172 m^2 g^{-1}) can be used to make a point-of-use arsenic water purifier. Its structure, while allowing ion penetration within, protects the composite as a whole from scale forming species, so as to maintain uptake kinetics. The synthesized material exhibits inherent green strength and has an uptake capacity of 100 mg g^{-1} in the field conditions, the highest arsenic adsorption capacity known so far, allowing the creation of affordable water purifiers. While FeOOH in its various forms are known to uptake arsenic in both As(III) and As(V) forms, a point of use gravity fed purifier requires highest uptake capacity to be viable. Uptake capacity of CM2LF for As(III) and As(V) follows Langmuir adsorption isotherm; the data are presented in Figure S6 (Supporting Information).

After evaluating the performance of the material in batch experiments, a prototype filter was developed. About 60 g of the composite (particle size ≈72 μm) was packed in a water

© 2016 WILEY-VCH Verlag GmbH & Co. KGaA, Weinheim

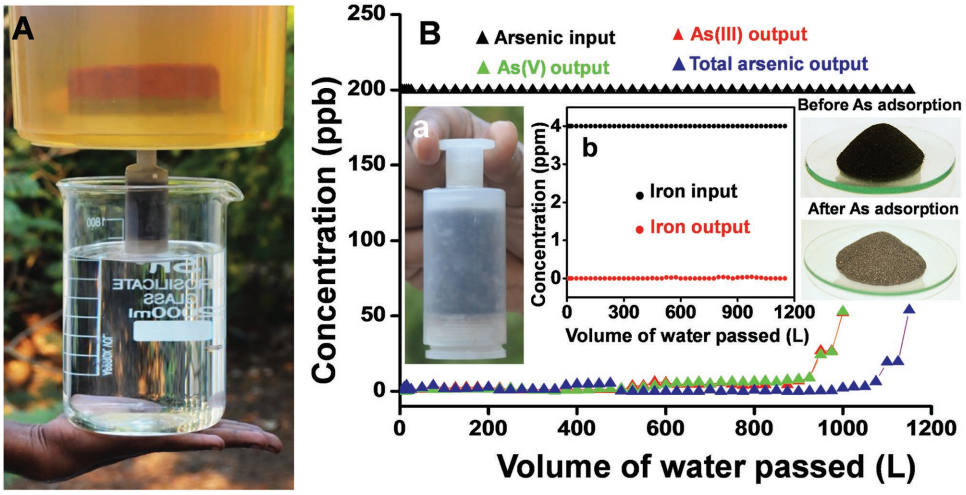

Figure 2. Set-up used for filtration containing arsenic (As(III + V)) and iron (Fe(II + III)) contaminated water using a cartridge with the reported material, along with a porous clay prefilter. B) Arsenic concentration in the water using a 60 g cartridge with the input as shown in A), inset (a) is the cartridge having 20 g adsorbent, inset (b) is iron output for the same input. The photographs of granular CM2LF before (black) and after (brown) As adsorption are in the inset.

purification cartridge (diameter, 10 mm; height, 35 mm) and a filter was assembled in an antigravity fashion. Output water was analyzed after acidification (5% HNO_3) and digestion, to ensure that all particulate matter that leached out, if at all, was also evaluated. In **Figure 2**A, we show a prototype used to conduct the experiments with over 1000 L of water at a flow rate of 12 to 15 mL min^{-1}, under gravity. Slight variation in the flow rate in the course of the long experiment was due to difference in the pressure head of the input water container. A particulate filter made from porous clay was sandwiched with a nanocomposite filter, shown in Figure 2Ba. The input water contains 4 mg L^{-1} (4 ppm) of Fe along with 200 µg L^{-1} (200 ppb) of a mixture of As(III) and As(V) in 1:1 ratio. This 1:1 composition is as seen in nature[24] and referred to as As(mix). Various combinations of ions Fe(II), Fe(III), As(III), As(V), and As(mix) have been tried to understand the performance of the material.

The flow rates were optimized for best performance. Data in Figure 2B show that As(III), As(V), and As(mix) were removed below the World Health Organization (WHO) limit of 10 µg L^{-1} for 1100 L synthetic and natural tap water samples using 60 g of the composite. The breakthrough was achieved at 1150 L, suggesting a capacity of 100 mg g^{-1} for the material. This capacity is 1.4 to 7.6 times larger than the best values reported in the literature.[25] The composite after arsenic adsorption shows a mild change in color (Figure 2B inset). The TEM-energy dispersive spectroscopy (EDS) and SEM-EDS elemental mappings of As(III) and As(V) saturated composites are presented in Figures S7 and S8 (Supporting Information), respectively, which confirm the presence of adsorbed arsenic homogeneously. As arsenic is generally found with Fe in the natural environment, tests were conducted with an input load of 4 mg L^{-1} Fe(II), which was removed to below the WHO limit of 300 µg L^{-1} over the entire range of volume investigated (Figure 2b). Fe(II) was chosen as the input as natural ground water from a depth of 50–120 ft from where it was extracted typically in affected areas through tube wells, where Fe is present in the +2 form, due to anaerobic conditions. Fe(II) becomes Fe(III) by aerial oxidation, intensifying the color of the water. Similar experiments were also conducted for Fe(III), As(III), As(V), and As(mix) separately and in various combinations of these and all the output values were below permissible limits. Experiments were conducted in the arsenic affected regions of West Bengal, Uttar Pradesh, Bihar, Assam, Jharkhand, Chhattisgarh, and Karnataka states of India in larger scale field trials as well, with similar results. Highest As contamination was seen in water sources of West Bengal, in the range of 200 µg L^{-1}, although even higher concentrations are seen occasionally. Therefore, this was chosen as the input concentration in test conditions.

Experiments were conducted to remove arsenic using the porous clay composite alone in presence and absence of iron (Fe(II/III)). A decrease of 40 µg L^{-1} was seen out of 200 µg L^{-1} As (mix) input using the porous filter alone without Fe(II/III). It was never possible to meet the water quality norm of 10 µg L^{-1} through this device in the absence of Fe(II)/Fe(III)/both. Studies revealed that As(III)/As(V)/As(mix) removal was due to particulates of Fe(II)/Fe(III) hydroxides which could not be passed through the porous clay. Dynamic light scattering (DLS) studies showed the existence of three major particle size distributions in this water samples (Figure S9, Supporting Information). All the arsenic and iron containing water samples used for testing in this study were maintained at pH ≈7.83.

Superior arsenic uptake capacity of the composite is due to its inherent structure. Arsenic uptake is uniform across the material and this does not change the inherent structure of the composite. This largely amorphous nature of the composite was also shown in the X-ray diffraction patterns (XRD), which reveals a metastable 2-line ferrihydrite structure in its most disordered form and it does not change upon As(III)/As(V) uptake. Uptake of arsenic appears to be surface adsorption as revealed by XPS studies (survey spectrum is shown in Figure S10A (Supporting Information), before and after As(III) and As(V) adsorption). Two broad peaks of Fe 2p were observed at 708.9 eV binding energy (BE) for Fe $2p_{3/2}$ and 722.3 eV for

© 2016 WILEY-VCH Verlag GmbH & Co. KGaA, Weinheim

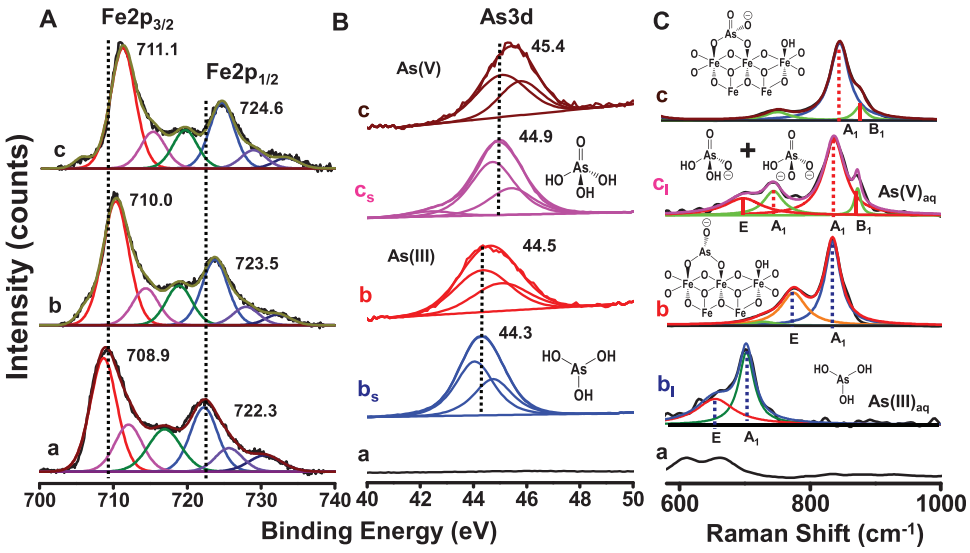

Figure 3. XPS of CM2LF showing A) Fe 2p and B) As 3d regions (a) before As adsorption, (b) after As(III) adsorption, and (c) after As(V) adsorption, independently compared with (b_s) standard As(III) of solid $NaAsO_2$ and (c_s) standard As(V) of solid Na_2HAsO_4 .$7H_2O$ respectively. The lines in A and B indicate relative peak shifts. C) Raman spectrum of (a) CM2LF solid, (b_l and c_l) standard aqueous 100×10^{-3} M solutions of As(III) and As(V) and (b and c) after adsorption of As(III) and As(V) on CM2LF. The structures in inset b_l and c_l show the speciation of As in solution at pH 7 and the structures in b and c show the probable structure of As(III/V) on CM2LF, respectively.

Fe $2p_{1/2}$, respectively for the initial material. The presence of satellite peak at 716.8 eV confirms +3 oxidation state of Fe (**Figure 3**Aa). The interaction of As(III)/As(V) does not change the oxidation state of Fe in CM2LF significantly. Similar Fe 2p doublet was observed at 710.0/723.5 and 711.1/724.6 eV, respectively for these samples, as shown in Figure 3Ab,c. Small change in the binding energy is due to the strong surface interaction of As with Fe(III). This explanation is supported by literature.[26,27] The C 1s core-level does not show any significant change while the other core levels, namely, As 3d (Figure 3B and Figure S10B, Supporting Information) and O 1s (Figure S10C, Supporting Information) show small changes upon arsenic interaction with CM2LF. There is a small shift of 0.2 and 0.5 eV, respectively for As(III) and As(V) to higher BE upon interaction with CM2LF, in comparison to the respective arsenic standards (Figure 3Bb_s,c_s). Data support physical interaction of As—O bonds with Fe in CM2LF. There is also a small shift in O 1s to higher BE upon As(III) and As(V) interaction with CM2LF (529.2 and 529.3 eV, respectively), in comparison to initial material (529.0 eV before arsenic adsorption), supporting strong interaction of O^{2-} with Fe(III) and As(III)/As(V) upon adsorption (Figure S10C, Supporting Information).

Raman spectrum of CM2LF is shown in Figure S11a (Supporting Information). The peaks around 230 and 300 cm^{-1} correspond to Fe—O and Fe—OH symmetric stretching. The standard arsenic materials, $NaAsO_2$ and $Na_2HAsO_4.7H_2O$ in solid state have characteristic peaks in the 700–900 cm^{-1} window due to symmetric stretching (A_1) of As—O bonds (see Figure S11, Supporting Information). As(III) in solution phase shows two peaks at pH 7 corresponding to the symmetric stretching mode A_1 at 702 cm^{-1} and the antisymmetric stretching mode E at 650 cm^{-1} due to the species, H_3AsO_3 (C_{3v} symmetry, Figure 3Cb_l). A redshift in the peak position was observed for As(III) after interaction with CM2LF, the peaks at 863 cm^{-1} (A_1) and 796 cm^{-1} (E) are due to the strong bidentate binding interaction of As—O with Fe—O as shown in Figure 3Cb. Similarly, in solution phase at pH 7, As(V) has two species $H_2AsO_4^-$ and $HAsO_4^{2-}$ in 1:1 ratio ($ABCD_2$ and AB_2CD type molecules both having C_s symmetry) exhibiting symmetric stretching (A_1) at 836 and 743 cm^{-1}, and symmetric bending (B_1 and E) at 875 and 696 cm^{-1}; assigned respectively to these two species (Figure 3Cc_l). Shifted peaks were observed at 852 cm^{-1} (A_1) and 884 cm^{-1} (B_1) after the interaction of As(V) with CM2LF. The near complete disappearance of the peaks at 680–750 cm^{-1} confirms that $H_2AsO_4^-$ converts to $HAsO_4^{2-}$ upon adsorption (Figure 3Cc). The interaction of $HAsO_4^{2-}$ with CM2LF is preferably bidendate in nature as shown in the inset of Figure 3Cc.

Figure 4 shows the mechanism of formation of CM2LF, where the ferric ions deposited on chitosan are converted to FeOOH nanoparticles (FeOOH NPs) upon incubation in alkaline medium at room temperature. It gradually makes nanocrystallites, confined in the chitosan network. The mechanical strength originates due to the formation of 3D cage-like structure of chitosan with embedded FeOOH NPs. These FeOOH NPs are accessible for water and dissolved ions. The interaction mechanism of As(III) and As(V) individually with CM2LF is shown Figures S12 and S13 (Supporting Information).

The effects of pH and common ion effect for the adsorption of As(III) and As(V) on CM2LF were studied. It was seen that pH in the range of 4–10 does not alter the adsorption capacity of CM2LF for As(III) and As(V), as shown in Figure S14 (Supporting Information). The effect of common ions on the As uptake is summarized in Table S1 (Supporting Information). CM2LF removes As(III) and As(V) efficiently even in the presence of other ions of relevance to drinking water. Total organic carbon (ToC) release from the components used in making

© 2016 WILEY-VCH Verlag GmbH & Co. KGaA, Weinheim

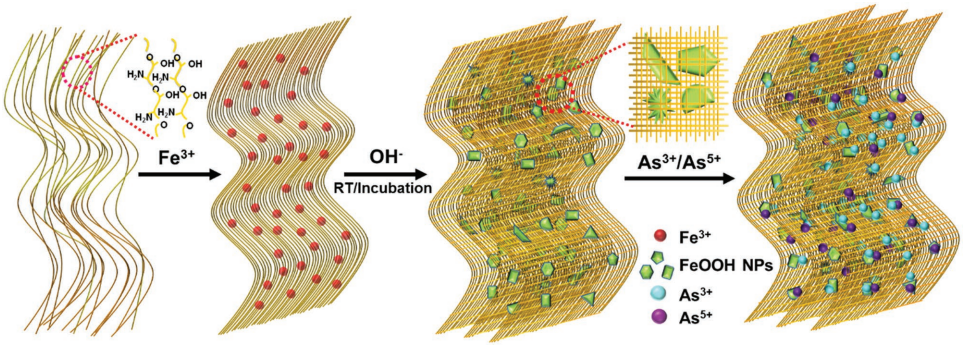

Figure 4. Schematic representation for the preparation of CM2LF and removal of As(III) and As(V) species from water.

CM2LF and the composite before and after As uptake was tested and these values were less than 1 mg L^{-1}, except for chitosan, as shown in Table S2 (Supporting Information). For chitosan, the ToC was 3.39 mg L^{-1} which may be due to the varying degree of polymerization; the smaller particles contribute to higher ToC. However, the acceptable United States Environmental Protection Agency (USEPA) limit for ToC in drinking water is 4 mg L^{-1}. Milli-Q water was used for experiments with CM2LF as the tap water routinely shows a ToC of 8.60 mg L^{-1}.

We have developed a reactivation protocol to regenerate the As saturated CM2LF. The composite was first soaked with Na_2SO_4 solution and incubated for 1 h at room temperature. The pH of the solution was subsequently adjusted to 4 using 1 M HCl solution. The solution was further incubated for about 3–4 h. The material was then washed with DI water to remove excess SO_4^{2-}/Cl^- ions. This reactivated material was used for arsenic adsorption for the next cycle. Using the above mentioned protocol we have reactivated and reused the same material for next seven cycles without any loss of arsenic adsorption capacity. The data are shown in Figure S14C and S14D (Supporting Information) for As(III) and As(V), respectively. The toxicity characteristic leaching protocol (TCLP, https://www.epa.gov/sites/production/files/2015-12/documents/1311.pdf) studies were conducted using the saturated composites to know the leaching of adsorbed arsenic and iron. The tests showed a leaching of 1 µg L^{-1} (total As), 2 µg L^{-1} (total As) and 24 µg L^{-1} (total Fe) for As(III), As(V) and iron, respectively.

The adsorption capacity of CM2LF was compared with pure ferrihydrite and chitosan separately with respect to the adsorbent dosage as shown in Figure S15 (Supporting Information). The maximum adsorption capacity of As was found to be 36.9 mg g^{-1} for ferrihydrite and 8.0 mg g^{-1} for chitosan in comparison to 100.0 mg g^{-1} for the composite. Performance data of CM2LF in batch experiments were also compared to other commercially available materials, viz., activated alumina, activated carbon, iron oxide (Fe_2O_3), silicon dioxide (SiO_2), GFH, and organic templated boehmite nanostructure (OTBN) are shown in Figures S16, S17, and S18 (Supporting Information). The arsenic adsorption capacities of commercial/noncommercial materials are reported as 15.9, 17.9, 20.2, 16.1, 70.0, and 13.1 mg g^{-1} for activated alumina,[3] activated carbon,[4,5] iron oxide,[5,6] silicon dioxide,[7] GFH,[8] and magnetite-reduced graphene oxide composite (M-RGO),[12] respectively. Data confirm that the arsenic removal capacity of CM2LF is 1.4 to 7.6 times better than all the compared materials. XPS data of all these commercial/noncommercial materials upon As(III) and As(V) adsorption and comparison of the data with As(III) and As(V) standards are presented in Figures S19, S20, and S21 (Supporting Information). The As 3d peaks of some of the materials shift slightly to lower BE, while some others shift slightly to higher BE but none of them show a drastic shift in these peaks, similar to CM2LF.

A domestic water filtration unit was prepared as shown in the photograph in the inset of Figure S22a (Supporting Information). A filter used three stage water filtration – first, a 0.5 µm polypropylene yarn wound cartridge filter for removal of particulates; second, iron removal media; and third, 900 g arsenic adsorbent, CM2LF. The water input and output are marked in the photograph. Performance data for the removal of arsenic and iron using three stage filtration, with a 1:1 ratio of As(III) and As(V), together at 200 µg L^{-1} and either of Fe(II) and Fe(III) at 4 mg L^{-1}, as contaminants are shown in Figure S22A (Supporting Information), for a total volume of 6000 L water passed (>15 L per day for a year). The output was below the WHO limit of 10 and 300 µg L^{-1} for As and Fe, respectively, throughout the experiment. The inset, Figure S22b (Supporting Information) shows water flow rate from the unit at an applied pressure of 7 psi. Reduced quantity of adsorbent and higher flow rates are possible in the optimized design, at different levels of operation, especially in the community scale.

To summarize, As(III) and As(V) as well as mixed forms of the same could be effectively scavenged by a composite with fast kinetics allowing the creation of an affordable arsenic-free drinking water solution for point-of-use applications. The unprecedented large capacity in field conditions is attributed to the inherent structure of the composite with confined metastable 2-line ferrihydrite in biopolymer cages, which allows the creation of effective adsorption sites. The arsenic adsorption capacity of the composite is 1.4 to 7.6 times better than the available compositions. Synthesis of the composition involves simple raw materials and the process requires no electrical power and no organic solvents. With this material, arsenic-free drinking water can be delivered for a family of five at an estimated cost of US $2 per year in resource limited settings.

Experimental Section

Materials: Ferric chloride ($FeCl_3.6H_2O$), sodium hydroxide (NaOH), sodium sulphate (Na_2SO_4), ferrous sulphate ($FeSO_4.7H_2O$), and ferric

© 2016 WILEY-VCH Verlag GmbH & Co. KGaA, Weinheim

sulphate ($Fe_2(SO_4)_3.XH_2O$) were purchased from Rankem Glasswares and Chemicals, Pvt. Ltd. India. Biopolymer (Chitosan) was purchased from Pelican Biotech & Chemicals Labs Pvt. Ltd. India. Sodium arsenite ($NaAsO_2$) and sodium arsenate ($Na_2HAsO_4.7H_2O$) were purchased from SD Fine Chemicals Limited. All chemicals were of analytical grade and were used without further purification. The porous filters developed by CSIR-Institue of Minerals and Materials Technology (IMMT) were purchased from Watsan Envirotech Private Limited. Deionized water was used throughout the experiments unless otherwise mentioned.

Synthesis of CM2LF: The granular composites, composed of iron oxyhydroxide–chitosan nanostructures, were synthesized by a green synthetic route, which in general involves the hydrolysis of a metal precursor–chitosan complex using an alkaline medium followed by washing and drying at ambient conditions. Metal ion precursor used for the preparation of the composite was Fe^{3+}. All syntheses were carried out in deionized water, while natural ground water or tap water was used for testing.

An iron oxyhydroxide-chitosan nanostructure was synthesized as follows: About 0.13 g chitosan was dissolved in 10 mL, 1% HCl by continuous stirring for 12 h. This was precipitated at pH 9 using 0.2 M NaOH. About 0.5 g Na_2SO_4 was added in one step. After 5 min of incubation, 10 mL, 1 M ferric hexachloride was added. The mixture was brought to pH 8, using 2 M sodium hydroxide by slow addition. The final composition was further incubated for about 12 h, at ambient temperature to embed the synthesized FeOOH nanoparticles in biopolymer cages. The resulting gel was washed with copious amount of water to remove soluble salts and was dried at room temperature (28–30 °C). The resulting composite, namely, CM2LF, was insoluble in water and appeared as black-red to brownish granules. The dried composite was crushed to specific sizes (optimized 52 × 72 µm) and used for arsenic adsorption. The yield was 1.0 g. The method of preparation of the composite is water positive by two to three orders of magnitude; i.e., it produces 500 L of clean water for every 1 L of water consumed for its production. The as-prepared granular composite was stable and did not disintegrate in water for over two years.

The CM2LF prepared within the chitosan matrix, which induces structural integrity, is biodegradable and inexpensive. Other polymers such as banana silk can also be used for this purpose. The organic polymer acts as a template, controls the size of the particles, and gives mechanical strength to the composite after drying at room temperature. When the ferrihydrite nanoparticles were prepared within the matrix, they bind strongly with it, due to which no nanoparticles get into the purified water. It is well-known that hydrous iron oxide, as found in nature, exhibits reasonable mechanical strength (as they occur in crystalline form). In the case of CM2LF composite, it is largely amorphous. Here, the role of chitosan is crucial in improving the mechanical strength of CM2LF composite by binding with ferric oxyhydroxide nanocrystals. As 2-line ferrihydrite has been examined extensively in terms of its structure,[28,29] we focused only on its arsenic uptake properties.

Testing Protocol for Arsenic Efficacy in Batch: 25 mg of CM2LF was shaken with 100 mL of natural tap water (see Table S1 in the Supporting Information for water quality parameters). Arsenic removal efficiency of CM2LF was measured by spiking the natural tap water with As(III) and As(V) separately at a concentration of 1.1 mg L^{-1} . Thereafter, the water was left standing for 1.5 h and subsequently the leftover arsenic concentration in treated water was analyzed using inductively coupled plasma mass spectrometry (ICP-MS) after acidification with 5% HNO_3. Experiments with water filtration cartridges are described in the main text.

Instrumentation: HRTEM images of the sample were obtained with JEM 3010 (JEOL, Japan) operating at 200 kV with an ultrahigh resolution polepiece. Elemental mapping using TEM was done on an Oxford Semistem EDS system. The samples for HRTEM were prepared by dropping the dispersion on amorphous carbon films supported on a copper grid and subsequent drying. ADF-STEM measurements were carried out using a Gatan GIF Quantum ER fully loaded Tecnai F20. This analysis was carried out at 200 kV and the data were acquired in digital micrograph and the chemical analysis was carried out with 1 eV energy resolution. This entire ADF-STEM analysis was carried out in Dual EELS mode to measure the accurate chemical shift. Identification of the phase(s) of all the samples was carried out by XRD (Bruker AXS, D8 Discover, USA) using Cu Kα radiation at λ = 1.5418 Å. XPS measurements were done using ESCA Probe TPD spectrometer of Omicron Nanotechnology. Polychromatic Mg Kα was used as the X-ray source (hν = 1253.6 eV). Samples were spotted as dropcast films on a sample stub. Constant analyzer energy of 20 eV was used for the measurements. Binding energy was calibrated with respect to C 1s at 284.5 eV. Surface enhanced Raman spectroscopy was performed using a CRM 200 micro Raman spectrometer of WiTec GmbH (Germany). The substrate was mounted on a sample stage of a confocal Raman spectrometer. The spectra were collected at 532 nm laser excitation. For Raman measurements, the corresponding nanomaterial/standard material (as in dried powder form)-coated glass substrates were analyzed keeping the laser and other parameters same. A super-notch filter placed in the path of the signal effectively cuts off the excitation radiation. The signal was then dispersed using a 600/1800 grooves per mm grating and the dispersed light was collected by a Peltier-cooled charge coupled device. Surface morphology, elemental analysis, and elemental mapping studies were carried out using a SEM equipped with EDS (FEI Quanta 200). For the SEM and EDS measurements, samples were spotted on an aluminum sample stub. Total arsenic and iron concentrations in water were detected using ICP-MS (Agilent Technologies, 7700x ICP-MS and PerkinElmer NexION 300X ICP-MS) with appropriate standards. Brunauer-Emmett-Teller (BET) surface area was measured using Micromeritics ASAP 2020. Samples were degassed at 200 °C for 4 h under vacuum and analysed at 77 K with ultra high pure nitrogen gas.

Supporting Information

Supporting Information is available from the Wiley Online Library or from the author.

Acknowledgements

The authors thank Avijit Baidya, Mohd. Azhardin Ganayee, Rahul Narayanan, and P. Srikrishnarka for taking photographs of the set-up used for arsenic testing, for their technical support in conducting Raman analysis, IR measurements, and help in making the Schematic and TOC figures, respectively. The authors thank Edamana Prasad and Madhu Babu for their help in measuring DLS measurements. The authors thank Ligy Philip and Ramprasad for help in ToC measurements. The authors also thank R. G. Robinson, Lini K. Nair, and Manu Santhanam (Department of Civil Engineering) for their help in conducting direct shear stress and compressive strength analyses. Radha Gobinda Bhuin is currently working at University Erlangen-Nürnberg, Egerlandstr, Germany. National Centre for Catalysis Research at IIT Madras thanked for the BET analyses. Authors thank the Department of Science and Technology (Government of India) for constantly supporting our research program on nanomaterials.

Received: August 9, 2016
Revised: October 16, 2016
Published online: December 5, 2016

[1] T. Pradeep, Anshup, *Thin Solid Films* **2009**, *517*, 6441.
[2] R. Damoiseaux, S. George, M. Li, S. Pokhrel, Z. Ji, B. France, T. Xia, E. Suarez, R. Rallo, L. Madler, Y. Cohen, E. M. V. Hoek, A. Nel, *Nanoscale* **2011**, *3*, 1345.
[3] T. F. Lin, J. K. Wu, *Water Res.* **2001**, *35*, 2049.

© 2016 WILEY-VCH Verlag GmbH & Co. KGaA, Weinheim

[4] B. Deng, M. Caviness, Z. Gu, *ACS Symp. Ser.* **2005**, *915*, 284.
[5] S. Yao, Z. Liu, Z. Shi, *J. Environ. Health. Sci. Eng.* **2014**, *12*, 58.
[6] Y. Jia, T. Luo, X.-Y. Yu, Z. Jin, B. Sun, J.-H. Liu, X.-J. Huang, *New J. Chem.* **2013**, *37*, 2551.
[7] H.-T. Fan, X. Fan, J. Li, M. Guo, D. Zhang, F. Yan, T. Sun, *Ind. Eng. Chem. Res.* **2012**, *51*, 5216.
[8] W. Driehaus, M. Jekel, U. Hildebrandt, *Aqua (Oxford)* **1998**, *47*, 30.
[9] T. S. Sreeprasad, S. M. Maliyekkal, K. P. Lisha, T. Pradeep, *J. Hazard. Mater.* **2011**, *186*, 921.
[10] W. Gao, M. Majumder, L. B. Alemany, T. N. Narayanan, M. A. Ibarra, B. K. Pradhan, P. M. Ajayan, *ACS Appl. Mater. Interfaces* **2011**, *3*, 1821.
[11] D. Koushik, S. Sen Gupta, S. M. Maliyekkal, T. Pradeep, *J. Hazard. Mater.* **2016**, *308*, 192.
[12] V. Chandra, J. Park, Y. Chun, J. W. Lee, I. C. Hwang, K. S. Kim, *ACS Nano* **2010**, *4*, 3979.
[13] U. Schwertmann, R. M. Cornell, *Iron Oxides in the Laboratory*, 2nd Ed., Wiley-VCH, Weinheim, Germany **2000**.
[14] A. Navrotsky, L. Mazeina, J. Majzlan, *Science* **2008**, *319*, 1635.
[15] S. Dixit, J. G. Hering, *Environ. Sci. Technol.* **2003**, *37*, 4182.
[16] J. Gimenez, M. Martinez, J. de Pablo, M. Rovira, L. Duro, *J. Hazard. Mater.* **2007**, *141*, 575.
[17] Y. Jia, L. Xu, Z. Fang, G. P. Demopoulos, *Environ. Sci. Technol.* **2006**, *40*, 3248.
[18] A. Ghosh, Y. Krishnan, *Nat. Nanotechnol.* **2014**, *9*, 491.
[19] S. Das, M. J. Hendry, J. Essilfie-Dughan, *Environ. Sci. Technol.* **2011**, *45*, 268.
[20] M. U. Sankar, S. Aigal, S. M. Maliyekkal, A. Chaudhary, A. A. Anshup Kumar, K. Chaudhari, T. Pradeep, *Proc. Natl. Acad. Sci. USA* **2013**, *110*, 8459.
[21] V. K. Mourya, N. N. Inamdar, A. Tiwari, *Adv. Mater. Lett.* **2010**, *1*, 11.
[22] K. Rout, M. Mohapatra, S. Anand, *Dalton Trans.* **2012**, *41*, 3302.
[23] V. Gade, T. Dave, V. Chauhan, S. Dasaka, In *Proc. Indian Geotechnical Conf., Roorkee*, Roorkee, India **2013**.
[24] D. Das, G. Samanta, B. K. Mandal, T. R. Chowdhury, C. R. Chanda, P. P. Chowdhury, G. K. Basu, D. Chakraborti, *Environ. Geochem. Health* **1996**, *18*, 5.
[25] S. Kumar, R. R. Nair, P. B. Pillai, S. N. Gupta, M. A. R. Iyengar, A. K. Sood, *ACS Appl. Mater. Interfaces* **2014**, *6*, 17426.
[26] A. P. Grosvenor, B. A. Kobe, M. C. Biesinger, N. S. McIntyre, *Surf. Interface Anal.* **2004**, *36*, 1564.
[27] R. P. Gupta, S. K. Sen, *Phys. Rev. B* **1974**, *10*, 71.
[28] K. M. Towe, W. J. Bradley, *J. Coll. Inter. Sci.* **1967**, *24*, 384.
[29] F. M. Michel, L. Ehm, S. M. Antao, P. L. Lee, P. J. Chupas, G. Liu, D. R. Strongin, M. A. Schoonen, B. L. Phillips, J. B. Parise, *Science* **2007**, *316*, 1726.

© 2016 WILEY-VCH Verlag GmbH & Co. KGaA, Weinheim

Copyright WILEY-VCH Verlag GmbH & Co. KGaA, 69469 Weinheim, Germany, 2016.

ADVANCED MATERIALS

Supporting Information

for *Adv. Mater.*, DOI: 10.1002/adma.201604260

Confined Metastable 2-Line Ferrihydrite for Affordable Point-of-Use Arsenic-Free Drinking Water

*Avula Anil Kumar, Anirban Som, Paolo Longo, Chennu Sudhakar, Radha Gobinda Bhuin, Soujit Sen Gupta, Anshup, Mohan Udhaya Sankar, Amrita Chaudhary, Ramesh Kumar, and Thalappil Pradeep**

Submitted to ADVANCED MATERIALS

Supporting Information

for *Adv. Mater.*, DOI: 10.1002/adma.201604260

Confined metastable 2-line ferrihydrite for affordable point-of-use arsenic free drinking water

*Avula Anil Kumar[1], Anirban Som[1], Paolo Longo[2], Chennu Sudhakar[1], Radha Gobinda Bhuin[1], Soujit Sen Gupta[1], Anshup[1], Mohan Udhaya Sankar[1], Amrita Chaudhary[1], Ramesh Kumar[1] and Thalappil Pradeep[1]**

Figure S1. Time dependent microscopic analyses (HRTEM) of CM2LF, amorphous vs. crystallization features of CM2LF

Figure S2. SEM and ADF-STEM analyses of CM2LF

Figure S3. Infrared spectrum (IR) of CM2LF

Figure S4. Direct shear test of CM2LF

Figure S5. Mohr-Coulomb failure pattern of CM2LF

Figure S6. Arsenic uptake kinetics of CM2LF for As(III) and As(V)

Figure S7. TEM-EDX analysis of CM2LF

Figure S8. SEM-EDX analysis of CM2LF

Figure S9. Dynamic light scattering (DLS) analysis of arsenic in presence of iron (Fe-As interaction) in solution

Figure S10. X-ray photoelectron spectrum (XPS) analysis of CM2LF

Figure S11. Raman spectrum of CM2LF

Figure S12. Proposed mechanism of As(III) adsorption on CM2LF

Figure S13. Proposed mechanism of As(V) adsorption on CM2LF

Figure S14. Adsorption efficiency of CM2LF on varying pH and reactivation and reuse of the composite

Figure S15. Comparison of pure ferrihydrite and chitosan with CM2LF

Figure S16. Performance data (batch study) of CM2LF in comparison to activated alumina and activated carbon with respect to arsenic removal

Figure S17. Performance data (batch study) of CM2LF in comparison to iron oxide and silicon dioxide with respect to arsenic removal

Figure S18. Performance data (batch study) of CM2LF in comparison to granular ferric hydroxide (GFH) and organic templated boehmite nanostructure (OTBN) with respect to arsenic removal

Figure S19. XPS data of activated alumina and activated carbon upon arsenic adsorption

Figure S20. XPS data of iron oxide and silicon dioxide upon arsenic adsorption

Figure S21. XPS data of GFH and OTBN upon arsenic adsorption

Figure S22. Performance data (cartridge study) for the proof of concept prototype of Inline domestic unit for arsenic and iron removal

Table S1. Effect of other ions on the As adsorption capacity of CM2LF

Table S2. ToC due to CM2LF before and after As adsorption

Table S3. Physicochemical characteristics of influent natural water

Supporting Information Text

Materials and Methods

High Resolution Transmission Electron Microscopy (HRTEM) images of the sample were obtained with JEM 3010 (JEOL, Japan) operating at 200 kV with an ultra-high resolution (UHR) pole piece. Elemental mapping on TEM was done on an Oxford semi STEM EDS system. The samples for HRTEM were prepared by dropping the dispersion on amorphous carbon films supported on a copper grid and dried. Surface morphology, elemental analysis and elemental mapping studies were carried out using a Scanning Electron Microscope (SEM) equipped with Energy Dispersive Analysis of X-rays (EDAX) (FEI Quanta 200). For the SEM and EDAX measurements, samples were spotted on the aluminium sample stub. Annular Dark-Field Scanning Tunneling Electron Microscopy (ADF STEM) measurements were carried out using a Gatan GIF Quantum ER fully loaded Tecnai F20. This analysis was carried out at 200 kV and data acquired in digital micrograph and chemical analysis was

carried out with 1 eV energy resolution. This entire ADF STEM analysis was carried out in DualEELS (Dual Electron Energy Loss Spectroscopy) mode to measure the accurate chemical shift. X-ray Photoelectron Spectroscopy (XPS) measurements were done using ESCA Probe TPD spectrometer of Omicron Nanotechnology. Polychromatic Mg Kα was used as the X-ray source (hν = 1253.6 eV). The samples were spotted as drop-cast films on a sample stub. Constant analyzer energy of 20 eV was used for the measurements. Binding energy was calibrated with respect to C 1s at 284.5 eV. Total arsenic and iron concentrations in water were detected using inductively coupled plasma mass spectrometry (ICP-MS) (Agilent Technologies, 7700x ICP-MS and PerkinElmer NexION 300D ICP-MS) with appropriate standards.

Mechanical testing of CM2LF: The shear strength of the composite was measured at dry and wet conditions, separately. Around ~ 90 g of granular media was packed in a 6 cm x 6 cm x 6 cm (L x B x H) sample holder and horizontal shear stress was measured under normal stress of 50, 100 and 200 kPa, respectively.

Supporting Information Figures

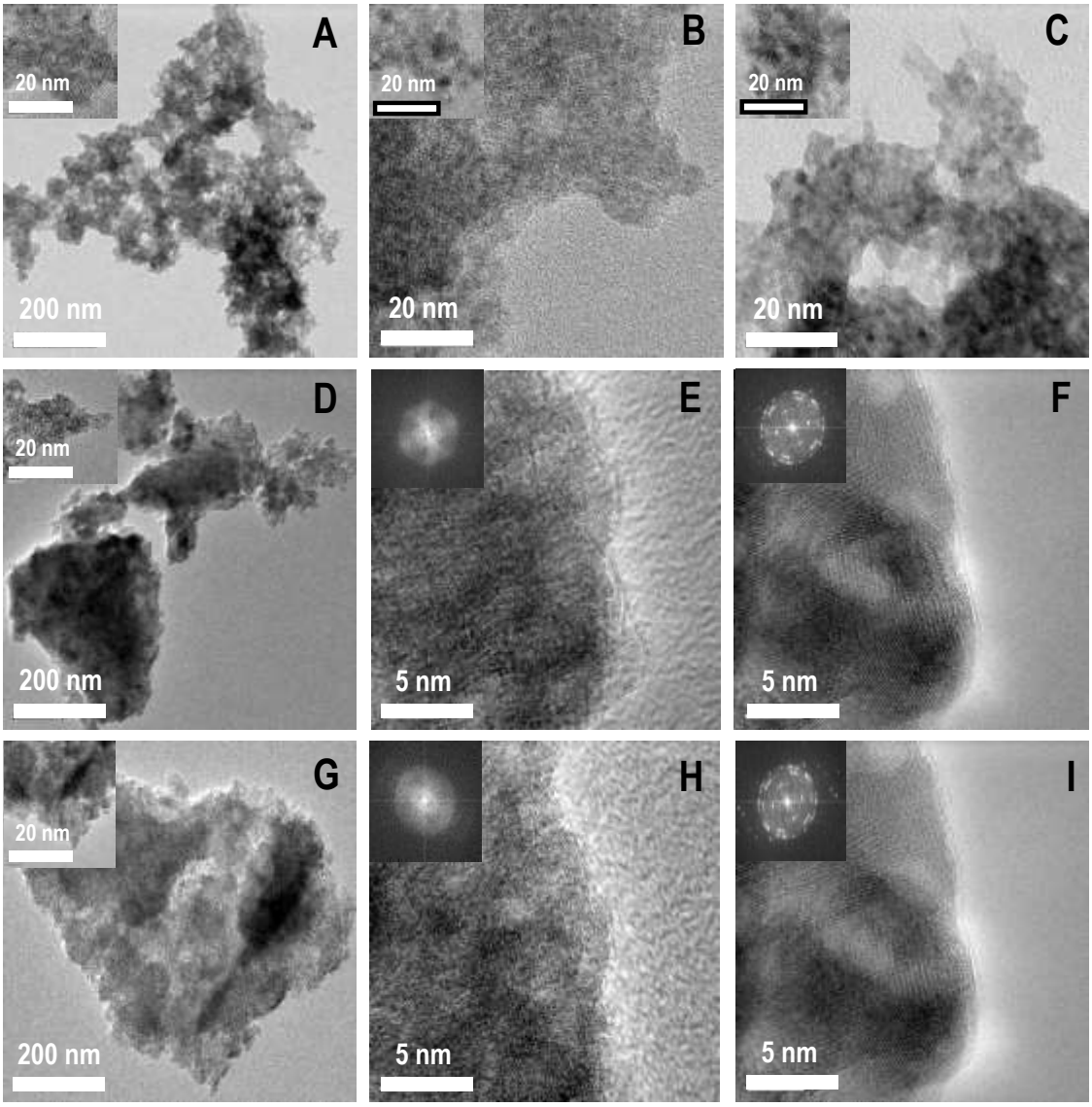

Figure S1. Time dependent TEM images of CM2LF, (A, D and G) initial material, As(III) adsorbed and As(V) adsorbed CM2LF before electron beam irradiation showing amorphous nature of the material (the insets shows the high resolution images). (B, E and H) Short time electron beam induced crystallization of the initial, As(III) adsorbed and As(V) adsorbed CM2LF showing a little crystalline behavior of the material (inset images). (C, F and I) Long time electron beam induced crystallization of the initial, As(III) adsorbed and As(V) adsorbed CM2LF showing the more crystalline nature of the material (inset images).

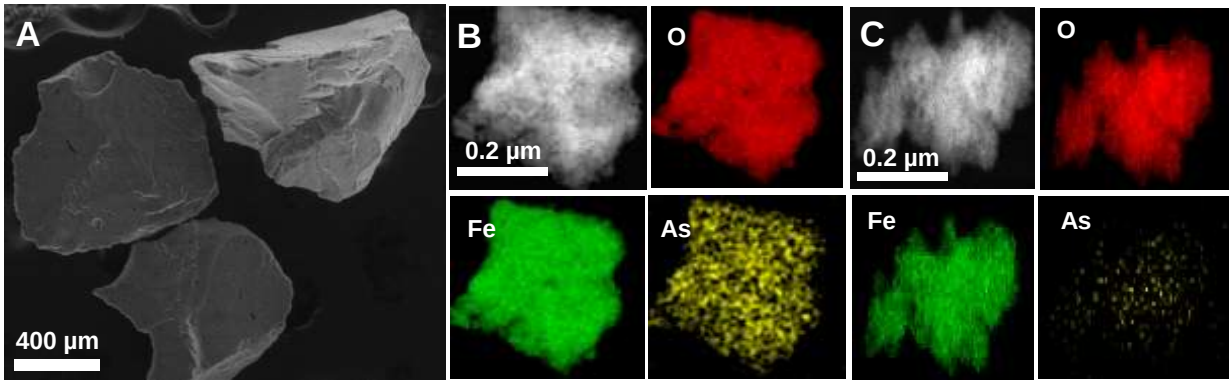

Figure S2. (A) SEM image of the initial granular material (52 X 72 µm), which was stored in water for about 6 months. (B and C) ADF-STEM images of As(III) and As(V) adsorbed material, respectively and the corresponding elemental maps of O, Fe and As(III).

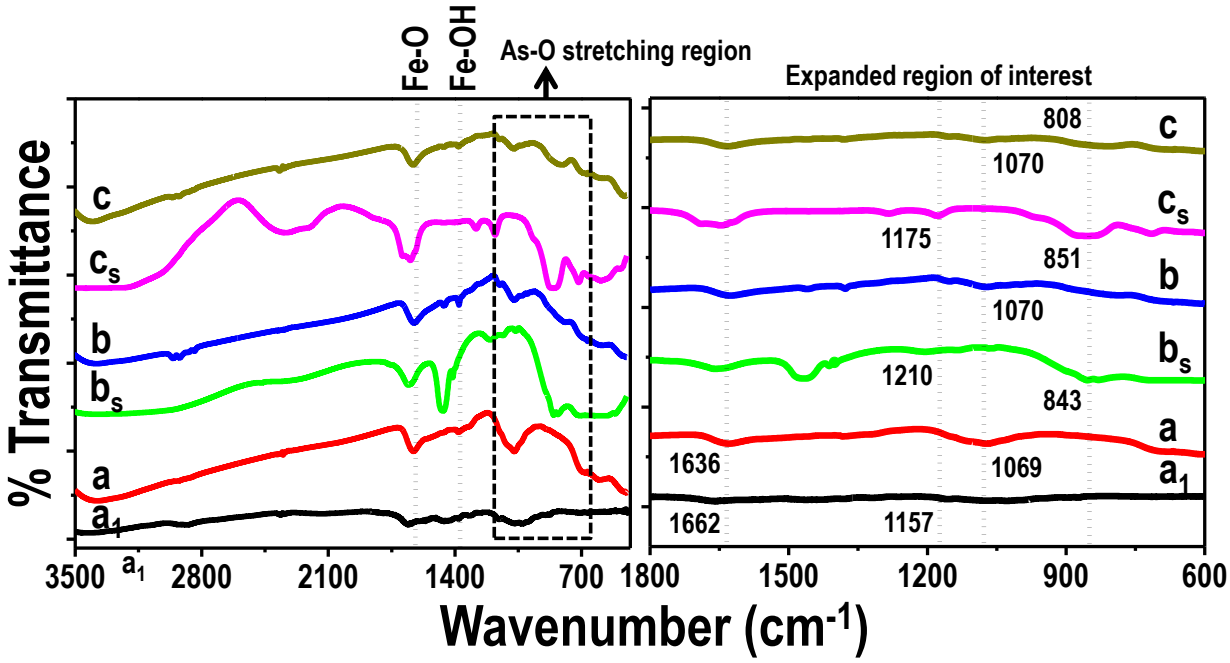

Figure S3. Infrared spectrum (IR) of (a_1) bio-polymer (chitosan), (a) the initial material (i.e., CM2LF), (b) after As(III) adsorption and (c) after As(V) adsorption on CM2LF, independently compared with respective arsenic standards (b_s) As(III) standard and (c_s) As(V) standard, respectively and the corresponding stretching and bending region of Fe-O, Fe-OH and As-O are shown in the expanded region. The corresponding peak shifting are also shown in the expanded region.

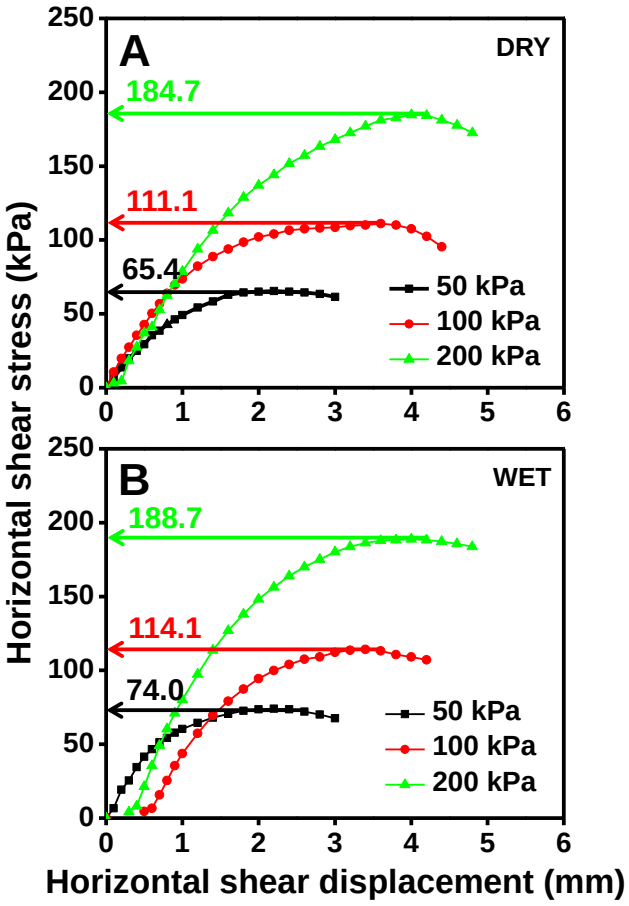

Figure S4. Direct shear test of CM2LF. (A and B) Plot of horizontal shear stress vs. horizontal shear displacement of loosely packed CM2LF measured at dry condition (A) and wet condition (B), respectively.

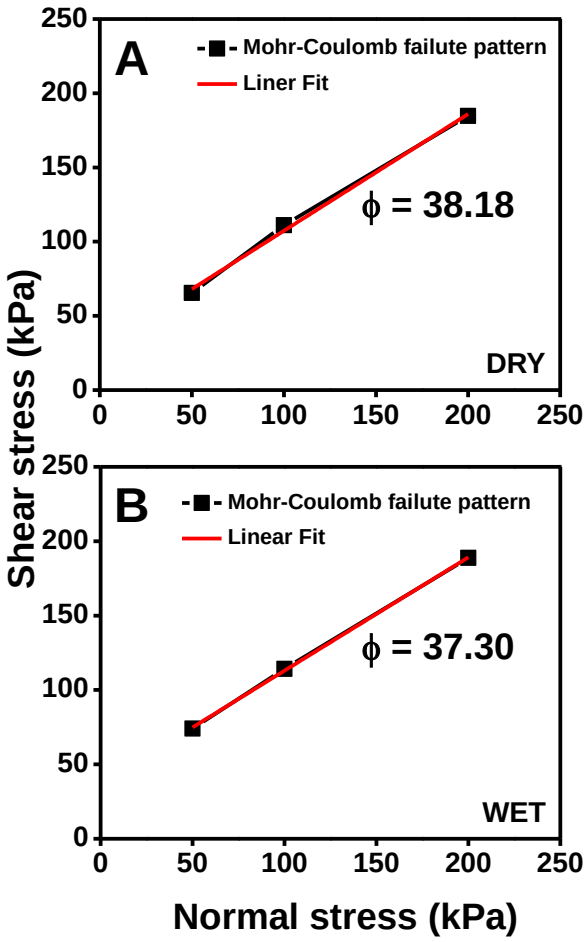

Figure S5. Mohr-Coulomb failure pattern of CM2LF. (A and B) Plot of shear stress vs. normal stress of loosely packed CM2LF showing the straight-line approximation of the Mohr-Coulomb failure pattern measured at dry condition (A) and wet condition (B), respectively.

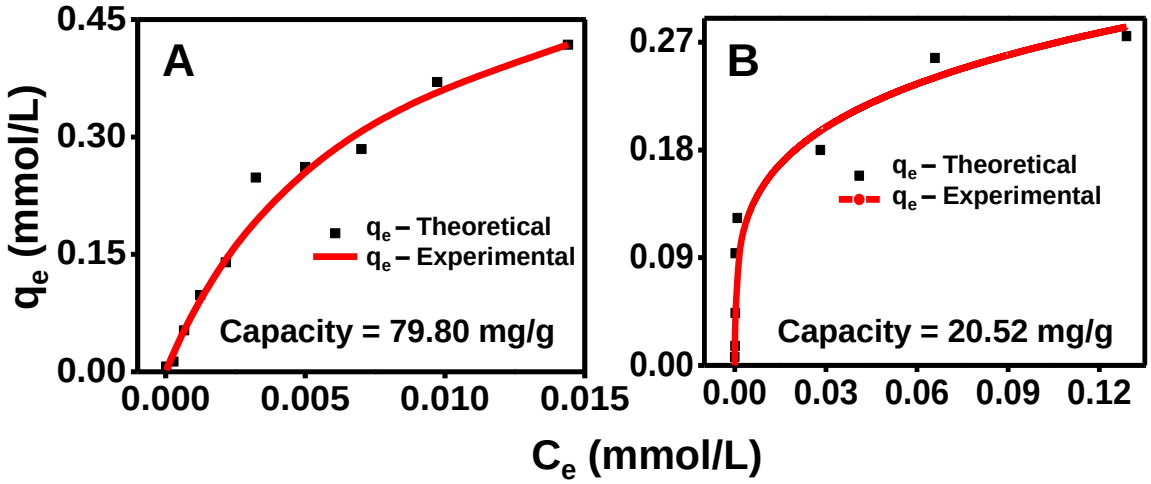

Figure S6. Arsenic uptake kinetics of CM2LF for As(III) and As(V). (A and B) Langmuir isotherm for As(III) adsorbed (mmol/g) as a function of As(III) concentration (mmol/L) (A) and Langmuir isotherm for As(V) adsorbed (mmol/g) as a function of As(V) concentration (mmol/L) (B) conducted with 30 mg initial adsorbent dose in 30 mL deionized water with 90 min as contact time, respectively. Fitted curve is based on Langmuir isotherm.

Arsenic adsorption isotherm of as-synthesized CM2LF composite was measured in the lab in 0.04 M NaCl at pH 7.0, to mimic field conditions. As-synthesized composite adsorbs approximately 1.064 mmol/g and 0.27 mmol/g each at an equilibrium concentration of 0.15 mM of As(III) and As(V), respectively. Langmuir isotherm was evaluated using Equation (1).

$$\frac{C_e}{q_e} = \frac{C_e}{q_{max}} + \frac{1}{q_{max}b} \qquad \text{Equation (1)}$$

where, C_e (mmol/L) is the equilibrium concentration of arsenic in the solution, q_e (mmol/L) is the quantity of arsenic adsorbed at equilibrium and q_{max} (mmol/L) is the monolayer adsorption capacity, and b (L/mmol) is the Langmuir adsorption constant, related to the free energy of adsorption.

The Langmuir isotherm was used to estimate the maximum adsorption capacity of CM2LF under the conditions 298 K, pH 7.0 with 90 min of contact time and 1.0 g/L adsorbent dose while varying initial arsenic concentration from 0.5 to 30 mg/L. The values of the isotherm

constants $1/q_{max}$ and $1/q_{max}b$, for As(III) adsorption are 1.60 and 0.0114, respectively while that for As(V) adsorption are 3.63 and 0.008, respectively.

The linear plot of C_e/q_e versus C_e (mmol/L) along with a high value correlation coefficient indicates that Langmuir isotherm provides a better fit of the equilibrium data. The Langmuir monolayer capacity (mg/g) of CM2LF for As(III) adsorption is calculated to be 79.80 mg/g while for As(V) adsorption is 20.52 mg/g. This difference is because the adsorbent works better at higher concentrations of As(III) and at lower concentrations of As(V). This is because basic pH is more suitable to remove As(III) while acidic pH is more suitable to remove As(V). The Langmuir model is based on the assumption of homogeneous monolayer coverage with all adsorption sites being identical and energetically equivalent.

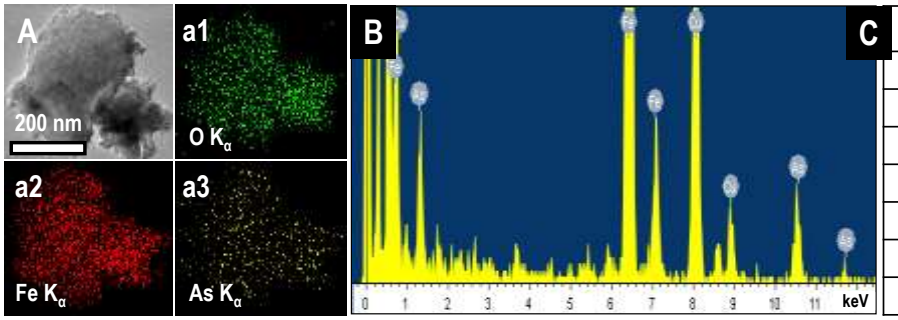

Element	Weight%	Atomic%
O K	33.44	64.20
Si K	0.60	0.66
Cl K	0.63	0.55
Ca K	0.50	0.38
Fe K	53.73	29.55
As K	11.10	4.66
Total	**100.00**	**100.00**

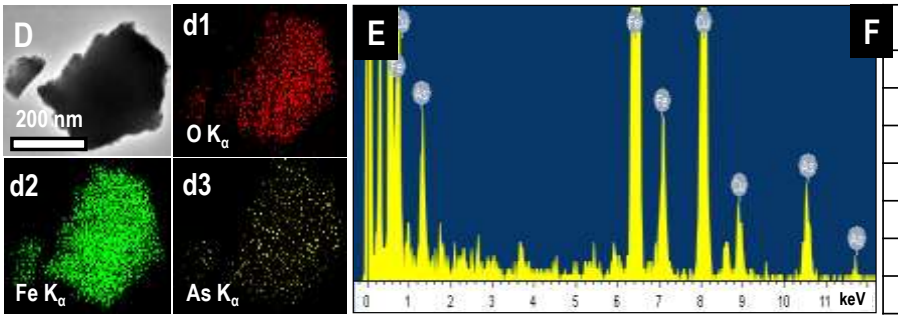

Element	Weight%	Atomic%
O K	31.51	61.85
Si K	0.98	1.09
Cl K	0.69	0.61
Ca K	2.52	1.98
Fe K	51.14	28.75
As K	13.15	5.72
Total	**100.00**	**100.00**

Figure S7. TEM-EDX analysis of CM2LF. (A) X-ray elemental mapping of different elements, (B) Elemental EDX spectrum and (C) Elemental EDX analysis of As(III) adsorbed CM2LF. Same data for As(V) adsorbed CM2LF.

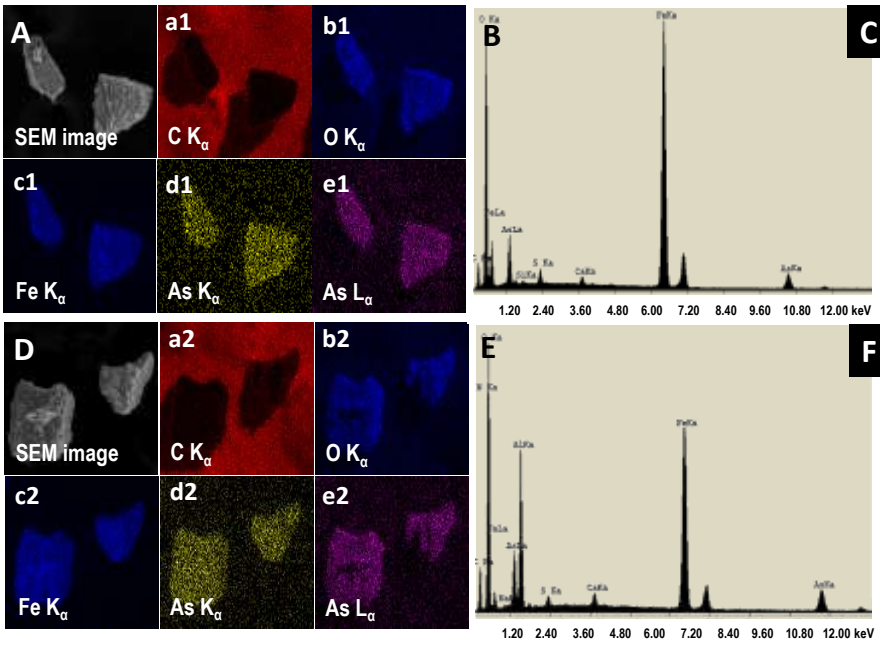

C

Element	Weight%	Atomic%
C K	16.47	29.81
O K	39.97	54.32
Si K	0.23	0.18
S K	0.81	0.55
Ca K	0.37	0.20
Fe K	27.23	10.60
As K	5.36	1.56
As L	9.56	2.77
Total	**100.00**	**100.00**

F

Element	Weight%	Atomic%
C K	22.70	38.10
O K	35.90	45.30
N K	2.40	3.50
S K	0.50	0.30
Ca K	0.50	0.20
Fe K	14.30	5.20
Fe L	10.40	3.80
As K	5.90	1.60
As L	7.40	2.00
Total	**100.00**	**100.00**

Figure S8. SEM-EDX analyses of CM2LF: (A) X-ray elemental mapping of different elements, (B) Elemental EDX spectrum and (C) Elemental EDX analysis of As(III) adsorbed CM2LF, respectively. Same data for As(V) adsorbed CM2LF.

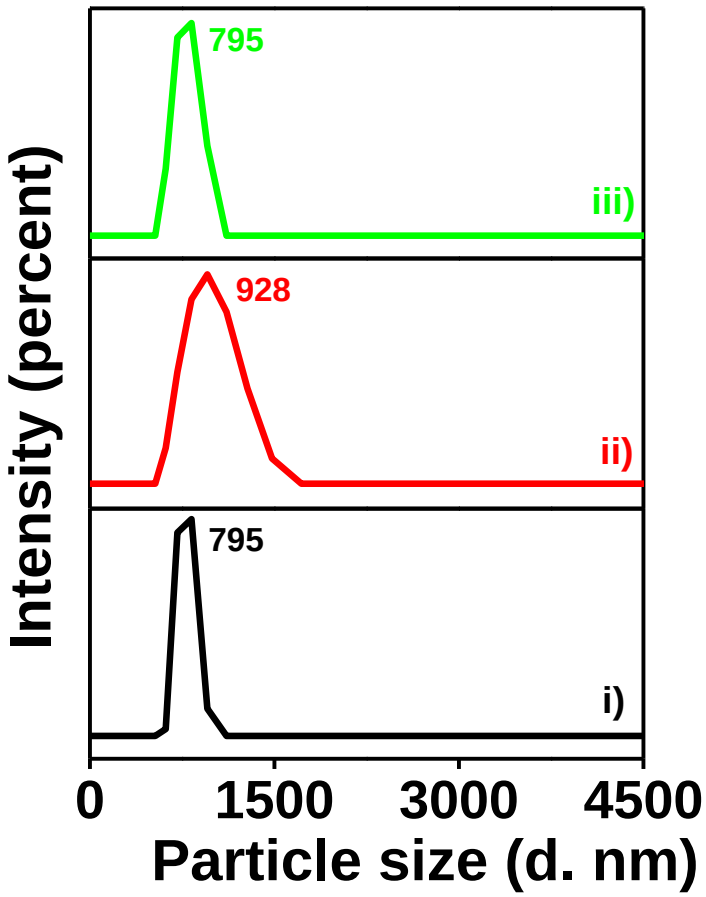

Figure S9. Dynamic light scattering (DLS) analysis of arsenic in presence of iron (Fe-As interaction) in solution. The Fe(II)/Fe(III) hydroxide particulates in presence of (i) As(III), (ii) As(V) and (iii) As(Mix.), which is showing the existence of only single major particle size distributions (~ 0.8 µm – 1 µm) in water.

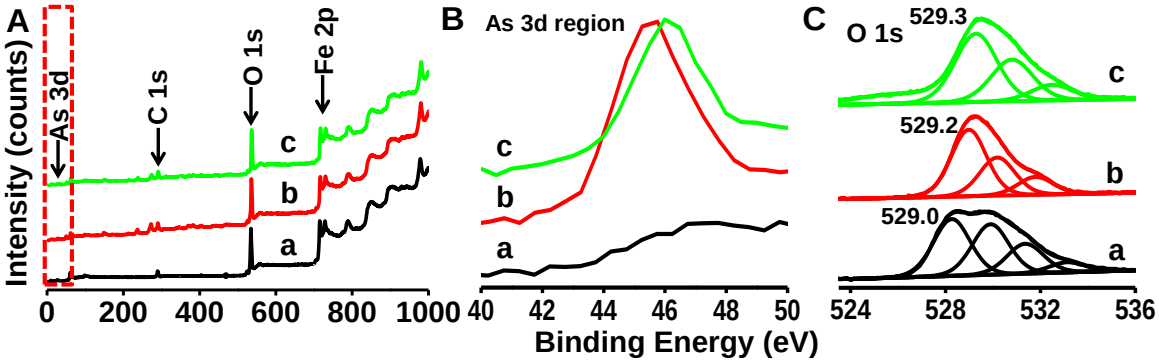

Figure S10. (A) X-ray photoelectron spectrum (XPS) analysis of CM2LF and (B) is the As 3d expanded region of the same plot (a) before As adsorption (b) after As(III) adsorption and (c) after As(V) adsorption. (C) Deconvoluted XPS spectrum of O 1s of CM2LF (a) before As adsorption (b) after As(III) adsorption and (c) after As(V) adsorption.

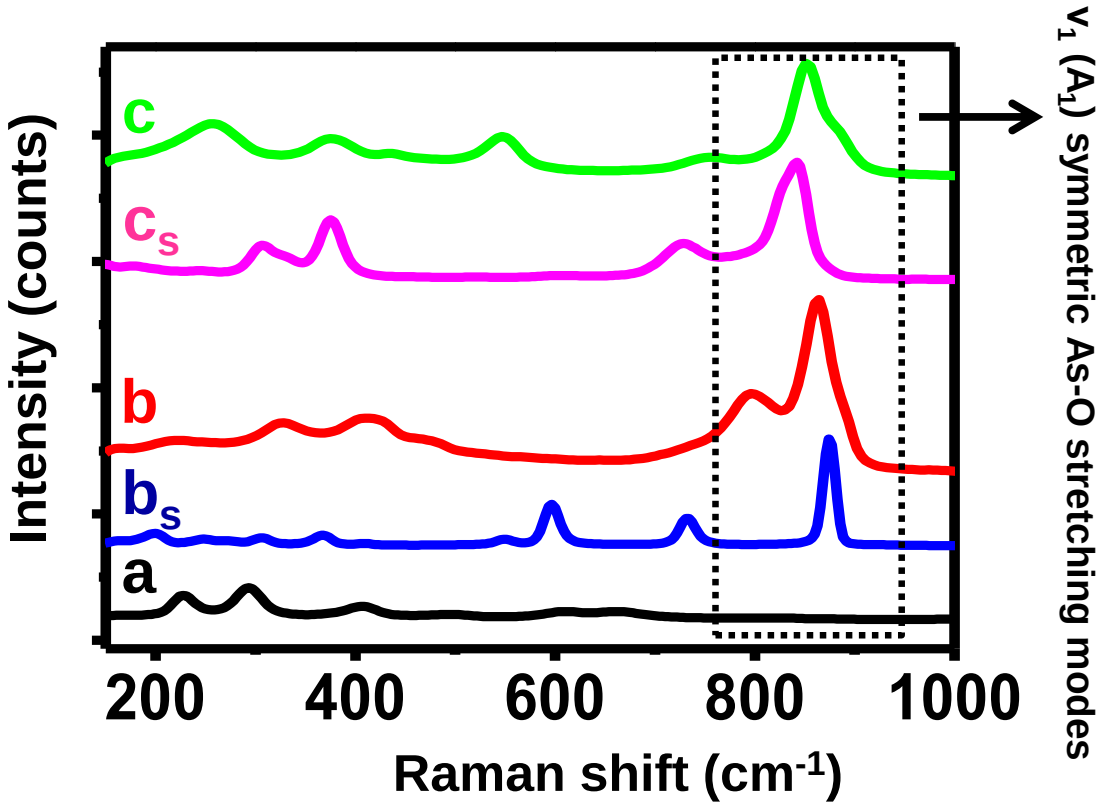

Figure S11. Raman spectrum of (A) CM2LF, (b_s) standard As(III) in solid state, (b) As(III) after treated with CM2LF, (c_s) standard As(V) in solid state and (c) A(V) after treated with CM2LF.

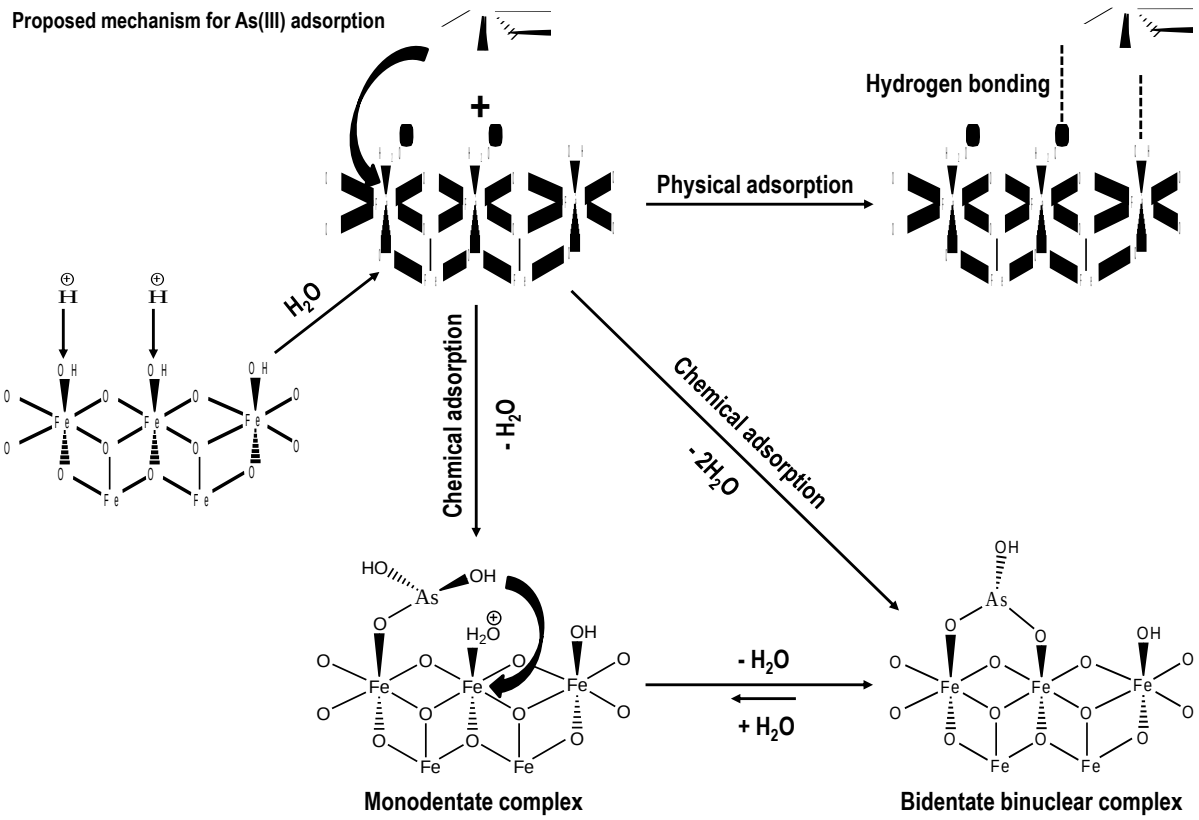

Figure S12. Adsorption mechanism of As(III) on CM2LF.

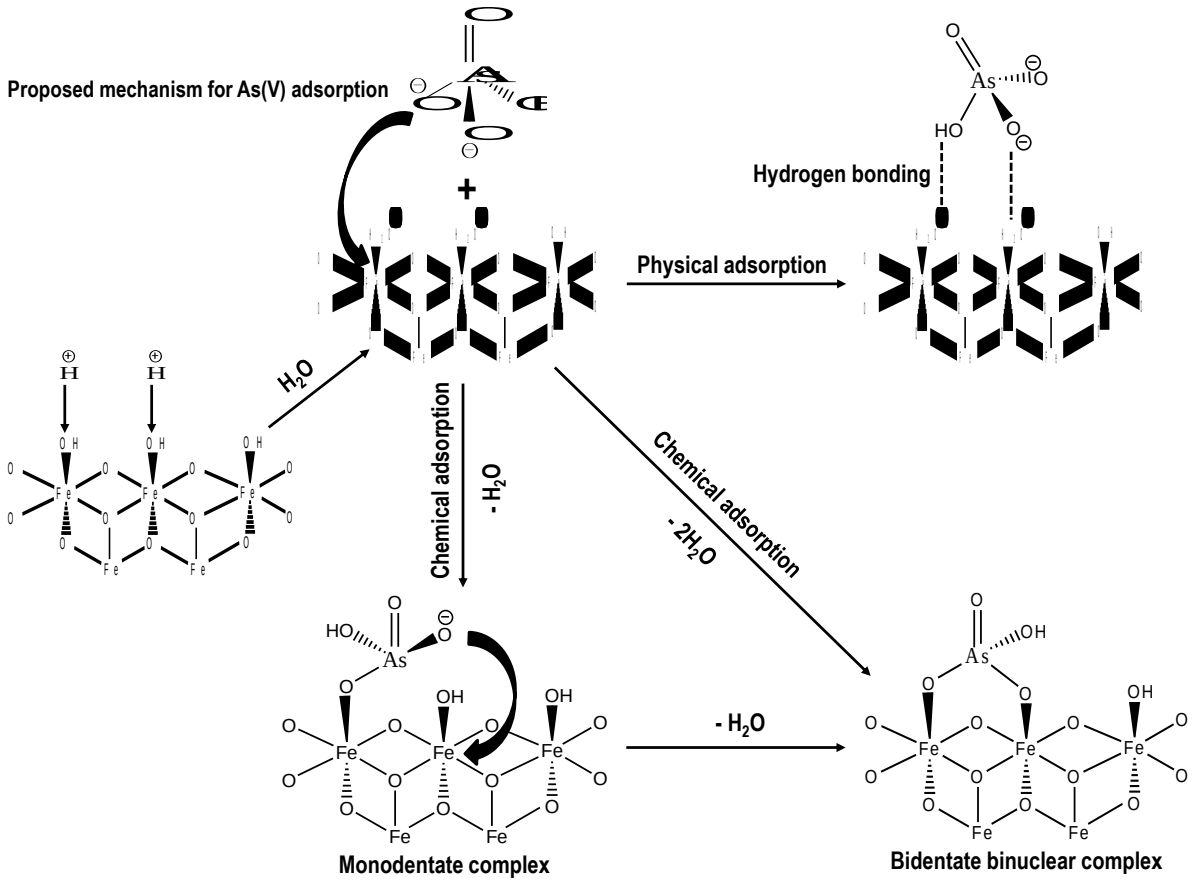

Figure S13. Adsorption mechanism of As(V) on CM2LF.

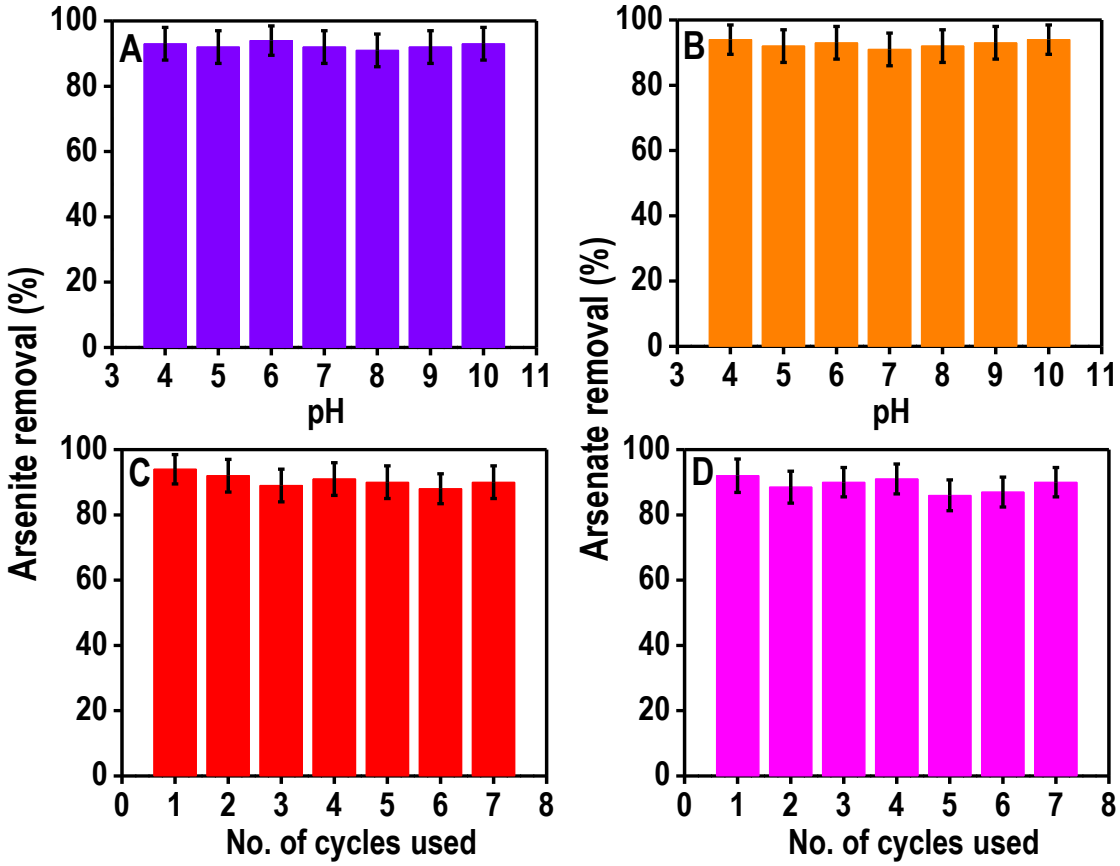

Figure S14. Adsorption efficiency of CM2LF for (A) As(III) and (B) As(V) as a function of pH. The re-use performance of the CM2LF composite upon activation for (C) As(III) and (D) As(V) removal (batch study) as a function of no. of cylces. An input arsenic concentration of 1.1 mg L^{-1} was used for both the species. Volume taken as 100 mL of ground water for 25 mg of the composite and the incubation time was 90 min.

.

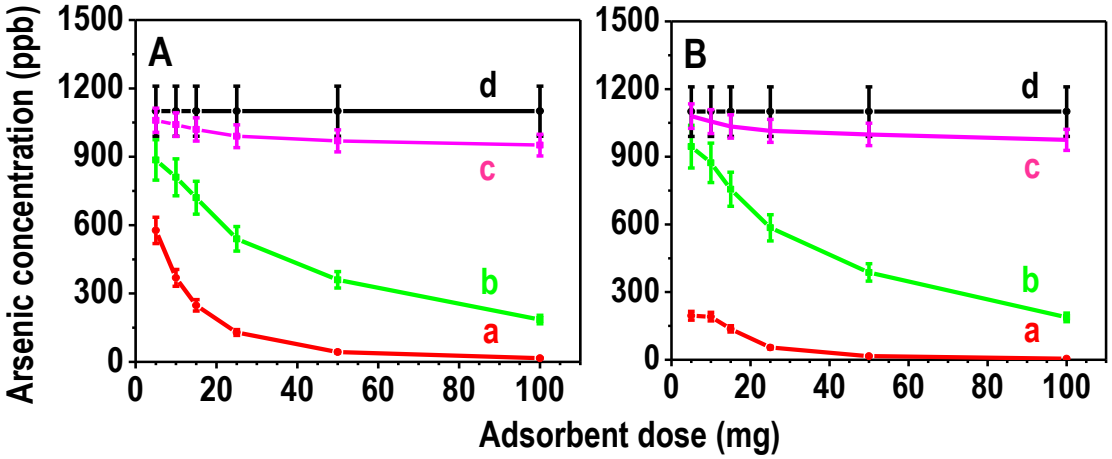

Figure S15. Performance data (batch study) of arsenic removal capacity of CM2LF compared with pure ferrihydrite and chiotsan. Residual (A) arsenite and (B) arsenate concentrations as a function of (a) CM2LF dosage, in comparison to (b) pure ferrihydrite and (c) chitosan, with an input arsenic concentration of 1.1 mg L^{-1}, which is shown as (d). Volume taken was 100 mL of ground water, for different doses, varying from 5-100 mg of the materials and the incubation time was 90 min.

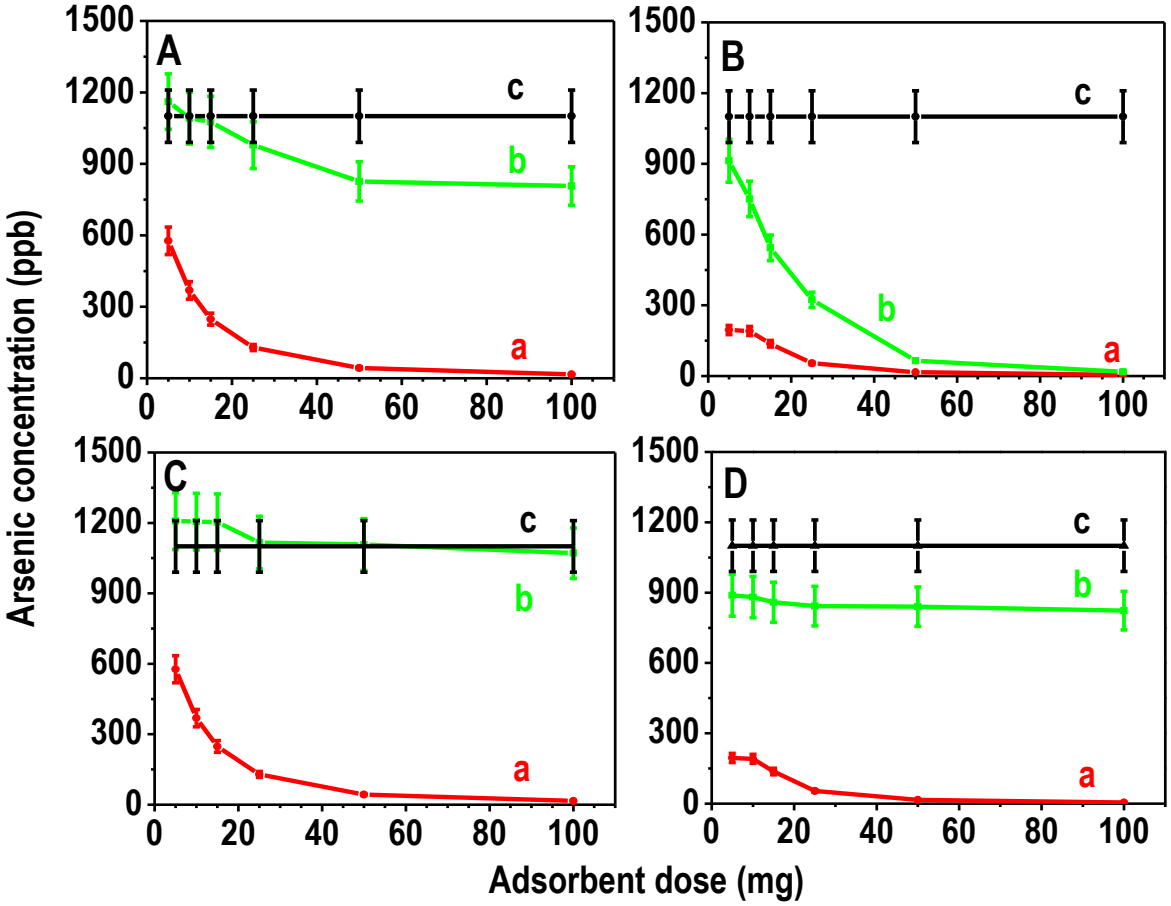

Figure S16. Performance data (batch study) of arsenic removal capacity of CM2LF compared with activated alumina and activated carbon. (A and B) Residual arsenite (A) and arsenate (B) concentrations as a function of (a) CM2LF dosage in comparison to (b) activated alumina with an (c) input arsenic concentration of 1.1 mg L^{-1}. (C and D) Residual arsenite (C) and arsenate (D) concentrations as a function of (a) CM2LF dosage in comparison to (b) activated carbon with an (c) input arsenic concentration of 1.1 mg L^{-1}. Volume taken was 100 mL ground water and the incubation time was 90 min.

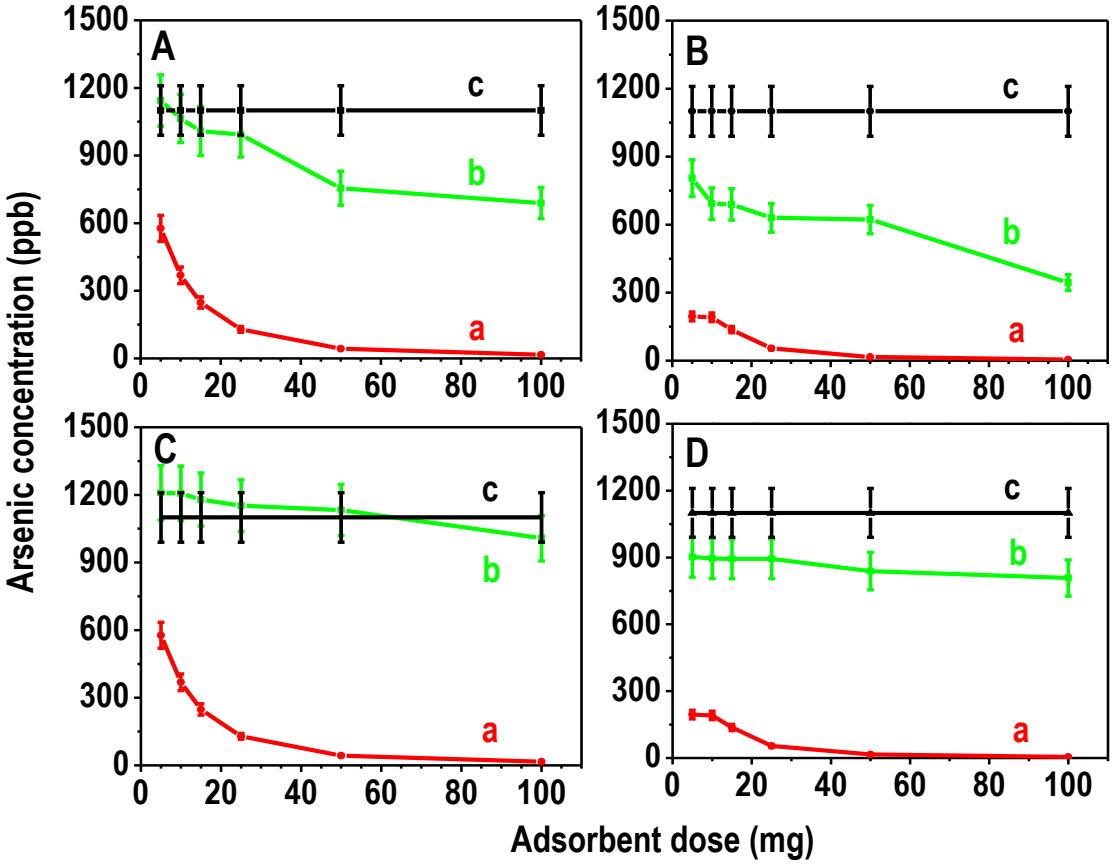

Figure S17. Performance data (batch study) of CM2LF in comparison to iron oxide (Fe_2O_3) and silicon dioxide (SiO_2) with respect to arsenic removal. (A and B) Residual arsenite (A) and arsenate (B) concentrations as a function of (a) CM2LF dosage in comparison to (b) iron oxide dosage with an (c) input arsenic concentration of 1.1 mg L^{-1}. (C and D) Residual arsenite (C) and arsenate (D) concentrations as a function of (a) CM2LF dosage in comparison to (b) silicon dioxide dosage with an (c) input arsenic concentration of 1.1 mg L^{-1}. Volume taken was 100 mL ground water and incubation time was 90 min.

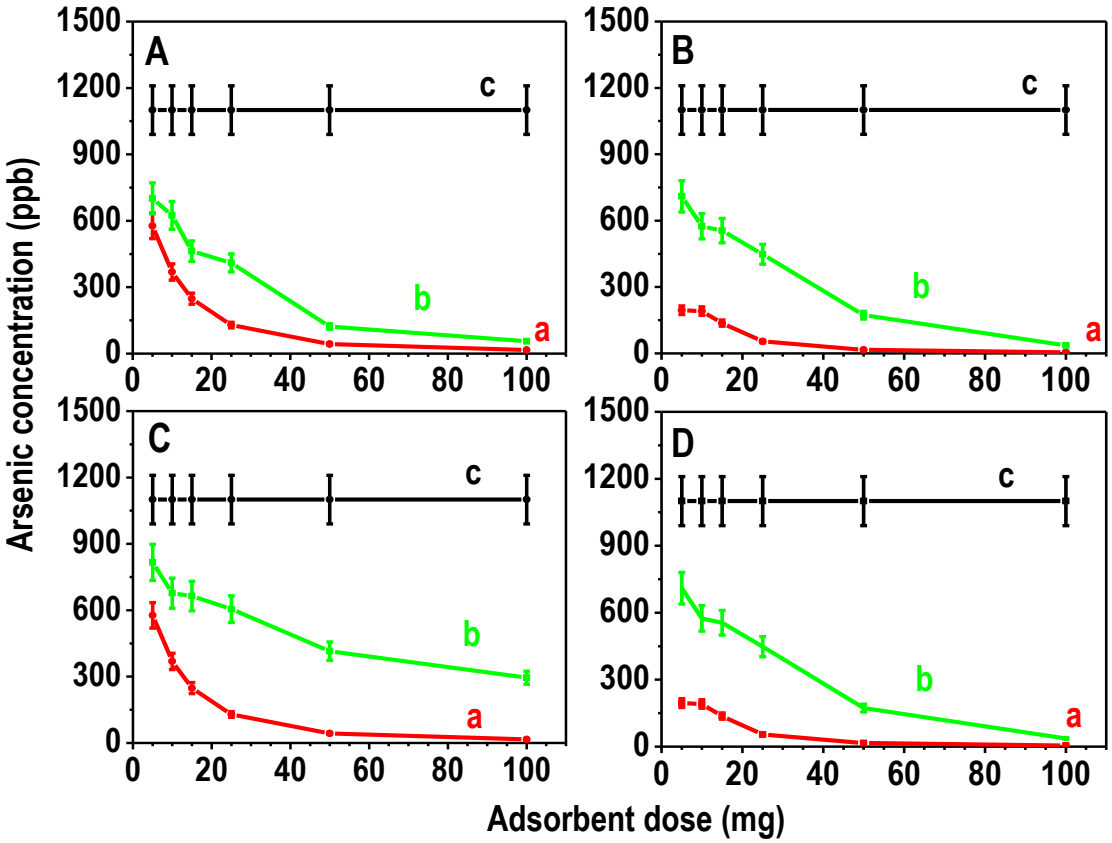

Figure S18. Performance data (batch study) of CM2LF in comparison to granular ferric hydroxide (GFH) and organic templated boehmite nanostructure (OTBN) with respect to arsenic removal. (A and B) Residual arsenite (A) and arsenate (B) concentrations as a function of (a) CM2LF dosage in comparison to (b) GFH dosage with an (c) input arsenic concentration of 1.1 mg L^{-1}. (C and D) Residual arsenite (C) and arsenate (D) concentrations as a function of (a) CM2LF dosage in comparison to (b) OTBN dosage, respectively with an (c) input arsenic concentration of 1.1 mg L^{-1}. Volume taken was 100 mL ground water and incubation time was 90 min.

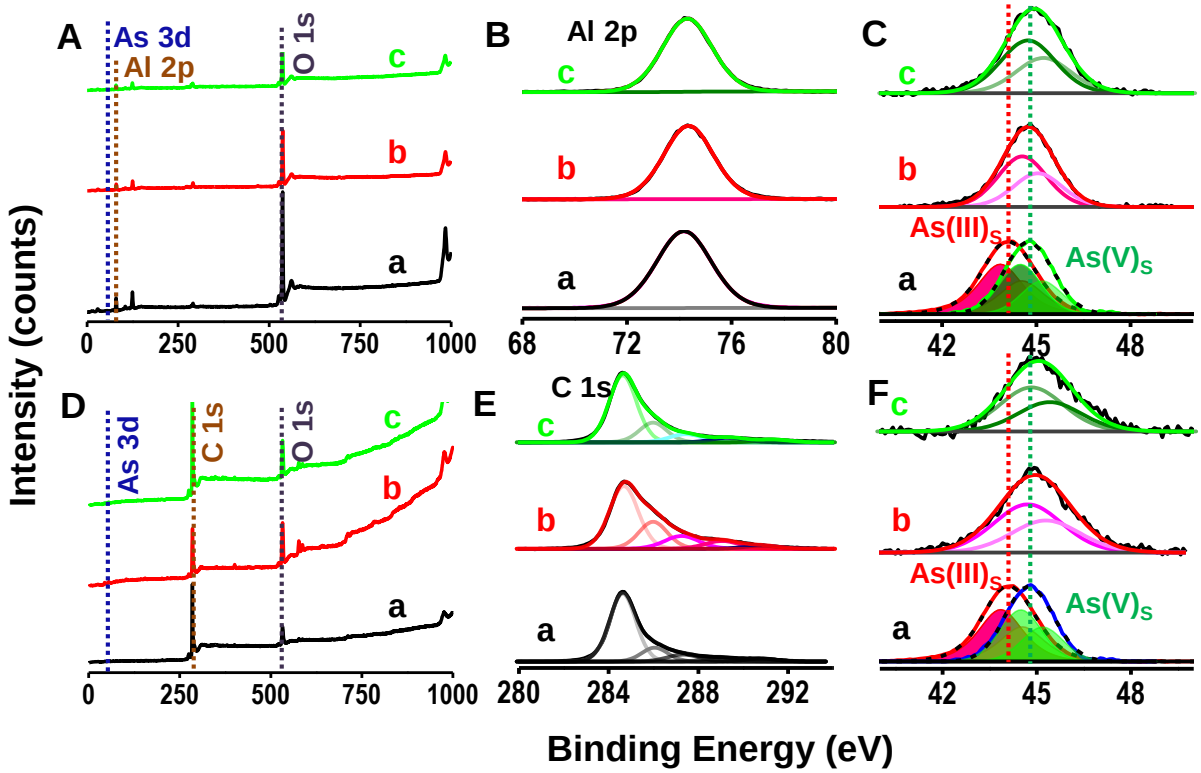

Figure S19. XPS data of activated alumina and activated carbon upon arsenic adsorption. (A) Survey spectrum, (B) Aluminium 2p (Al 2p) region and (C) Arsenic 3d (As 3d) region of activated alumina (a) before As adsorption, (b) after As(III) adsorption and (c) after As(V) adsorption, independently compared with (b_s) standard As(III) and (c_s) standard As(V), respectively. (D) Survey spectrum, (E) Carbon 1s (C 1s) region and (F) Arsenic 3d (As 3d) region of activated carbon (a) before As adsorption, (b) after As(III) adsorption and (c) after As(V) adsorption, independently compared with (b_s) standard As(III) and (c_s) standard As(V), respectively.

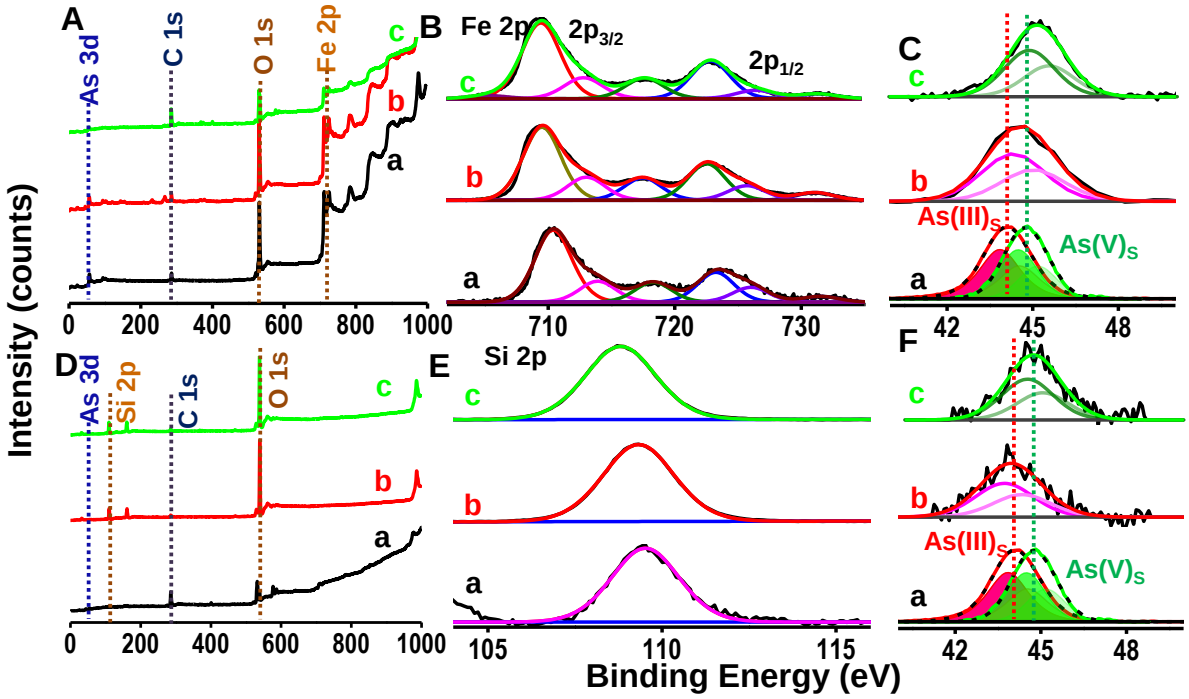

Figure S20. XPS data of iron oxide and silicon dioxide upon arsenic adsorption. (A) Survey spectrum, (B) Iron 2p (Fe 2p) region and (C) Arsenic 3d (As 3d) region of iron oxide (a) before As adsorption, (b) after As(III) adsorption and (c) after As(V) adsorption, independently compared with (b_s) standard As(III) and (c_s) standard As(V), respectively. (D) Survey spectrum, (E) Silicon 2p (Si 2p) region and (F) Arsenic 3d (As 3d) region of silicon dioxide (a) before As adsorption, (b) after As(III) adsorption and (c) after As(V) adsorption, independently compared with (b_s) standard As(III) and (c_s) standard As(V), respectively.

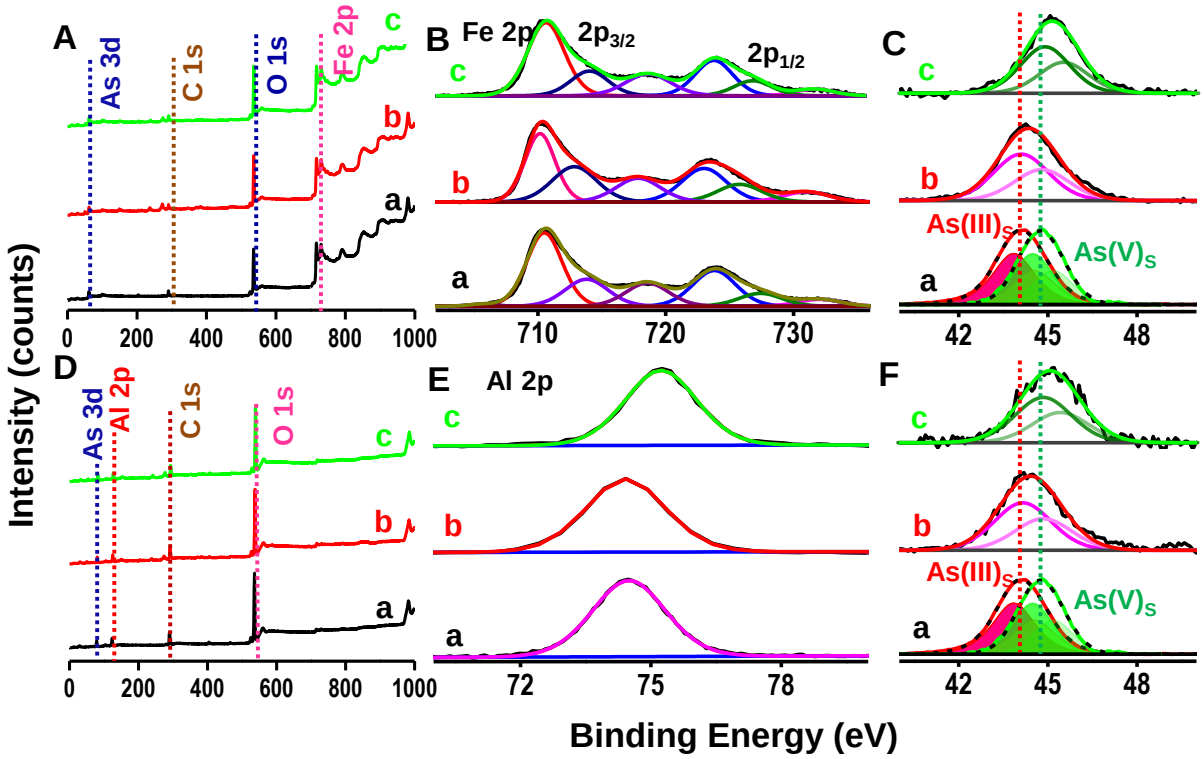

Figure S21. XPS data of GFH and OTBN upon arsenic adsorption. (A) Survey spectrum, (B) Iron 2p (Fe 2p) region and (C) Arsenic 3d (As 3d) region of GFH (a) before As adsorption, (b) after As(III) adsorption and (c) after As(V) adsorption, independently compared with (b_s) standard As(III) and (c_s) standard As(V), respectively. (D) Survey spectrum, (E) Aluminium 2p (Al 2p) region and (F) Arsenic 3d (As 3d) region of OTBN (a) before As adsorption, (b) after As(III) adsorption and (c) after As(V) adsorption, independently compared with (b_s) standard As(III) and (c_s) standard As(V), respectively.

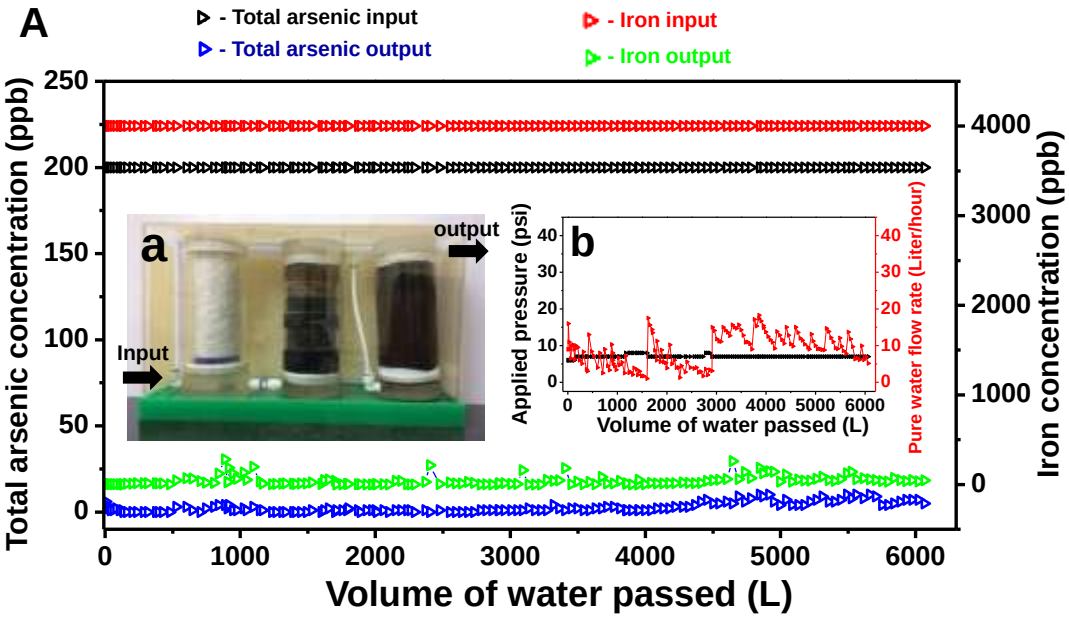

Figure S22. (A) Performance data for the removal of arsenic and iron. Inset (a) shows the proof of concept prototype of Inline domestic unit for removal of arsenic (As(III) + As(V)) and iron (Fe(II) + Fe (III)) contamination from water using three stage filtration, having first cartridge with 0.5 µm polypropylene yarn-wound candle filter for removal of micro-particulates, second cartridge with iron removal media and third cartridge with 900 g arsenic adsorbent. Inset (b) shows pure water flow rate from the unit at corresponding applied pressure. Slight variation in flow rate is due to the change in head pressure in week long experiments.

Table S1.

Arsenic uptake capacity of CM2LF under various ionic strengths with an input arsenic concentration of 1.1 mg L^{-1}, respectively for both As(III) and As(V). 100 mL arsenic contaminated ground water was taken for 25 mg of the composite and the incubation time was 90 min.

Type of ion	Concentration of ion used	Input As(III)	Uptake As(III)	Input As(V)	Uptake As(V)
Fluoride	0.6 ppm	1.1 ppm	1.09 ppm	1.1 ppm	1.09 ppm
Chloride	87 ppm	1.1 ppm	1.09 ppm	1.1 ppm	1.08 ppm
Nitrate	1.9 ppm	1.1 ppm	1.09 ppm	1.1 ppm	1.10 ppm
Sulphate	33 ppm	1.1 ppm	1.09 ppm	1.1 ppm	1.09 ppm
Silicate	16 ppm	1.1 ppm	1.09 ppm	1.1 ppm	1.09 ppm
Sodium	54 ppm	1.1 ppm	1.08 ppm	1.1 ppm	1.10 ppm
Potassium	2.5 ppm	1.1 ppm	1.09 ppm	1.1 ppm	1.10 ppm
Magnesium	15 ppm	1.1 ppm	1.09 ppm	1.1 ppm	1.09 ppm
Calcium	29 ppm	1.1 ppm	1.09 ppm	1.1 ppm	1.09 ppm
Carbonate	100 ppm	1.1 ppm	1.09 ppm	1.1 ppm	1.09 ppm
Bicarbonate	100 ppm	1.1 ppm	1.09 ppm	1.1 ppm	1.09 ppm

Table S2.

ToC leaching from various components used in making the CM2LF composite in comparison to the CM2LF before and after arsenic saturation. Volume taken was 100 mL Milli-Q water for 100 mg of the composite and the incubation time was 90 min. Milli-Q water was taken for the experiments for the composite, as the tap water routinely shows a ToC of 8.60 ppm.

Sample analysed	ToC
Blank water	0.17 ppm
Blank Chitosan	3.39 ppm
Chitosan @ pH 9	0.57 ppm
CM2LF without Arsenic	0.65 ppm
Saturated CM2LF with As(III)	0.69 ppm
Saturated CM2LF with As(V)	0.76 ppm

Table S3.

Physicochemical characteristics of influent natural water.

(Note: All parameters are expressed in mg L^{-1}, except for pH and conductivity)

Parameters	Value
Total coliforms (CFU/mL)	1-2 x 10^3
pH @ 25°C	7.8
Conductivity (µS/cm)	640.0
Fluoride	0.57
Chloride	86.34
Nitrate	1.84
Sulphate	32.41
Silicate	15.87
Lithium	ND
Sodium	53.74
Ammonium	ND
Potassium	2.33
Magnesium	14.34
Calcium	28.72

ND - not detected

Natural drinking water (without treatment so that there is a residual bacterial count in it) was used for testing to ensure that the material functions in the field.

Biopolymer-reinforced synthetic granular nanocomposites for affordable point-of-use water purification

Mohan Udhaya Sankar[1], Sahaja Aigal[1], Shihabudheen M. Maliyekkal[1], Amrita Chaudhary, Anshup, Avula Anil Kumar, Kamalesh Chaudhari, and Thalappil Pradeep[2]

Unit of Nanoscience and Thematic Unit of Excellence, Department of Chemistry, Indian Institute of Technology Madras, Chennai 600 036, India

Edited by Eric Hoek, University of California, Los Angeles, CA and accepted by the Editorial Board April 4, 2013 (received for review November 21, 2012)

Creation of affordable materials for constant release of silver ions in water is one of the most promising ways to provide microbially safe drinking water for all. Combining the capacity of diverse nanocomposites to scavenge toxic species such as arsenic, lead, and other contaminants along with the above capability can result in affordable, all-inclusive drinking water purifiers that can function without electricity. The critical problem in achieving this is the synthesis of stable materials that can release silver ions continuously in the presence of complex species usually present in drinking water that deposit and cause scaling on nanomaterial surfaces. Here we show that such constant release materials can be synthesized in a simple and effective fashion in water itself without the use of electrical power. The nanocomposite exhibits river sand-like properties, such as higher shear strength in loose and wet forms. These materials have been used to develop an affordable water purifier to deliver clean drinking water at US $2.5/y per family. The ability to prepare nanostructured compositions at near ambient temperature has wide relevance for adsorption-based water purification.

hybrid | green | appropriate technology | frugal science | developing world

Safe drinking water is a significant, but simple indicator of development. Its availability at point of use can save over 2 million human lives (1) (of the 3.575 million deaths caused by water, sanitation, and hygiene issues, 42.6% are due to diarrhea alone: 3.575 million × 0.426 = 1.523 million lives), can avoid over 2 billion diarrheal infections (2), and can contribute over $4 billion to the global gross domestic product (3) (formula used: Σ (number of deaths attributed to diarrhea in each country × corresponding country's per capita gross domestic product). Considering the challenges associated with traditional disinfectants (4), solutions based on state-of-the-art science and technology hold the key for safe drinking water (5) and novel approaches are being looked at (6, 7). It has been long known that silver, especially in nanoparticle form, is an effective disinfectant and works for a wide spectrum of bacteria and viruses (8, 9). Numerous approaches are available for the synthesis of biocidal silver nanoparticles or colloids, including the use of matrices (10–12). The biocidal property of silver nanoparticles, usually in the size range of 10–20 nm, is attributed to the release of trace quantities of silver ions in water (13–16), which, although being sufficient for microorganism killing, does not exhibit toxicity to humans (17, 18). [Toxicity due to silver nanoparticles themselves is also known (16)]. Although a number of silver-based biocidal compositions have been synthesized, those have not been able to reach the masses in large volumes (e.g., silver nanoparticle-loaded ceramic candles) (19). Massive deployment has been hampered due to the following reasons: (*a*) Drinking water contains many species (e.g., inorganic ions and organics) that anchor on the surface of the nanoparticles, making sustained silver ion release difficult (15); (*b*) suitable anchoring substrates that limit the scaling of nanoparticle surfaces while simultaneously preventing their release into water are not available; and (*c*) continued retention of the nanoparticles in the matrix is difficult.

In this work, we demonstrate a unique family of nanocrystalline metal oxyhydroxide-chitosan granular composite materials prepared at near room temperature through an aqueous route. The origin of crystallinity in the composition is attributed to abundant -O- and -OH functional groups on chitosan, which help in the crystallization of metal oxyhydroxide and also ensure strong covalent binding of the nanoparticle surface to the matrix. X-ray photoelectron spectroscopy (XPS) confirms that the composition is rich with surface hydroxyl groups. Using hyperspectral imaging, the absence of nanoparticle leaching in the water was confirmed. Further, a unique scheme to reactivate the silver nanoparticle surface is used for continual antimicrobial activity in drinking waters. Several other composites have been developed that can scavenge other contaminants in water. We demonstrate an affordable water purification device based on such composites developed over several years and undergoing field trials in India, as a potential solution for widespread eradication of the waterborne disease burden.

Results and Discussion

The antimicrobial composition consists of an aluminum oxyhydroxide–chitosan composite (referred to as BM) with silver particles of 10–20 nm diameter embedded in it (Fig. 1*A* and *SI Appendix*, Fig. S1) and is capable of sustained release of silver ions [40 ± 10 parts per billion (ppb)] in natural drinking water over an extended volume of water passing through it, to achieve effective removal of microorganisms (*SI Appendix*, Fig. S2; see Fig. 3*C*). The antimicrobial composite (referred to as Ag-BM) is unique as it is made in water at near room temperature, using a biopolymer, and dried in ambient conditions to obtain water-insoluble granules, yielding Na_2SO_4 as the major by-product (>90%), thereby making it a green synthesis. The concentration of silver ion leached into drinking water from the prepared composite at relevant temperatures (5–35 °C) (*SI Appendix*, Fig. S3) is significantly less than the maximum permissible limit of 100 ppb (secondary standard, US Environmental Protection Agency), thereby requiring no secondary filtration to remove excess silver ions. This controlled release at temperatures of relevance to drinking-water applications over extended periods is an important advantage of the composite. X-ray diffraction patterns of BM and Ag-BM show the presence of

ENGINEERING

Author contributions: M.U.S., A.C., A., and T.P. designed research; M.U.S., S.A., S.M.M., A.C., A., A.A.K., and K.C. performed research; M.U.S., S.A., A., and T.P. analyzed data; and M.U.S., S.A., A.C., A., and T.P. wrote the paper.

The authors declare no conflict of interest.

This article is a PNAS Direct Submission. E.H. is a guest editor invited by the Editorial Board.

[1]M.U.S., S.A., and S.M.M. contributed equally to this work.

[2]To whom correspondence should be addressed. E-mail: pradeep@iitm.ac.in.

This article contains supporting information online at www.pnas.org/lookup/suppl/doi:10.1073/pnas.1220222110/-/DCSupplemental.

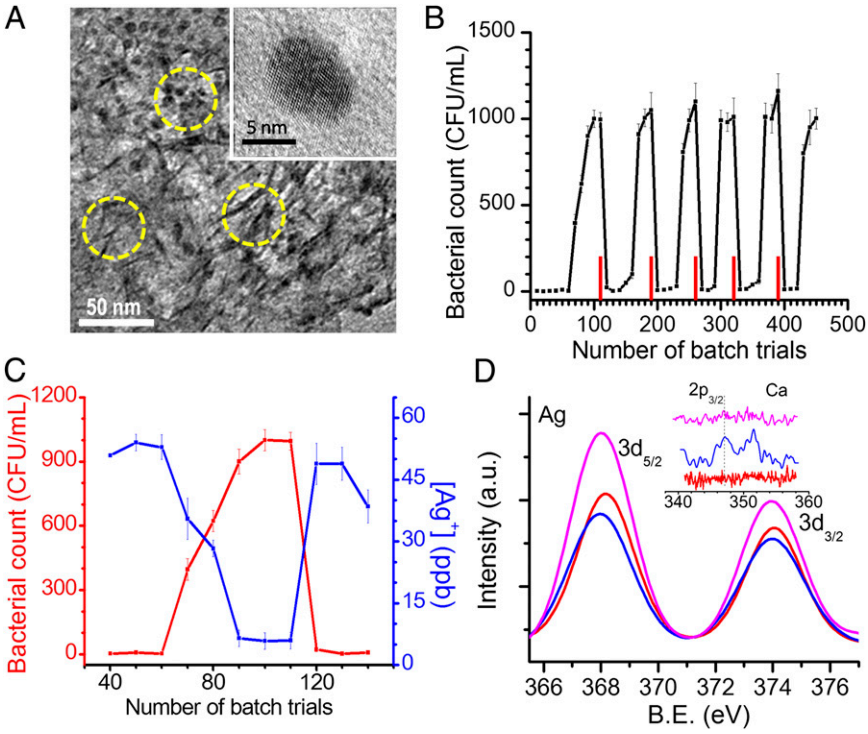

Fig. 1. Characterization of composite and exhibits of its unique antimicrobial activity. (*A*) Transmission electron micrograph of Ag-BM. The composite matrix appears as nanosheets of 3- to 4-nm thickness and the embedded nanoparticles are seen as dots. Some sheets and particles are indicated by circles. The matrix made of the boehmite–chitosan acts like a cage in which the nanoparticles are trapped. The particle sizes are much smaller than those of a typical aqueous phase synthesis. *Inset* shows an expanded view of one particle. (*B*) Bacterial load measured in water as a function of batch upon spiking 10^5 CFU/mL of *E. coli*. Red bars indicate the point of reactivation. (*C*) Silver ion concentration measured by ICP-MS (blue trace) and corresponding bacterial count in CFU/mL for one of the cycles (number of trials: 40th–140th) (red trace) from batch measurements. (*D*) X-ray photoemission spectra of initial (red trace), saturated (blue trace), and reactivated (pink trace) composites in the Ag 3d region and the Ca 2p region (*Inset*). The intensity of Ca 2p (*Inset*) is weak as the coating is thin. The reactivated composite shows an increased Ag 3d intensity due to removal of scale-forming species and better exposure of the nanoparticle surface.

nanocrystalline AlOOH of mean crystallite size of 3.5 nm calculated from the Scherrer formula (*SI Appendix*, Fig. S4).

High-resolution electron micrographs show that the silver nanoparticles are trapped within the AlOOH–chitosan cages, which allow them to be preserved with reduced contact with scale-forming chemical species, yet allowing sufficient interaction with water, due to which sustained release of Ag^+ is possible (Fig. 1*A* and *SI Appendix*, Figs. S1 and S5). The inorganic cages formed by AlOOH are seen as dark lines of 3–4 nm thickness in the transmission electron microscopy (TEM) image and are held together by the chitosan matrix (see below for a discussion of the materials). The nanoparticles are small enough to release Ag^+ and are single crystalline (Fig. 1*A*, *Inset*). This uniformity and reduced particle size are difficult to achieve for silver in a fast, aqueous-phase synthesis.

The composite was tested for antibacterial activity in batch mode (*Materials and Methods*) for more than 400 trials continuously and it exhibited a cyclic pattern of antibacterial action in natural drinking water (Fig. 1*B*). A typical cycle (number of trials: 10th–140th) represents antibacterial performance of Ag-BM at its peak, followed by a drop in performance due to a gradual decrease in Ag^+ release, resulting in an increase in bacterial count in the output water, and finally after reactivation (regaining the ability to leach silver ions) an immediate recovery of performance where Ag^+ release is back to normal (40 ± 10 ppb, Fig. 1*C*).

The concept of reactivation is an important reason behind Ag-BM's long-lasting antimicrobial performance. As seen in Fig. 1*B*, the performance of Ag-BM drops after a certain number of trials (60 trials) due to its continuous exposure to scalants present in water, even though the silver content within the BM matrix is still significant. This drop in performance is explained by studying the XPS of the spent Ag-BM, where the Ag $3d_{5/2}$ peak is at a reduced intensity in comparison with the initial composite (Fig. 1*D*). Factors such as deposition of sparingly soluble species, principally in the form of $CaCO_3$ and silicate precursors, are responsible for the partial filling of the composite with a thin layer of scalants, reducing silver release. The existence of Ca 2p and Si 2p peaks in the XPS spectra of spent Ag-BM proves this (Fig. 1*D*, *Inset* and *SI Appendix*, Fig. S6). SEM-EDAX elemental imaging and spectra also support the presence of deposits containing Ca and Si (*SI Appendix*, Fig. S7). Surface imaging by atomic force microscopy (AFM) shows increased inhomogeneity in the saturated Ag-BM (*SI Appendix*, Fig. S8). The proof of scaling is further substantiated by trials done in natural drinking water and ultrapure water (resistivity: 18 MΩ.cm). In natural drinking water, Ag-BM is subjected to deposition of sparingly soluble species, which limits its efficacy after a period; whereas, due to the nonexistence of these species in ultrapure water, the life of the composite is prolonged and is almost indefinite (*SI Appendix*, Fig. S9). Additionally, the antibacterial efficacy of Ag-BM was tested under prevalent water quality parameters of total dissolved solids (TDS), pH, and total organic carbon (TOC) and performance of the composite was acceptable (*SI Appendix*, Fig. S10). Of the several methods tested, the simplest, most effective, and field implementable one for regaining Ag^+ release is incubating the inactive Ag-BM in water [deionized water or natural drinking water (*SI Appendix*, Fig. S11)] at 70–100 °C for 3–4 h. In a batch experiment, when a finite bacterial colony count (10–50 CFU/mL) was observed in the output, the trials were continued a few more times to ensure the drop in performance and thereafter, the composite was reactivated. The number of trials that can be done after every reactivation slowly reduces with increasing trials. Acid-digested initial Ag-BM showed 0.432% silver by weight, and after 450 trials, it reduced to 0.306%, which corresponds to 71% of Ag still left in the BM matrix. Theoretically, leaching of 29% silver amounts to an average concentration of 50 ppb over 500 batch trials, using 2 g composite. The tests were stopped after 450 trials and Ag-BM was not reactivated further, although the same method may be continued. Innovative reactivation methods may also be used, not limited to the heat treatment method alone (*SI Appendix*, Fig. S12). By using diluted lemon juice, readily available in every home, further reactivation can be done, possibly until the composite gets exhausted completely, i.e., when requisite silver ions cannot be released from the matrix any further.

The composite was tested for antiviral activity in batch mode (*Materials and Methods*) for more than 200 trials continuously in

natural drinking water. The antiviral performance is similar to the antibacterial performance. When the performance deteriorates, the activity is regained after reactivation (*SI Appendix*, Fig. S13).

When a nanocomposite-based approach is used for drinking-water purification, the possibility of nanoparticle release in drinking water exists. To confirm the effective trapping of nanoparticles in the matrix and absence of any observable nanoparticle release in water, dark-field microscopy was done on the bacteria. Microscopic images (Fig. 2 and *SI Appendix*, Figs. S14 and S15) show that although nanoparticles are seen within the bacterial contour of citrate-protected Ag nanoparticle-treated bacterial cells, no nanoparticle is seen in bacterial cells treated with Ag-BM. However, lysis is observed in both cases as observed in the discontinuity of the cell membrane (Fig. 2 *B* and *C* and 2 *D* and *E*, *Insets*). The hyperspectral images of bacterial cells treated with citrate-protected Ag nanoparticles show distinct size-dependent surface plasmon features of the nanoparticles (Fig. 2*D*) that are absent in the case of Ag-BM–treated bacterial cells (Fig. 2*E*). The data conclusively established that silver ions released from Ag-BM are responsible for the antibacterial activity and there is no observable nanoparticle release in water. It is also confirmed that during the interaction of water with the composition, AlOOH–chitosan does not undergo dissolution; aluminum release in water is less than 6 ppb (aluminum secondary standard: 50–200 ppb, US Environmental Protection Agency) and total organic carbon is nearly 0.1 ppm (*SI Appendix*, Fig. S16). Independent spectroscopic measurements of Ag-BM–treated water samples and the cyclic nature of antibacterial performance also support this. The antibacterial activity of Ag-BM was also shown by fluorescence microscopy study of treated bacteria where a mixture of nucleic acid-binding fluorescent dyes [green fluorescent SYTO9 dye and red fluorescent propidium iodide (PI) dye] were used (*SI Appendix*, Fig. S17).

A water purification device (Fig. 3 *A* and *B*) containing 50 g of Ag-BM in cartridge form was assessed for performance under standard test conditions. This filter ran up to 1,500 L with a bacterial input load of 10^5 CFU/mL without the need for reactivation (Fig. 3*C* and *SI Appendix*, Fig. S2). Therefore, by using 120 g composite, safe drinking water can be provided for a family of five for 1 y (assuming daily drinking water consumption of 10 L). This translates to an annual expense of $2 per family. (Cost of media, sediment prefilter, plastic assembly, and cartridge packing are included in the cost calculation.) By reactivating this composite, the life of the cartridge can be enhanced further, thereby reducing the cost. The water purification device has a second-stage axial filtration based on an activated carbon block (Fig. 3*A*) with a nominal pore size of <4 μm, which enables it to remove cysts through physical filtration, and the cyst removal capacity is higher than 5 log (input count, 10^6 particles per liter; output count, <3 particles per liter), in accord with the National Science Foundation (NSF) protocol P231 (*SI Appendix*, Fig. S18). The carbon block has an additional function of removing any organic and bacterial biomass as well, besides removing traces of silver ions or silver bound with microbial debris. However, residual silver ion content may be advantageous in some cases to prevent microbial contamination in water upon storage as well as to prevent bio-fouling of the composite during periods of nonuse.

Considering the fact that some parts of the world have severe chemical contamination in ground water (20), causing life-threatening diseases, suitable unique composites may be packed into the carbon filter to remove harmful chemical contaminants such as arsenic, pesticides, mercury, lead, iron, etc., so that chemically and microbiologically pure water is obtained, depending on the region of use. Composite preparation at room temperature is crucial for addressing health-related contaminants as the method preserves active adsorption sites (for example, surface hydroxyl groups undergo dehydration on exposure to higher temperature).

For example, to remove iron, 100 g iron oxyhydroxide–chitosan composite (*Materials and Methods*) was taken. Feed water containing freshly prepared 5 ± 1 ppm of Fe^{2+} was passed through the composite at a flow rate of 50 mL/min. The output water was tested for both Fe^{3+} and Fe^{2+} by spectrophotometric methods. The column was run for 1,500 L and the output concentration was consistently below 0.3 ppm, thereby adhering to the World Health

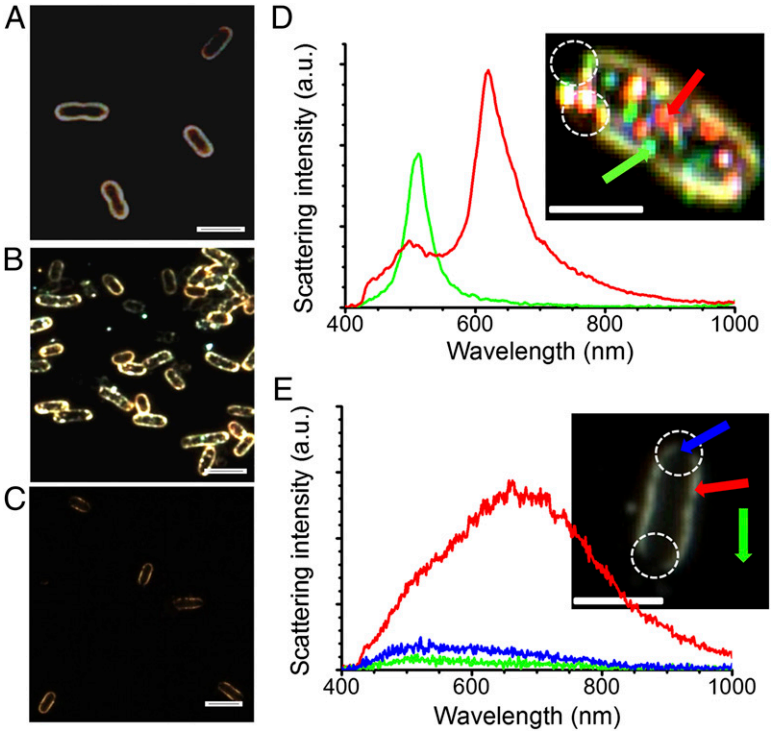

Fig. 2. Microscopic examination of bacterial lysis through dark-field and hyperspectral imaging. (*A*–*C*) Dark-field microscopy images of bacteria in water, bacteria treated with citrate-protected Ag nanoparticles, and bacteria treated with Ag-BM, respectively. (*A*) Continuous bacterial contour. (*B*) Nanoparticles within and outside the bacterial contour, which are seen as bright dots. (*C*) Discontinuous bacterial contour with the absence of nanoparticles from Ag-BM. (*D*) Scattering spectra of single nanoparticles embedded in the bacterial contour. (*Inset*) Hyperspectral image from which the spectra are taken. The spectral traces and the arrows correspond to the same particles. (*E*) Scattering spectra of lysed bacterial border after treating with Ag-BM. *Inset* shows the hyperspectral image of a bacterium treated with Ag-BM. The color of the traces and the points from which spectra are collected (shown by arrows) are the same. Blue and green traces in *E* are nearly the same, indicating that the lysed regions appear like background. Lysis is shown by white circles in the images in *D* and *E*. (Scale bars in all images: 2 μm.) Scattering from nanoparticles is approximately an order of magnitude larger compared with the bacterial contour.

ENGINEERING

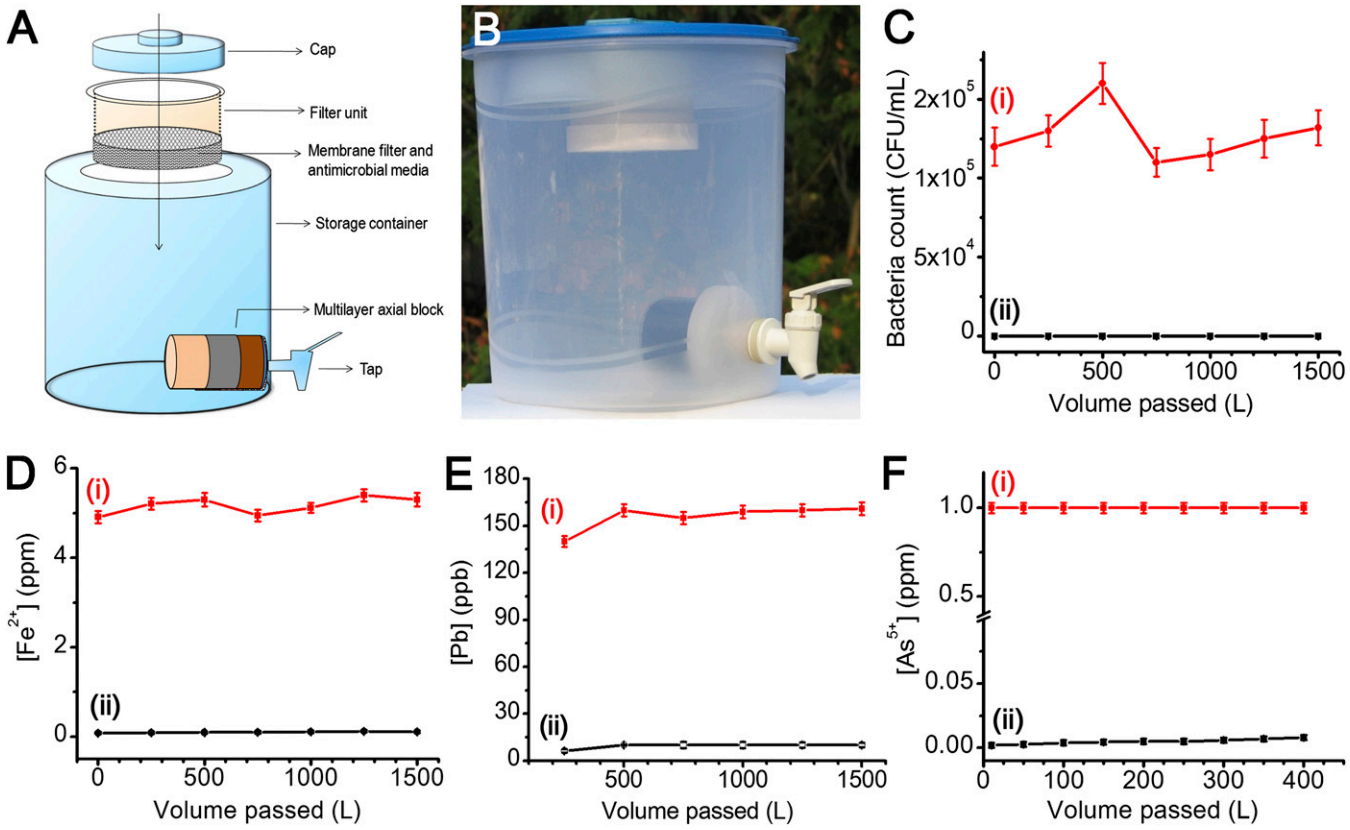

Fig. 3. Water purification device undergoing field trials in India and its performance evaluation. (*A*) Schematic diagram of the device. (*B*) Actual photograph of the device. Construction and assembly of the device are simple and can be done locally. The antimicrobial composition is used as granules and kept in the membrane filter. Carbon block is positioned just before the tap. Carbon block may also be used as a multilayer axial block, comprising adsorbents for specific regional contaminants such as arsenic, iron, and lead. (*C*–*F*) Column data for the removal of (*C*) *E. coli*, (*D*) Fe^{2+}, (*E*) Pb^{2+}, and (*F*) As^{5+}. Input (*i*) and output (*ii*) concentrations are indicated in *C*–*F*.

Organization (WHO) norms (Fig. 3*D*). Similarly, to remove lead, 50 g of nano-MnO_2–loaded BM composite was packed in a column and fed with 1,500 L of water spiked with 150 ± 10 ppb of Pb^{2+}. The total concentration of lead in the output water (Pb exists in ionized as well as hydrolyzed form at the pH of drinking water), measured by inductively coupled plasma mass spectrometry (ICP-MS), was consistently below 10 ± 1 ppb, adhering to the WHO norms (Fig. 3*E*). Additionally, arsenic mitigation from drinking water was effectively carried out using iron oxyhydroxide–chitosan composite. Twenty grams of granular composite was packed in a column and fed with 400 L of water spiked with 1 ppm of arsenic (As^{5+}) at a flow rate of 50 mL/min. Total arsenic concentration in the output water, measured by ICP-MS, was less than 10 ppb, below the permissible limit (Fig. 3*F*). Similar performance was seen with an input As^{3+} concentration of 1 ppm. Please note that the input concentrations were the maximum concentrations usually encountered in the field. The carbon block shown in Fig. 3 *A* and *B* may also be used as a multilayer axial block, comprising the above adsorbents for specific regional contaminants such as arsenic, iron, and lead.

To use the composition in a water purification cartridge, it is important that it has satisfactory wet strength to stay intact as a granular composition. Compositions that are obtained as powders offer poor hydraulic conductivity, leading to excessive pressure drop in the water purification cartridge operated with gravity pressure. To find the shear strength of the granular media, a direct shear test was conducted at different normal stresses. The maximum horizontal shear stress exhibited by the iron oxyhydroxide–chitosan composite under each normal stress is shown in *SI Appendix*, Fig. S19 *A* and *B*. These data are plotted in *SI Appendix*, Fig. S20 *A* and *B*. Straight-line approximation of the Mohr–Coulomb failure pattern gave the angle of internal friction (Φ) to be 41.76° and 44.07° for dry and wet media, respectively, showing that the prepared granular media's shear strength is equivalent to that of the Indian standard sand (~35–40°). The compressive strength of the iron oxyhydroxide–chitosan composite was found to be 25 MPa, comparable to that of concrete.

The essence of the approach to prepare the composition is described graphically in Fig. 4. Al^{3+}-complexed chitosan solution (pH 0.8) was treated with an alkali (Fig. 4 *A*, *ii*). Alkali treatment initiates aluminum ion hydrolysis (leading to the formation of aluminum hydroxide nanoparticles) followed by chitosan precipitation (random coiled water-insoluble chitosan network) (Fig. 4 *A*, *iii*). Fig. 4*B* shows photographs of aluminum hydroxide in the dispersed form at a solution pH 4–6 and settled residue of aluminum hydroxide–chitosan at pH 7 and above. Generally, Al^{3+} upon alkaline hydrolysis converts to an aluminum hydroxide gel and prolonged heating of the gel to temperatures above 80 °C leads to redissolution of aluminum hydroxide and subsequent crystallization to aluminum oxyhydroxide. Abundant -O- and -OH groups of chitosan act as nucleation centers for the formation of boehmite nanocrystals and this crystallization is promoted even at room temperature. There are crucial advantages associated with boehmite crystallization at room temperature: (*i*) Surface hydroxyl concentration stays highest whereas exposure to elevated temperature causes their destruction, thereby giving reduced adsorption capacity, and (*ii*) reduced production cost as heating can be avoided completely.

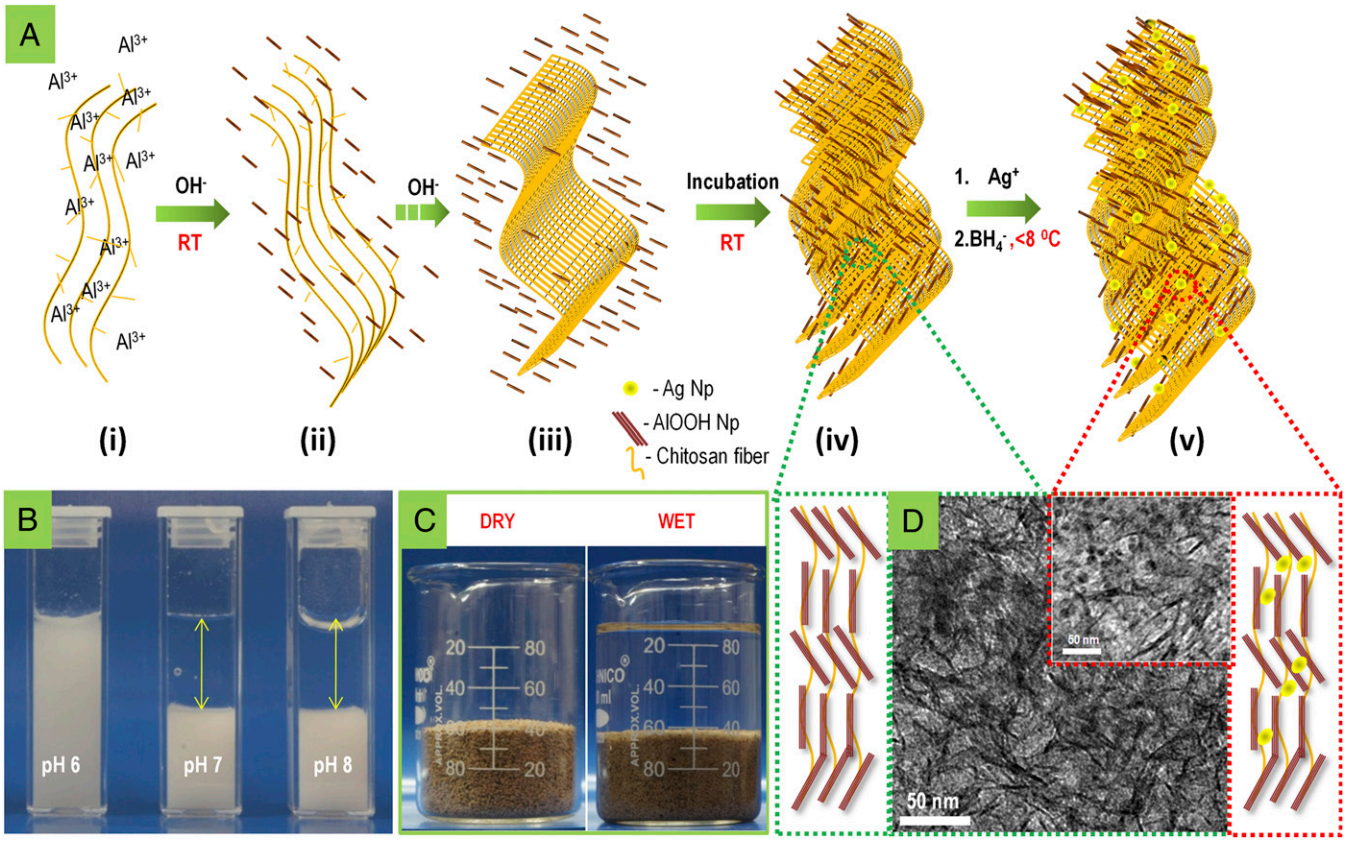

Fig. 4. Mechanism for the preparation of composite and origin of its physical strength in water due to network structure. (*A*) Mechanistic scheme for the formation of Ag-BM composite, as learned through various experiments. (*i–v*) (*i*) Al^{3+} complexes with chitosan solution; (*ii* and *iii*) alkali treatment leads to formation of aluminum hydroxide nanoparticles and random coiled chitosan network; (*iv*) aluminum hydroxide nanoparticles bind to chitosan network, possibly through covalent sharing of oxygen, leading to the formation of aluminum oxyhydroxide; and (*v*) silver nanoparticles form on the aluminum oxyhydroxide–chitosan network. (*B*) Photographs of the system during synthesis. Presence of aluminum hydroxide in the supernatant is clearly visible below pH 6 whereas bound aluminum hydroxide settles at pH 7 and pH 8, leading to a clear supernatant. (*C*) Photographs of the composite granules and of the same in water to illustrate that the material is stable in water. (*D*) Graphical representation and corresponding TEM images showing the aluminum oxyhydroxide-chitosan network without (green box) and with (red box) embedded silver nanoparticles.

We have observed that chitosan has the ability to bind colloidal nanoparticles in a proportion higher than 500 wt/wt% (Fig. 4 *A*, *iv*). Note that the role of chitosan is not merely as a flocculating agent for the precipitation of colloidal nanoparticles. In flocculation, colloidal particles undergo charge neutralization while binding with the flocculating agent. As a consequence, there is a reduction in the capacity to remove charge-bearing contaminants (such as arsenic or fluoride). However, the heavy metal ion-binding capability of aluminum oxyhydroxide–chitosan vis-à-vis equivalent chitosan is similar (Zn^{2+} binding ability: 53 mg/g and 56 mg/g, respectively, at an equilibrium concentration of 50 ppm). This means that functional groups for metal ion binding are largely available, even after hydrolysis of aluminum. A covalent interaction between chitosan and AlOOH ensures that charged sites on AlOOH are available for ion adsorption. Please note that typical sites on an oxide surface are MOH, MOH_2^+, and MO^-, with respective fractions determined by the pH.

Chitosan and AlOOH synergistically participate in the structural integrity of the composite. Chitosan undergoes swelling in water, due to destruction of hydrogen bonding. This behavior is similar to that observed in cellulose. Similarly, AlOOH disintegrates into finer particles upon exposure to water. However, the nanoscale AlOOH–chitosan composite, having a molecular-scale interaction of the individual components, does not exhibit any sign of disintegration in water. We propose that chitosan reinforces the AlOOH structure and vice versa, which imparts exceptional stability and strength to the composite in water (Fig. 4*C*). This molecularly assembled AlOOH–chitosan composite, exhibiting a cage-like structure, plays a critical role in stabilizing the silver nanoparticles (schematically illustrated in Fig. 4*D*). Upon addition of silver ions to AlOOH–chitosan, chitosan binds with silver due to its heavy metal ion-binding capacity. Upon addition of $NaBH_4$, silver ions reduce to zero valent nanoparticles, which are trapped in the AlOOH–chitosan cages (Fig. 4*A*, *v*). The presence of silver nanoparticles in the cage ensures their stabilization, while decreasing their exposure to scalants simultaneously, allowing release of silver ions in natural drinking water.

Conclusions

In their entirety, the proposed device and materials present a compelling solution for achieving the United Nations millennium development goal of sustainable access to safe drinking water. We believe that frugal science (21) based on nanotechnology can make a lasting impact on society. There are over 200 million households in India. Dissemination of this technology in various forms such as cartridges, sachets, etc., can generate large employment opportunities in the villages. The production of composites and water filter devices and their deployment and servicing can contribute to the local economy. Various modifications of the composite with different compositions have been developed with comparable performances.

Materials and Methods

The granular composites, composed of metal oxyhydroxide–chitosan nanostructures, were synthesized by a green synthetic route, which in general comprises hydrolysis of a metal precursor–chitosan complex using an alkaline medium followed by washing and drying at ambient conditions. Metal ion precursors that may be used for the preparation of composites are Al^{3+}, Fe^{3+}, Fe^{2+}, Mn^{2+}, Cu^{2+}, Zn^{2+}, Ti^{4+}, and Ce^{4+}. All syntheses were carried out in water.

Synthesis of the Composite for Bacteria and Virus Removal. An aluminum oxyhydroxide–chitosan nanostructure embedded with silver nanoparticles was synthesized by a two-step process: (*i*) Synthesis of the aluminum oxyhydroxide–chitosan nanostructure (referred to as BM): 1.5 g chitosan was dissolved in 0.5% nitric acid solution and to this mixture, 100 mL of 0.5 M aluminum sulfate was added dropwise. After 3 h incubation, 140 mL of 2 M sodium hydroxide was added dropwise to precipitate aluminum and chitosan. The resultant precipitate was further stirred for 1 h and subsequently washed with copious amounts of water. This precipitate is called BM. (*ii*) Synthesis of silver nanoparticle in BM: After redispersing the precipitate in water, 100 mL of 5 mM silver nitrate was added and incubated for 1 h. Afterwards, 100 mL of 10 mM sodium borohydride was added dropwise at <10 °C and the mixture was stirred continuously. The final precipitate was subsequently washed with copious amounts of water, dried at room temperature (28–30 °C), crushed, and used for further studies. The resulting composite was insoluble in water and appears as light yellow granules, referred to as Ag-BM. The method of composite preparation is water positive by two to three orders of magnitude; i.e., it produces 500 L of clean water for every 1 L of water consumed for material production.

Synthesis of Composite for Heavy Metal Removal. An aluminum oxyhydroxide–chitosan nanostructure embedded with nano-MnO_2 particles was synthesized through a two-step process: (*i*) synthesis of BM and (*ii*) MnO_2 nanoparticles incorporation in BM. Briefly, after redispersing the BM precipitate in water, a freshly prepared MnO_2 nanoparticles suspension was added dropwise and the mixture was stirred continuously. The final precipitate was subsequently washed with copious amounts of water, dried at room temperature, crushed, and used for further studies. The resulting composite was insoluble in water and appeared as black granules.

Synthesis of Composite for Arsenic and Iron Removal. The iron oxyhydroxide–chitosan nanostructure was prepared by the route described in *Synthesis of Composite for Bacteria and Virus Removal* for the preparation of BM. Ferric sulfate was used as the metal ion precursor for iron. The final precipitate was dried at room temperature, crushed, and used for further studies. The resulting composite was insoluble in water and appeared as brown granules.

Synthesis of Silver Nanoparticles for Hyperspectral Imaging. Silver nanoparticles used for hyperspectral imaging (HSI) are prepared through $NaBH_4$ reduction method. $AgNO_3$ (1 mM) was mixed with 1 mM trisodium citrate solution in equal volumes. An equal volume of 10 mM ice-cooled solution of $NaBH_4$ was then added dropwise to the above solution with stirring. The solution turns golden yellow and exhibits an absorption maximum at 390 nm, corresponding to an average particle diameter of 5–10 nm.

Testing protocol for antibacterial and antiviral efficacy. Two grams of Ag-BM was shaken with 100 mL of natural drinking water (see *SI Appendix*, Table S1 for water quality parameters). Antibacterial activity of Ag-BM was measured by spiking the natural drinking water with *Escherichia coli* (*E. coli* ATCC 25922) at a concentration of $\sim 1 \times 10^5$ CFU/mL, whereas antiviral activity was measured by spiking the water with bacteriophage MS2 at a concentration of $\sim 1 \times 10^3$ PFU/mL. Thereafter, the water was left standing for 1 h and subsequently the surviving microorganism count was measured by conventional pour plate (*E. coli*) and plaque assay (bacteriophage MS2) techniques. Colony counts were performed after incubation at 37 °C for 48 h (*E. coli*) and 16 h (bacteriophage MS2). It should be noted that the input bacteria and virus concentration may vary slightly in studies extending for weeks as the cultures are prepared on a daily basis.

Testing protocol for the water purification device. For the water purification device studies, 50 g of the composite was packed in a water purification cartridge (diameter, 70 mm; height, 2 mm) and assembled as a gravity-fed water purifier. The feed water was passed at a flow rate of 1,000 mL/min. The input tap water was periodically subjected to a bacterial load of $\sim 1 \times 10^5$ CFU/mL and the output water was plated in accordance with the protocol to understand the biocidal performance activity. Cyst removal studies were conducted following the NSF protocol P231 and NSF/American National Standards Institute standard 53. Polystyrene beads with a nominal size of 4–6 μm were used as a surrogate for cysts. An input concentration of $\sim 1 \times 10^6$ particles per liter was passed through the carbon block. Input and output concentrations were directly examined by a scanning electron microscope. Output water was concentrated ×1,000 before examination.

Details of the fluorescence microscopy protocol, mechanical testing of composite, and material characterization techniques used in this study are described in *SI Appendix*, *Methods* and *SI Appendix*, *Material Characterization*.

ACKNOWLEDGMENTS. We thank M. S. Bootharaju, S. Banupriya, P. R. Sajanlal, Robin John, and Rakhil Akkali for their technical support in conducting X-ray photoelectron spectroscopy, transmission electron microscopy, field emission scanning electron microscopy, atomic force microscopy, and fluorescence microscopy measurements, respectively. We thank Dr. R. G. Robinson and Dr. Manu Santhanam (Department of Civil Engineering) for their technical support in direct shear test and compressive strength analyses. We thank the Department of Science and Technology (Government of India) for constantly supporting our research program on nanomaterials.

1. Prüss-Ustün A, Bos R, Gore F, Bartram J (2008) *Safer Water, Better Health* (WHO, Geneva).
2. Clasen TF, Haller L (2008) *Water quality interventions to prevent diarrhoea: Cost and cost-effectiveness* (WHO, Geneva).
3. (2004) *The World Factbook 2004* (Central Intelligence Agency, Washington, DC).
4. Sedlak DL, von Gunten U (2011) Chemistry. The chlorine dilemma. *Science* 331(6013): 42–43.
5. Shannon MA, et al. (2008) Science and technology for water purification in the coming decades. *Nature* 452(7185):301–310.
6. (2009) *Nanotechnology Applications for Clean Water*, eds Savage N, et al. (William Andrew Publication, Norwich, NY).
7. Kim SJ, Ko SH, Kang KH, Han J (2010) Direct seawater desalination by ion concentration polarization. *Nat Nanotechnol* 5(4):297–301.
8. Pradeep T, Anshup (2009) Noble metal nanoparticles for water purification: A critical review. *Thin Solid Films* 517(24):6441–6478.
9. De Gusseme B, et al. (2010) Biogenic silver for disinfection of water contaminated with viruses. *Appl Environ Microbiol* 76(4):1082–1087.
10. Kumar A, Vemula PK, Ajayan PM, John G (2008) Silver-nanoparticle-embedded antimicrobial paints based on vegetable oil. *Nat Mater* 7(3):236–241.
11. Dai J, Bruening ML (2002) Catalytic nanoparticles formed by reduction of metal ions in multilayered polyelectrolyte films. *Nano Lett* 2(5):497–501.
12. Jain P, Pradeep T (2005) Potential of silver nanoparticle-coated polyurethane foam as an antibacterial water filter. *Biotechnol Bioeng* 90(1):59–63.
13. Liu J, Hurt RH (2010) Ion release kinetics and particle persistence in aqueous nano-silver colloids. *Environ Sci Technol* 44(6):2169–2175.
14. Kittler S, Greulich C, Diendorf J, Köller M, Epple M (2010) Toxicity of silver nanoparticles increases during storage because of slow dissolution under release of silver ions. *Chem Mater* 22(16):4548–4554.
15. Jin X, et al. (2010) High-throughput screening of silver nanoparticle stability and bacterial inactivation in aquatic media: Influence of specific ions. *Environ Sci Technol* 44(19):7321–7328.
16. Marambio-Jones C, Hoek EMV (2010) A review of the antibacterial effects of silver nanomaterials and potential implications for human health and the environment. *J Nanopart Res* 12(5):1531–1551.
17. Nowack B (2010) Chemistry. Nanosilver revisited downstream. *Science* 330(6007): 1054–1055.
18. Berger TJ, Spadaro JA, Chapin SE, Becker RO (1976) Electrically generated silver ions: Quantitative effects on bacterial and mammalian cells. *Antimicrob Agents Chemother* 9(2):357–358.
19. Franz AM (2004) A *performance* study of ceramic candle filters in Kenya including tests for coliphage removal (Massachusetts Institute of Technology, Cambridge, MA). Available at http://dspace.mit.edu/bitstream/handle/1721.1/31120/61162474.pdf.
20. Qiu J (2011) Environmental science. China to spend billions cleaning up groundwater. *Science* 334(6057):745.
21. Whitesides G (2011) The frugal way: The promise of cost-conscious science. *The World in 2012*, ed, Franklin D, The Economist, pp 154.

Supporting Information for

Biopolymer-reinforced synthetic granular nanocomposites for affordable point-of-use water purification

Mohan Udhaya Sankar[a,1], Sahaja Aigal[a,1], Shihabudheen M. Maliyekkal[a,1], Amrita Chaudhary[a], Anshup[a], Avula Anil Kumar[a], Kamalesh Chaudhari[a] and Thalappil Pradeep[a,2]

[a]DST Unit of Nanoscience (DST UNS) and Thematic Unit of Excellence,
Department of Chemistry, Indian Institute of Technology Madras,
Chennai 600 036, India.

[2]Correspondence and requests for composites should be addressed to T.P. (pradeep@iitm.ac.in)

Supporting Information	Title	Page No.
SI	Methods	3
SI	Material characterization	3

Supporting Figure	Title	Page No.
S1.	Transmission electron micrograph and EDAX elemental mapping of Ag-BM	5
S2.	Performance trials for gravity-fed water purifier device containing Ag-BM as water purification composite	6
S3.	Silver ion leaching as a function of temperature	7
S4.	X-ray diffraction pattern of BM and Ag-BM	8
S5.	Field emission scanning electron microscopic image of Ag-BM	9

S6.	XPS survey spectra of Ag-BM	10
S7.	SEM-EDAX elemental spectrum and elemental imaging	11
S8.	AFM images of surface roughness of Ag-BM	12
S9.	Effect of water quality on performance of Ag-BM	13
S10.	Effect of variations in input water quality on antibacterial performance of Ag-BM	14
S11.	Effect of water quality used for reactivation of Ag-BM	15
S12.	Antibacterial performance for Ag-BM reactivation by alternate methods	16
S13.	Antiviral performance trials for Ag-BM in batch	17
S14.	Hyperspectral imaging of *E. coli*	18
S15.	Hyperspectral imaging of silver nanoparticles	19
S16.	Analysis of aluminium and TOC leaching	20
S17.	Fluorescence microscopy images of treated bacteria	21
S18.	Cyst removal performance tested with 4-6 micron polystyrene spheres	22
S19.	Direct shear test (horizontal shear stress vs. horizontal displacement)	23
S20.	Mohr-coulomb failure pattern (shear stress vs. normal stress)	24

Supporting Table	**Title**	**Page No.**
S1.	Physicochemical characteristics of influent natural drinking water	25

SI Methods

Fluorescence microscopy protocol: 1L of 10^6 CFU/mL *E. coli* containing water was contacted with Ag-BM for an hour and it was repeatedly centrifuged at 20,000 rpm to obtain a bacterial pellet. This pellet was resuspended in 1 mL of 0.85% saline to obtain a final bacterial concentration of 10^9 CFU/mL. Staining was done according to Invitrogen Molecular Probes protocol. Briefly, 3 µL of a fluorescent probe mixture containing 3.34 µM green fluorescent nucleic acid stain SYTO 9 and 15 µM red fluorescent nucleic acid stain PI was combined with 1 mL of bacterial suspension. The mixture was incubated in dark for 15 min at room temperature and a 5 µL aliquot was placed on a glass slide, which was then covered by a cover slip, sealed and examined under Fluorescence microscope. Excitation was done for SYTO 9 at 465-495 nm and at 530-560 nm for PI. Emission was collected using a band pass filter for SYTO 9 at 515-555 nm and a long pass filter for PI at 590 nm.

Mechanical testing of composite: The shear strength of the media was measured at dry and wet conditions, separately. Around ~140 g of granular media was packed in a 6 cm x 6 cm x 6 cm (LxBxH) sample holder and horizontal shear stress was measured under normal stress of 50, 100 and 200 kPa.

SI Material characterization

The identification of the phase(s) of the as-prepared sample was carried out by X-ray powder diffraction (Bruker AXS, D8 Discover, USA) using Cu-Kα radiation at λ = 1.5418 Å. Surface morphology, elemental analysis and elemental mapping studies were carried out using a Scanning Electron Microscope (SEM) equipped with Energy Dispersive Analysis of X-rays (EDAX) (FEI Quanta 200). Field Emission SEM measurements were done with FEI Nova NanoSEM 600 instrument. High Resolution Transmission Electron Microscopy (HRTEM) images of the sample were obtained with JEM 3010 (JEOL, Japan) operating at 300 keV. Elemental mapping was done with a TEM EDAX. X-ray Photoelectron Spectroscopy (XPS) measurements were done using

ESCA Probe TPD of Omicron Nanotechnology. Polychomatic Mg Kα was used as the X-ray source (hv = 1253.6 eV). Binding energy was calibrated with respect to C 1s at 284.5 eV. Total silver, arsenic and lead concentrations in water were estimated using inductively coupled plasma mass spectrometry (ICP-MS) (Agilent Technologies, 7700x ICP-MS and PerkinElmer NexION 300 ICP-MS). Atomic Force Microscopy (AFM) measurements were done using a Witec GmbH confocal Raman microscope (CRM-Alpha300 S). Bacteria treated with silver nanoparticles and those treated with Ag-BM, were viewed under the Cytoviva microscope, attached to a Hyperspectral imaging (HSI) system. The system captures the VNIR (400-1000 nm) spectrum within each pixel of the scanned field of view. The bacteria were treated for a period of 2 h, and 2 µL of the same were spotted on glass slides. The spotted samples were allowed to dry for over 4 h before imaging. Imaging was done at 100x magnification, using a halogen lamp (400-1000 nm) as the light source. Nikon ECLIPSE 80i fluorescence microscope was used to image stained bacteria.

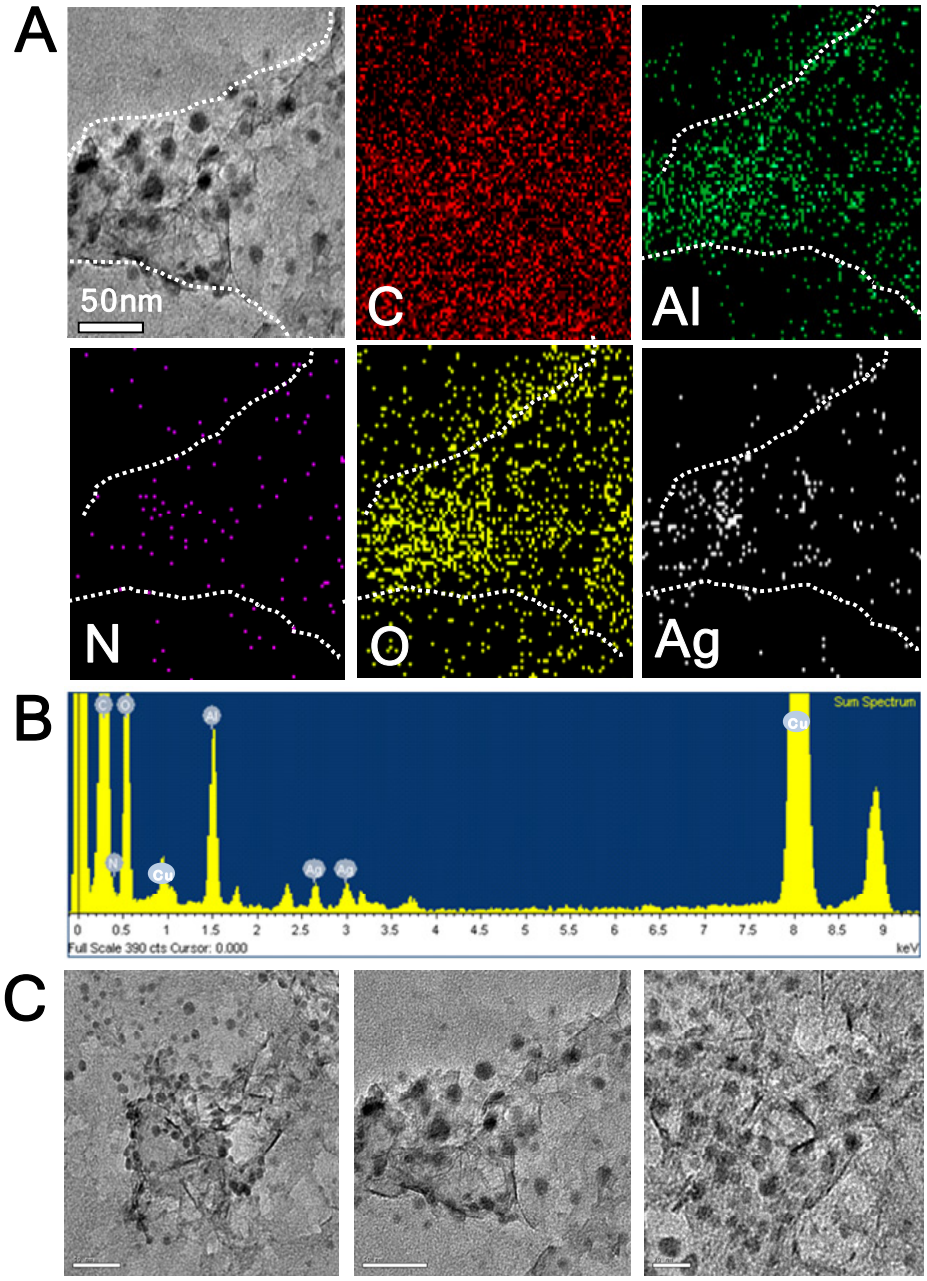

Fig. S1. Transmission electron micrograph and EDAX elemental mapping of Ag-BM. (*A*) EDAX elemental imaging of Ag-BM**.** Top extreme left is the TEM image and others are elemental maps from the region. **(*B*)** EDAX spectrum of **(*A*)** confirming the presence Ag. **(*C*)** HRTEM micrographs of Ag-BM (Scale bar is 50 nm). The uniform carbon image is due to the grid and the material. Al and O are present uniformly due to AlOOH and their pattern resembles the pattern of the sample (marked). Ag is also present in this region. The spatial resolution of EDAX resolution is good enough to see isolated particles. The Cu lines are due to the grid used.

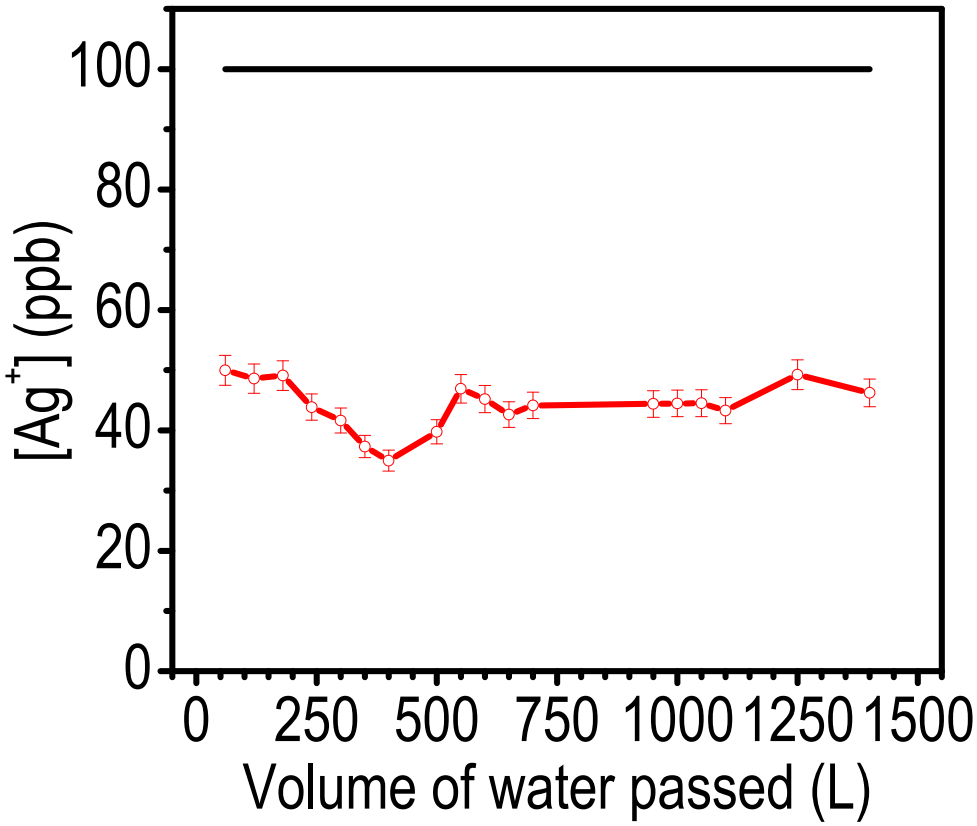

Fig. S2. Performance trials for gravity-fed water purifier device containing Ag-BM as the water purification composite. Analysis of silver ion concentration in output water measured by ICP-MS (red) in cartridge study (refer: *Materials and Methods*). The permissible limit for silver ion concentration in drinking water is shown as black line. Cartridge was run for 1500 L without any reactivation.

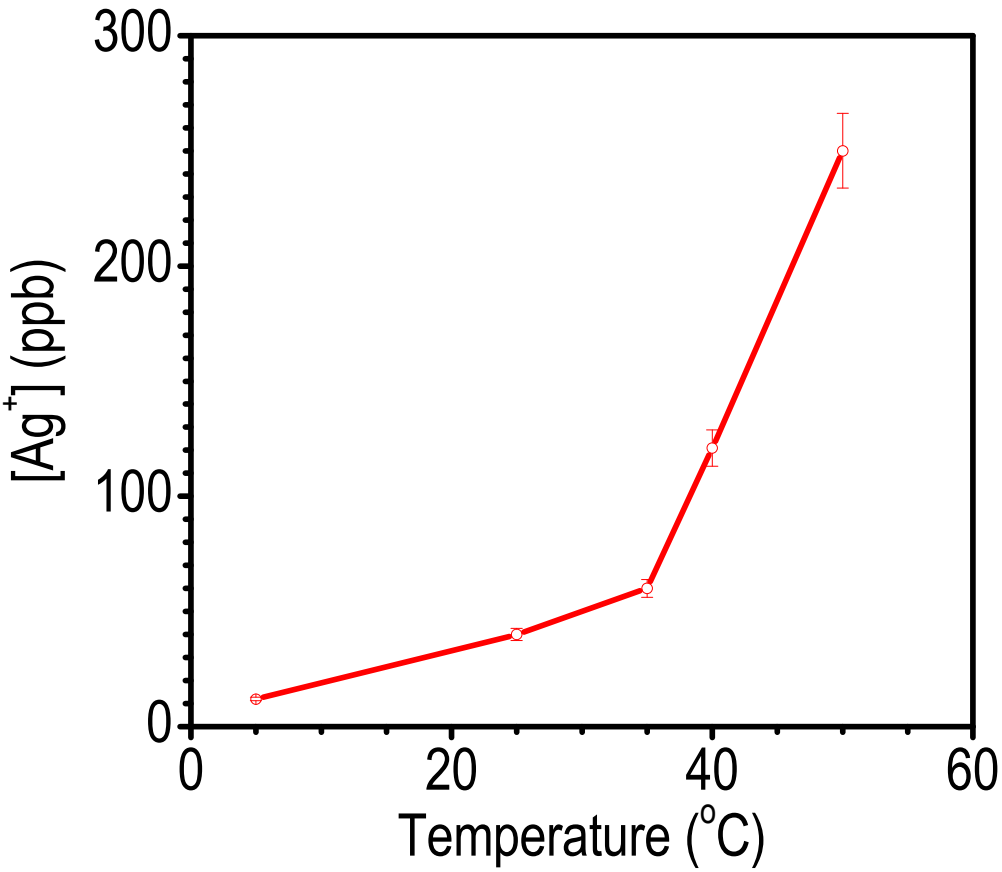

Fig. S3. Silver ion leaching as a function of temperature. Silver ion leaching from Ag-BM in water at temperatures of 5, 25, 35, 40 and 50 ^{0}C (measured using ICP-MS). The amount of silver ions leached in water at RT (25-35 ^{0}C) is 40 ± 10 ppb, when trials were done in batch.

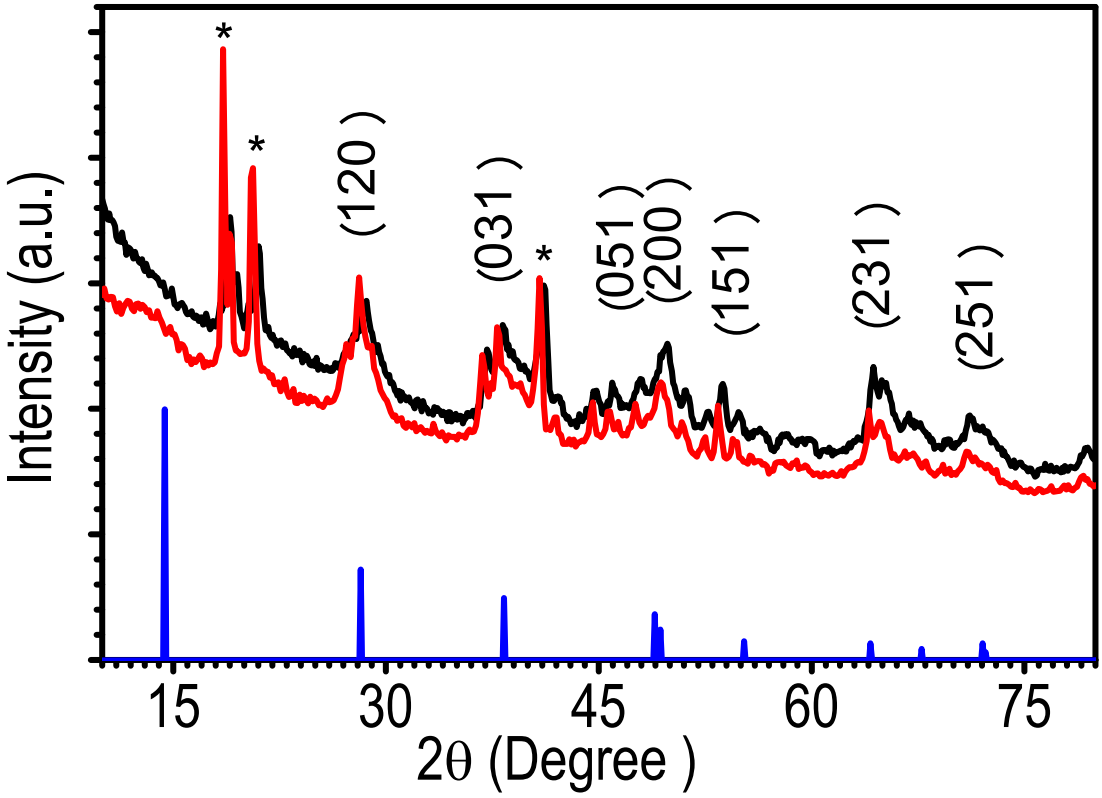

Fig. S4. X-ray diffraction patterns of BM and Ag-BM. XRD patterns of BM (black) and Ag-BM (red). BM showed peaks corresponding to (120), (013), (051), (151), (200), (231) and (251) planes. All these peaks can be indexed to orthorhombic-AlOOH shown in blue colour (JCPDS # 83-2384). The broadened XRD peaks imply that the crystallite size of BM particles is very small. The mean crystallite size calculated from the Scherrer formula shows that AlOOH nanocrystals are of an average size of 3.5 nm. The presence of organic template (chitosan) is also clear from the XRD data. The peaks marked by * corresponding to 2θ (in degrees) = 18.7°, 20.6° and 41.2° are attributed to the presence of the organic template. There is a definite difference in the full-width at half maxima (FWHM) for the peaks corresponding to AlOOH and organic template. Addition of Ag to BM doesn't lead to new diffraction features, presumably due to low concentration of Ag.

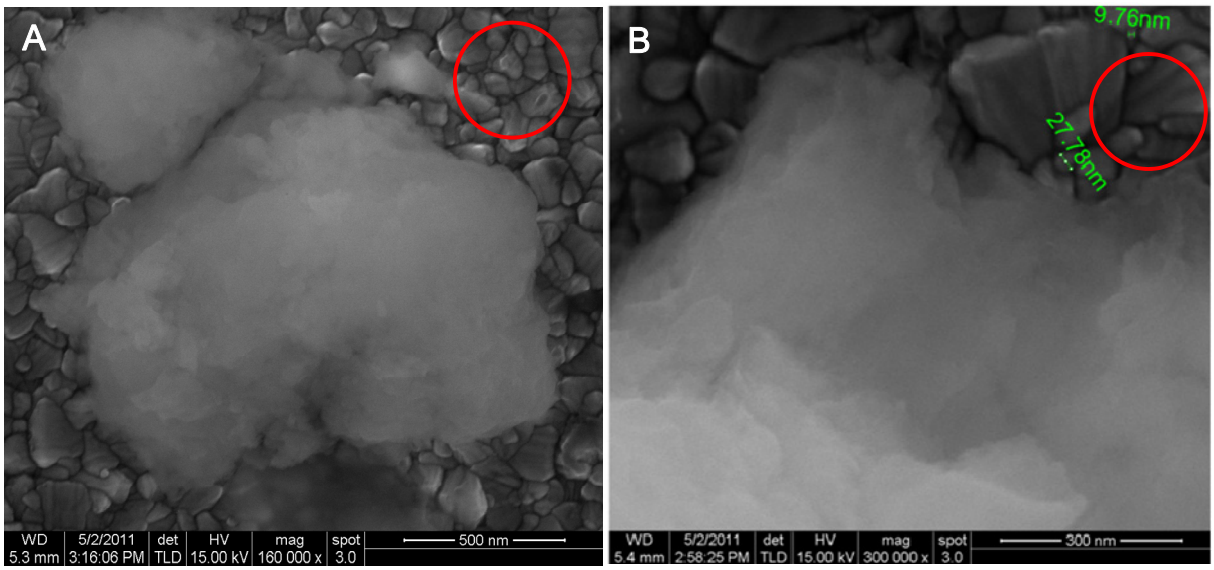

Fig. S5. Field emission scanning electron microscopic image of Ag-BM. FESEM images of an Ag-BM grain at two magnifications. Silver nanoparticles are not seen on the surface of the BM composite, although the substrate particles (ITO, indium tin oxide) in similar size range (10-30 nm) are clearly visible. A part of the ITO coated glass substrate is highlighted by the red circle to illustrate this point. This indicates that silver nanoparticles are embedded and well protected in the BM matrix.

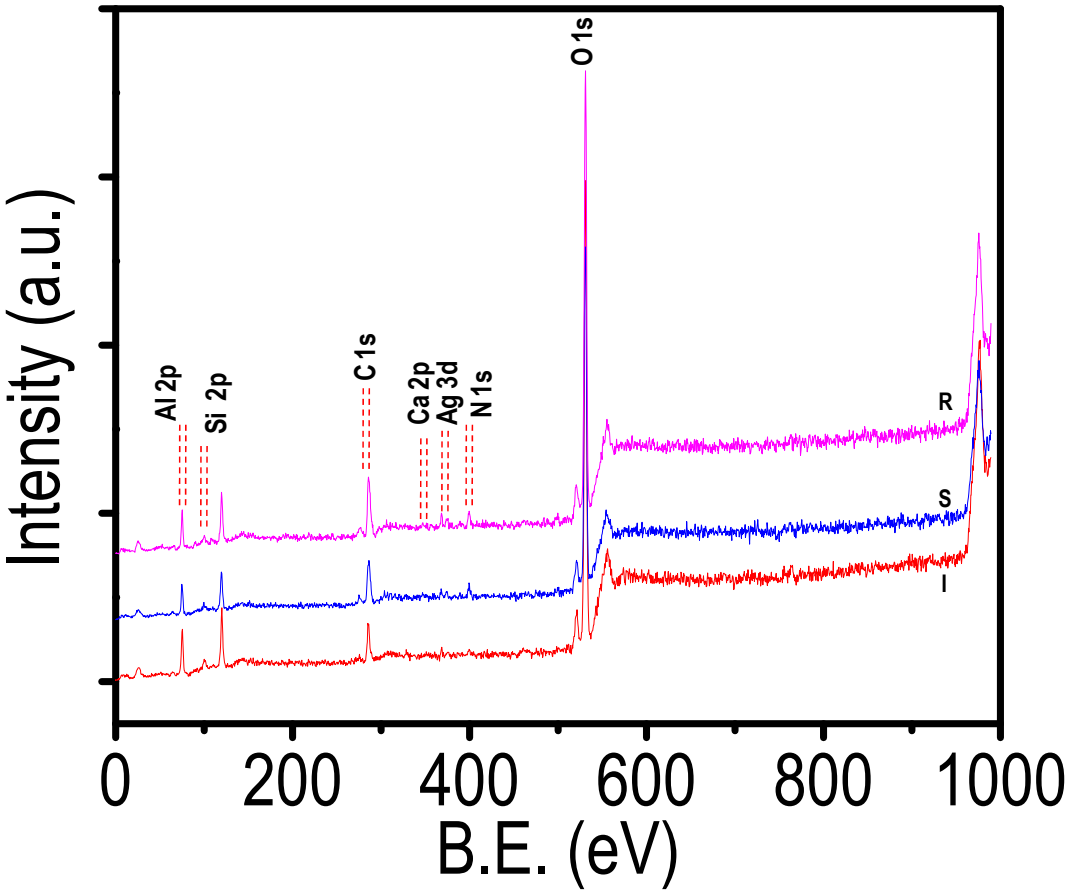

Fig. S6. XPS survey spectra of Ag-BM. XPS survey spectra of Ag-BM samples (I) Prior to use, (S) upon saturation of anti-bacterial activity and (R) upon reactivation in distilled water at 70 °C. The spectra are essentially the same except in Ca 2p and Si 2p regions, which are marked. N 1s is also present in I, although with reduced intensity.

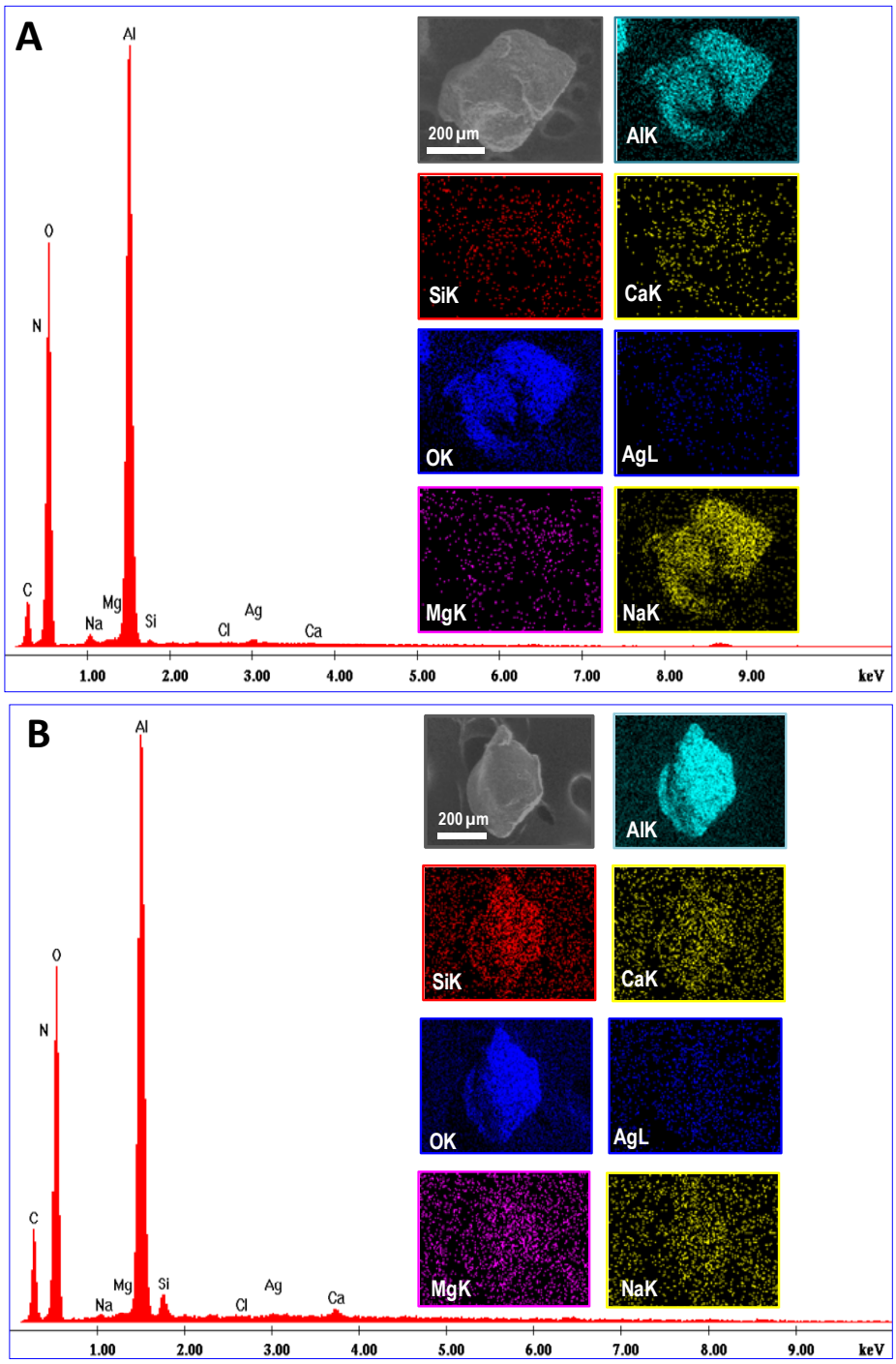

Fig. S7. SEM-EDAX elemental spectrum and elemental imaging. SEM-EDAX of **(*A*)** freshly prepared Ag-BM and **(*B*)** saturated Ag-BM. Natural drinking water (without treatment so that there is a residual bacterial count in it) was used for testing. Presence of deposits containing Ca and Si is seen on the saturated Ag-BM material.

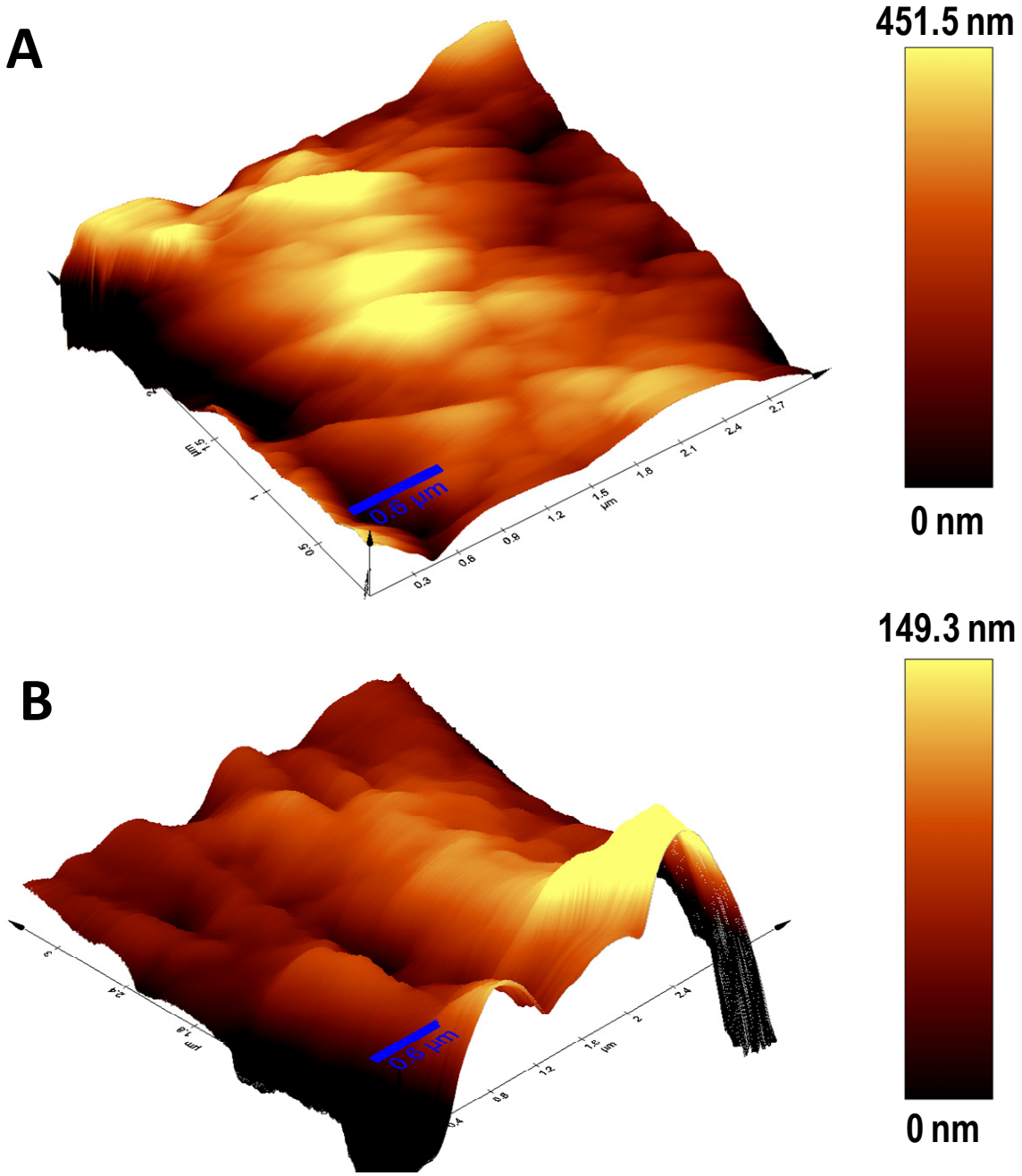

Fig. S8. AFM images of surface roughness of Ag-BM. 3D AFM images of surface roughness of (***A***) initial Ag-BM and (***B***) saturated Ag-BM. The high profile is also shown. Increased inhomogeneity, possibly due to deposits is seen in *B*.

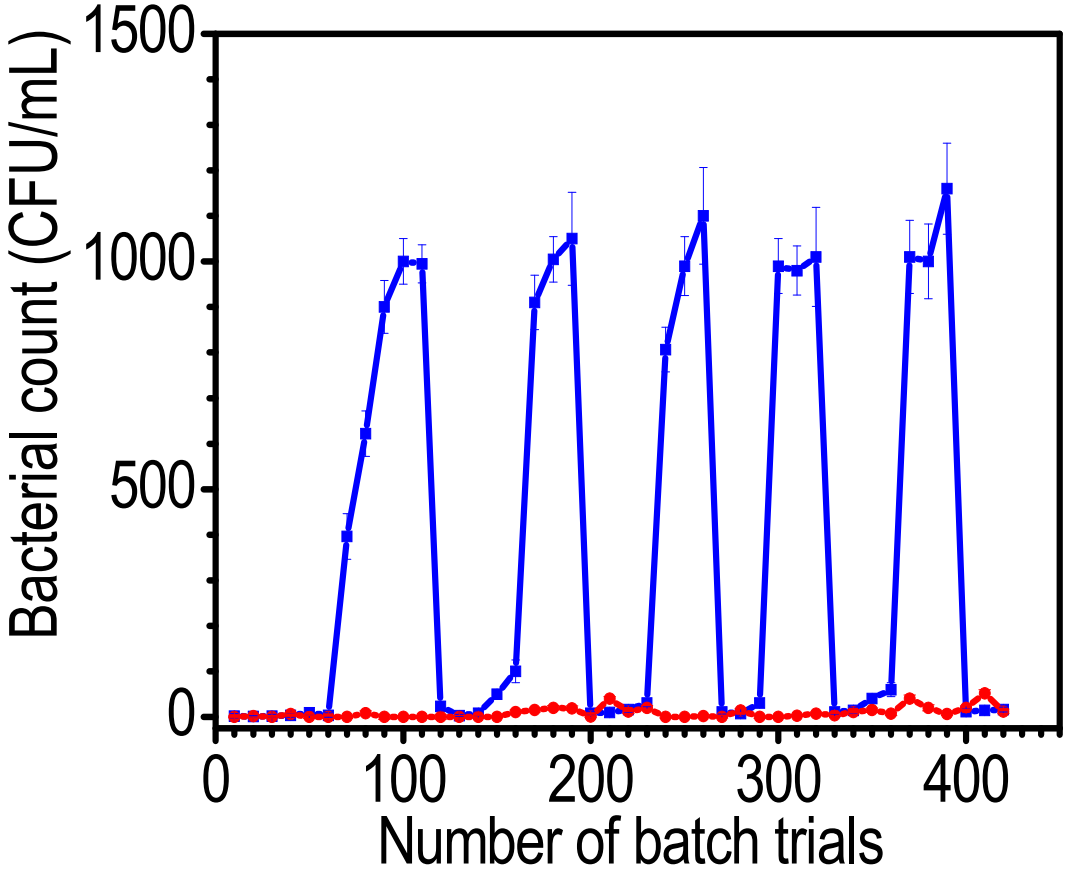

Fig. S9. Effect of water quality on performance of Ag-BM. Performance comparison for Ag-BM shaken in tap water (blue trace) and ultrapure water (red trace). The antibacterial efficacy of the composite in ultrapure water is due to the absence of interfering species typically found in tap water. As in other batch experiments, 2g of the composite was shaken in 100 mL of ultrapure water spiked with 0.85% NaCl (to avoid osmotic rupture) and bacterial input load of 10^5 CFU/mL and the solution was plated after 1 h. The composite works indefinitely without the need for reactivation.

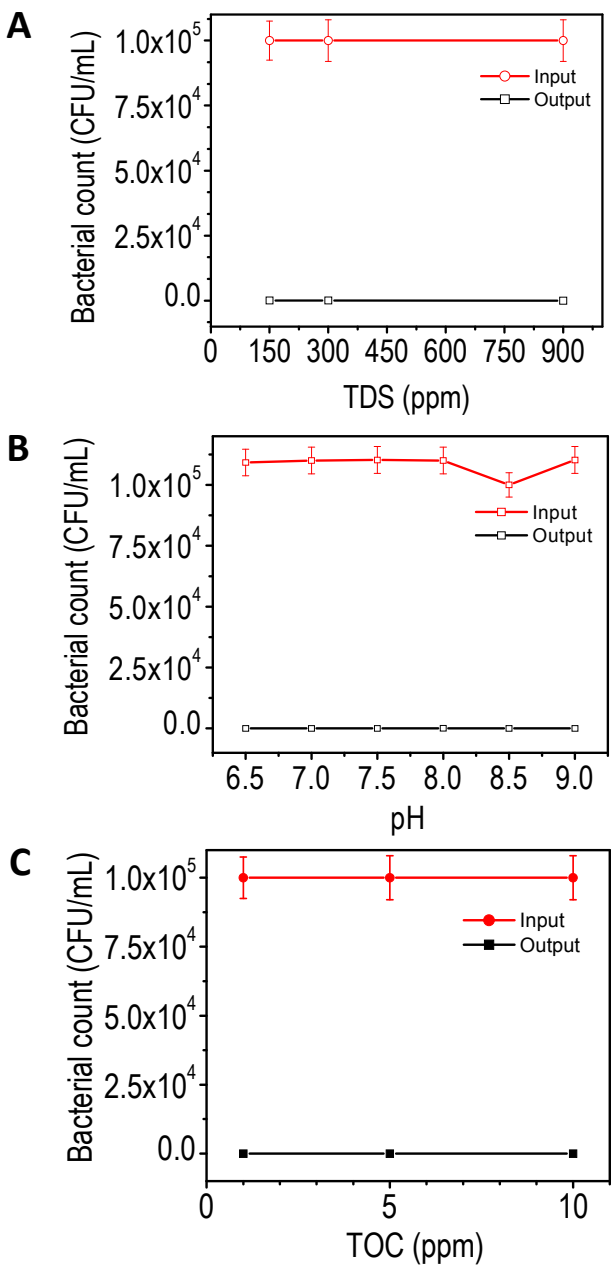

Fig. S10. Effect of variations in input water quality on antibacterial performance of Ag-BM. Performance of Ag-BM against *E. coli* was tested in batch, by varying **(*A*)** the ionic strength of synthetic challenge water (pH held constant at 7.0±0.2), **(*B*)** pH of the synthetic challenge water (TDS held constant at 300 ppm) and **(*C*)** the organic (humic acid) content of the synthetic challenge water (pH and TDS held constant at 7.0±0.2 and TDS 300 ppm, respectively). The average input concentration was $1X10^5$ CFU/mL. Activity of the composite does not diminish with variation in TDS, pH as well as TOC of synthetic challenge water.

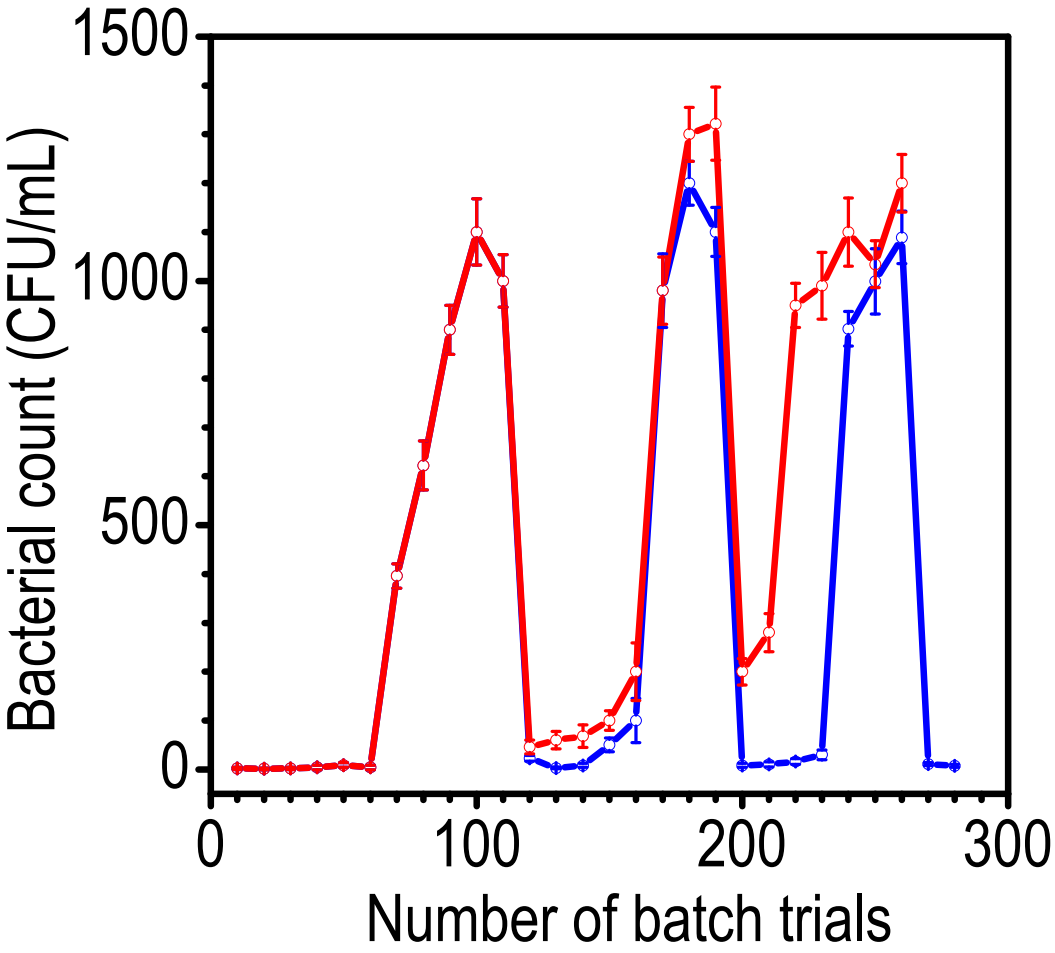

Fig. S11. Effect of water quality used for reactivation of Ag-BM. Performance comparison for Ag-BM reactivated with distilled water (blue trace) and tap water (red trace) at 70 °C. Unlike reactivation of composite in tap water, reactivation in distilled water leads to nearly complete recovery of anti-bacterial performance (output count came to zero). The composite exhibits only 2 cycles of reactivation before getting exhausted in tap water. On the contrary, the composite can be reactivated for at least 5 cycles, if reactivation is conducted in distilled or quality drinking water.

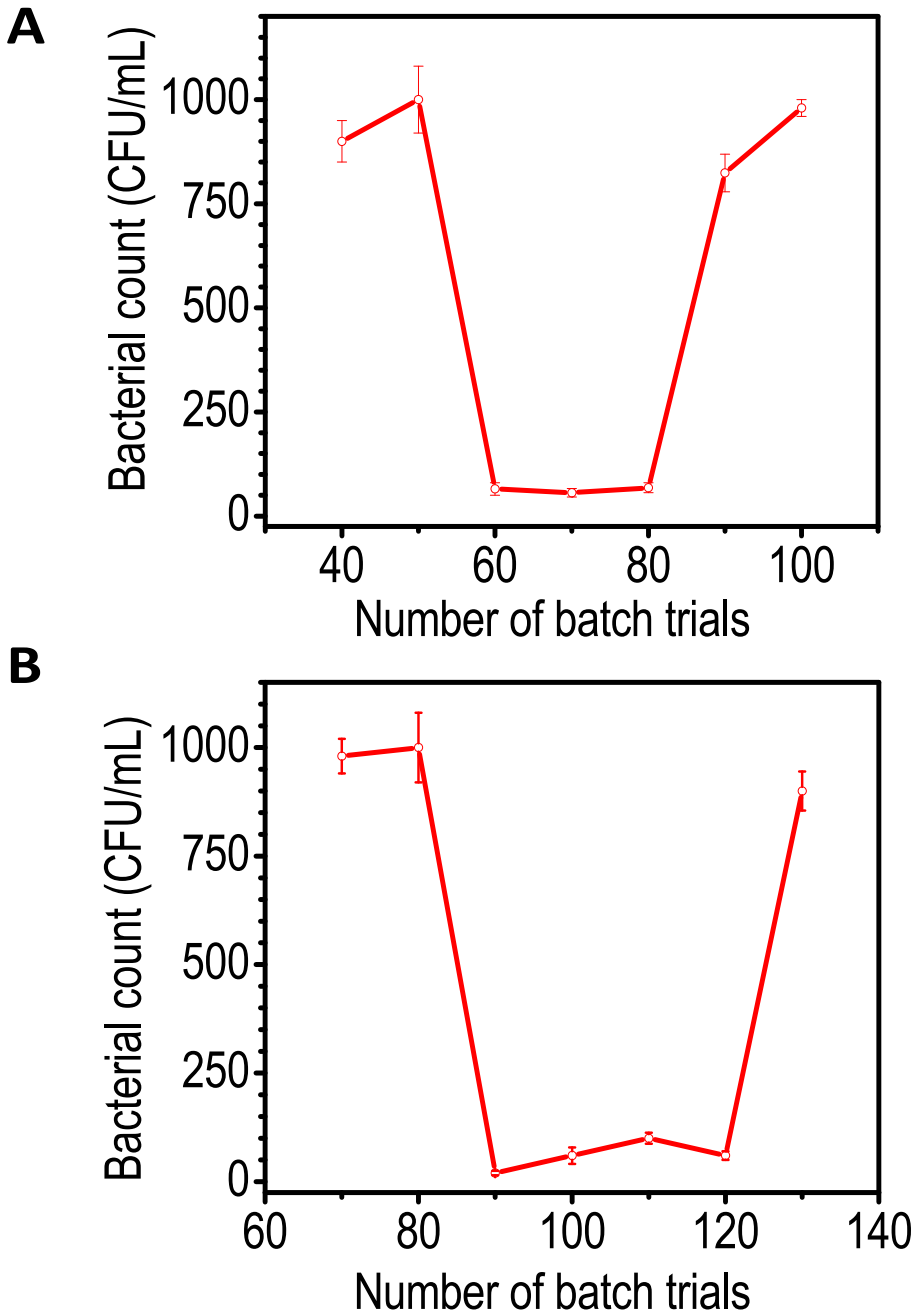

Fig. S12. Antibacterial performance for Ag-BM reactivation by alternate methods. Reactivation using **(*A*)** citric acid (10 mM) (alternatively, 4 drops of fresh lemon juice is used, pH 5.5±0.5) and **(*B*)** hydrogen peroxide (100 ppm). It is evident that chemical methods of reactivation are equally efficient in recovering the performance of the composite.

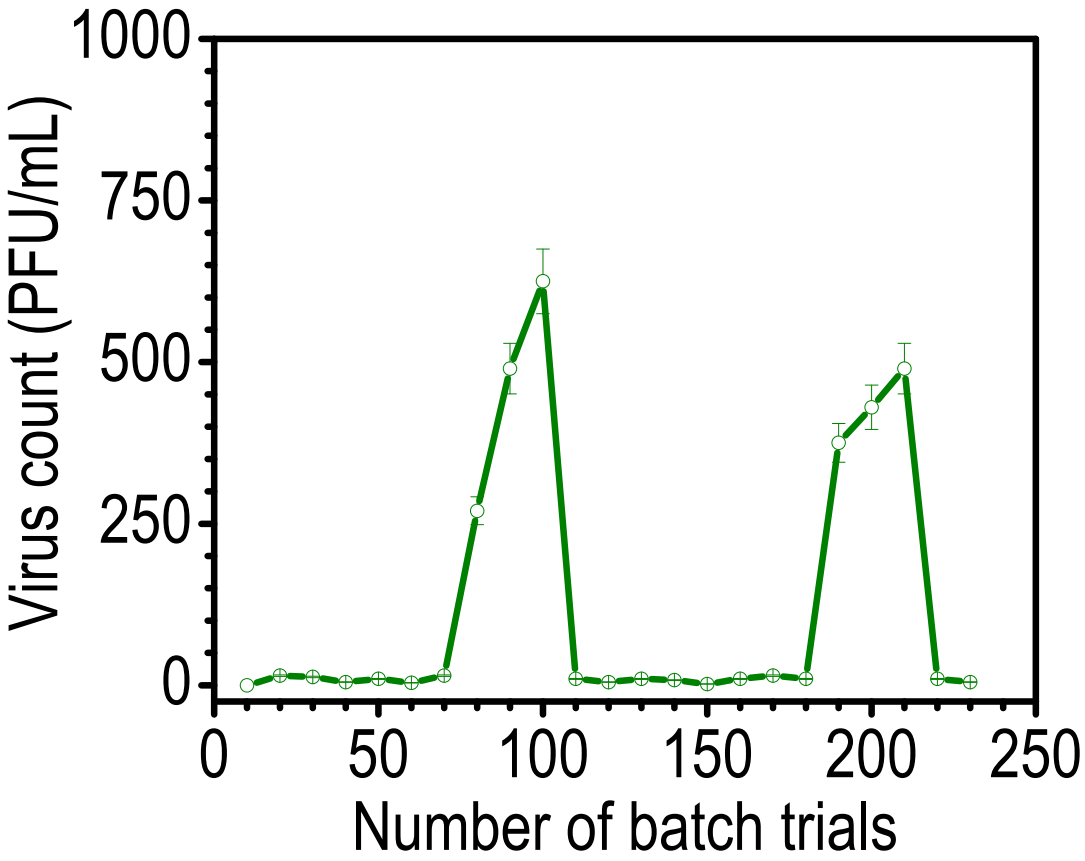

Fig. S13. Antiviral performance trials of Ag-BM in batch. Performance of Ag-BM against MS2 bacteriophage was tested in batch. The average input concentration was 1000 PFU/mL. The composite was reactivated after the 3 consecutive saturation points (trial numbers 80-100 and 190-210) were obtained. The antiviral performance is comparable to antibacterial performance as the composite regains its property after reactivation.

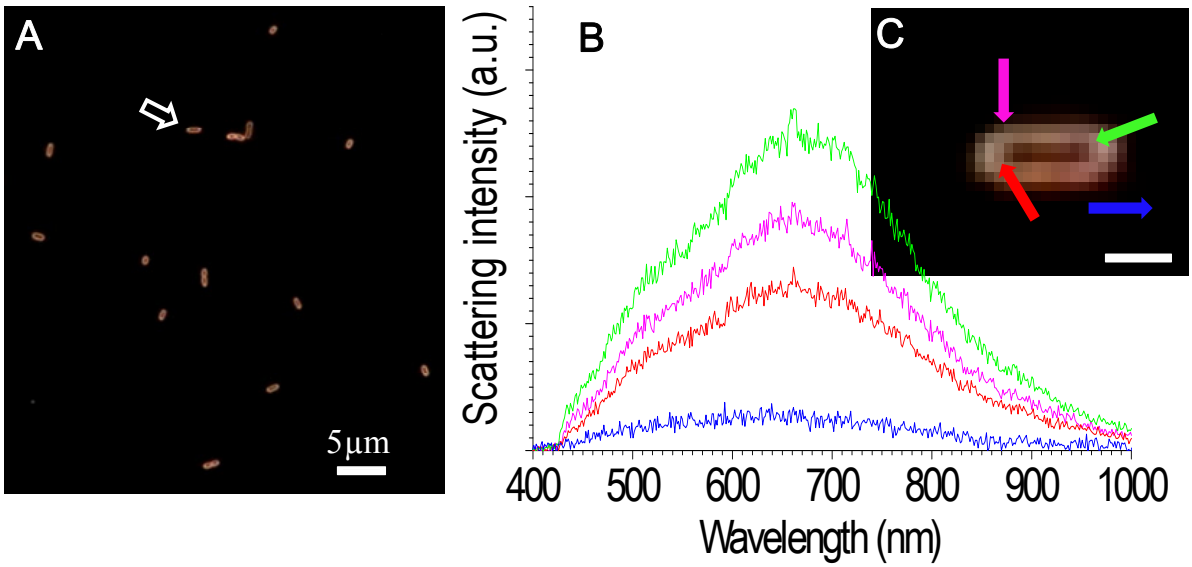

Fig. S14. Hyperspectral imaging of *E. coli*. (*A*) Hyperspectral image of *E. coli*, **(*B*)** spectra collected at various borders of *E. coli* and **(*C*)** expanded hyperspectral image of *E. coli* used for collection of spectra. The scale bar is 1 µm. The spectrum essentially resembles the lamp spectrum as there are no absorbing species in a bacterium.

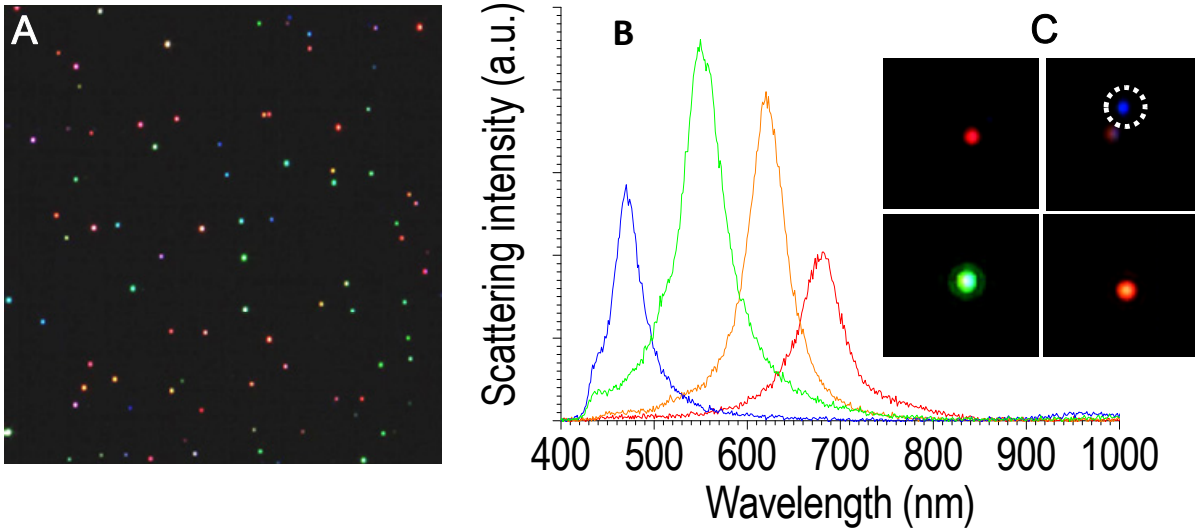

Fig. S15. Hyperspectral imaging (HSI) of silver nanoparticles. HSI images of **(*A*)** nanoparticles in water, **(*B*)** spectra collected for single nanoparticles showing different colors due to differences in absorption maxima and **(*C*)** zoomed images of the corresponding nanoparticles.

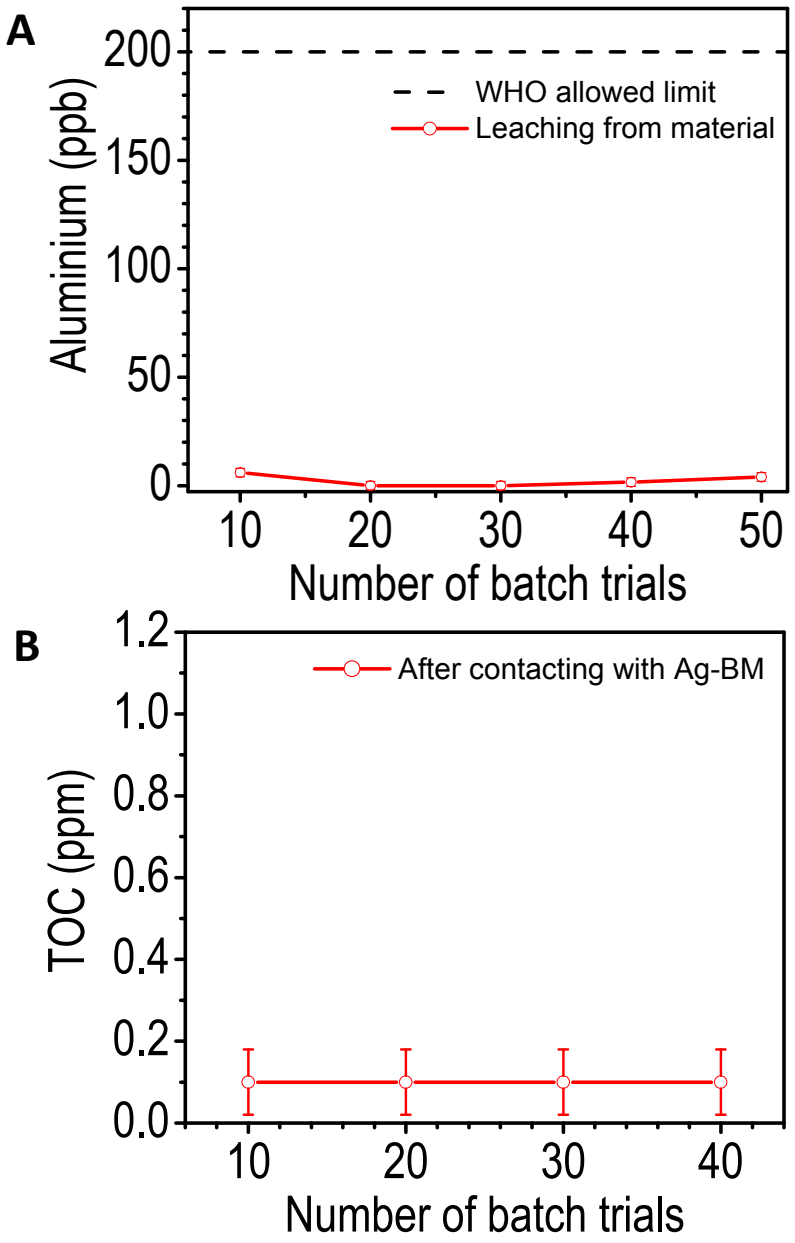

Fig. S16. Analysis of aluminium and TOC leaching. (*A*) Analysis of aluminum concentration in output water measured by ICP-MS (red) in batch trials. The maximum permissible limit for aluminum ion concentration in drinking water is shown as red line. **(*B*)** Analysis of leached total organic carbon (TOC) in output water. The limit of detection of TOC measurement was estimated to be 80 ppb.

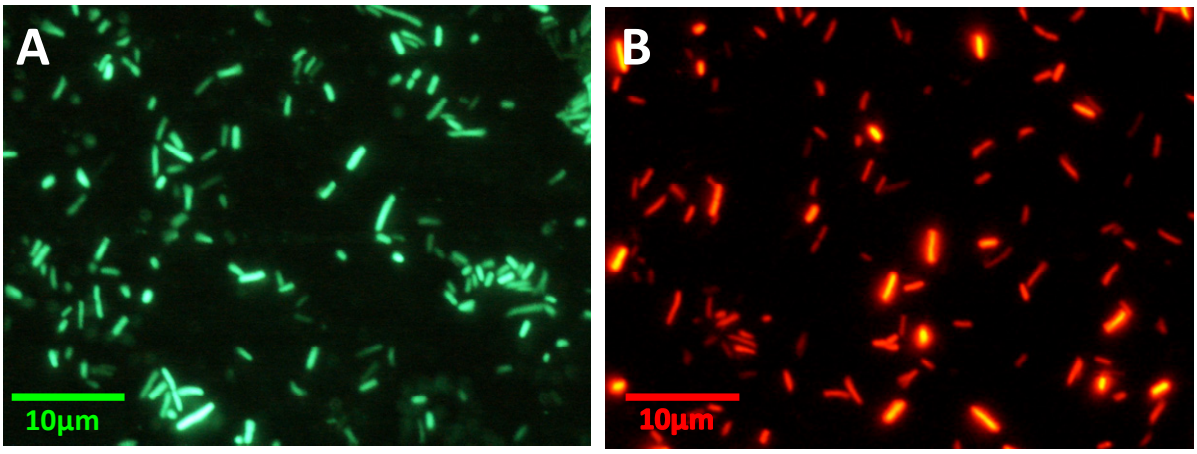

Fig. S17. Fluorescence microscopy study of treated bacteria. Fluorescence microscopy images of bacteria (*E. coli*) after staining with SYTO 9 (green) and PI (red). **(*A*)** Untreated and **(*B*)** treated with Ag-BM composite for 1h. Each image is a result of superposition of an image taken for the green fluorescent dye and red fluorescent dye using the appropriate filters. The scale bar is 10 µm. Fluorescence microscopy study supports that bacteria are killed within 1h after treating with Ag-BM.

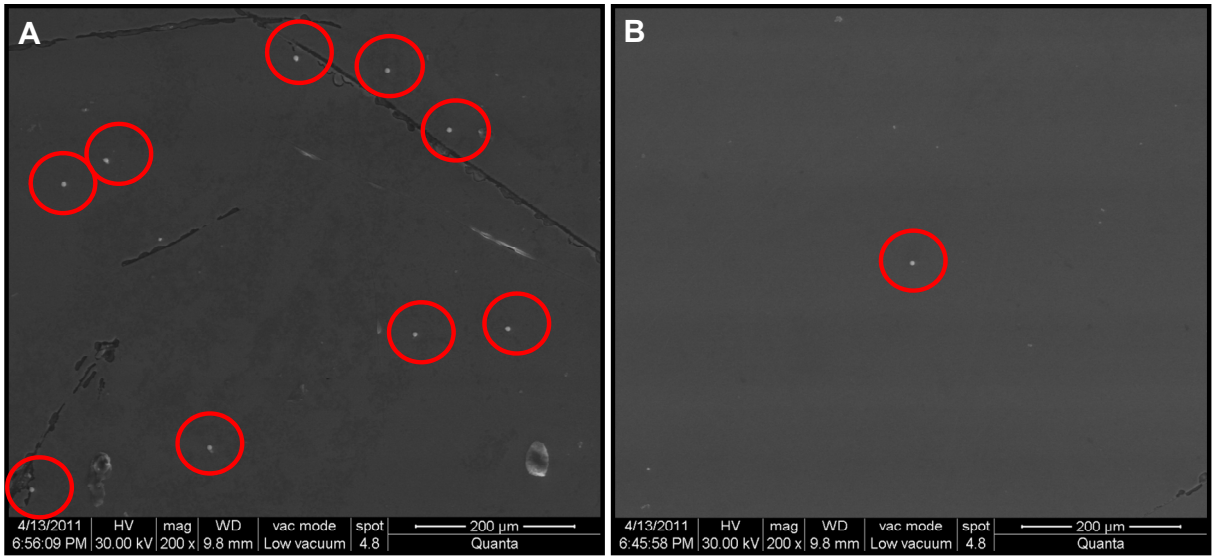

Fig. S18. Cyst removal performance tested with 4-6 micron polystyrene spheres. SEM images of 4-6 micron polystyrene spheres. **(*A*)** Input count: 10^6 particles/L and **(*B*)** output count: 1 particle is seen in the 1000 times concentrated sample (<3 particles/L). The input water containing polystyrene spheres was passed through the porous carbon block as per NSF P231 protocol (polystyrene spheres are used as representative for cyst, in terms of size) and removal capacity is higher than 5 log. The porous carbon block removes cysts through physical filtration.

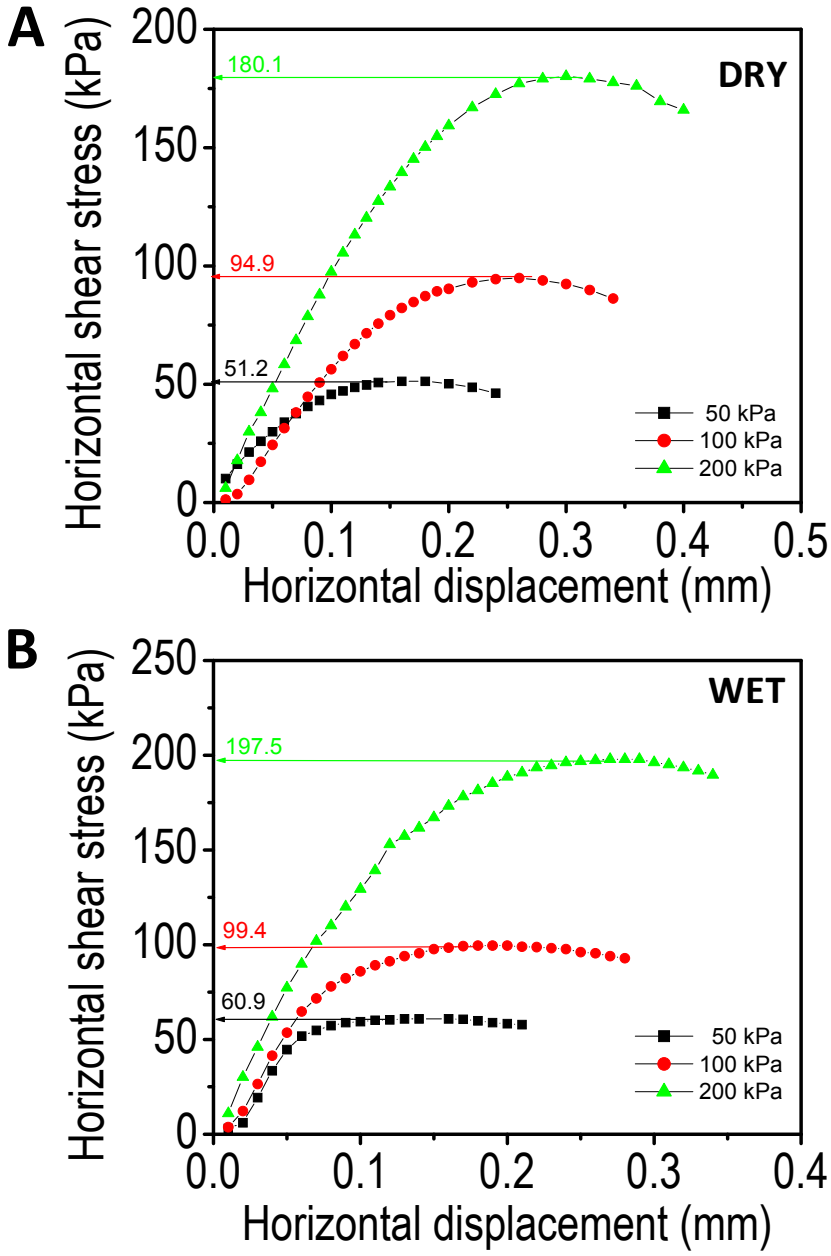

Fig. S19. Direct shear test (Horizontal shear stress vs. Horizontal displacement). Plot of horizontal shear stress vs. horizontal displacement of loosely packed media obtained from direct shear tests: **(*A*)** measured at dry condition and **(*B*)** measured at wet condition.

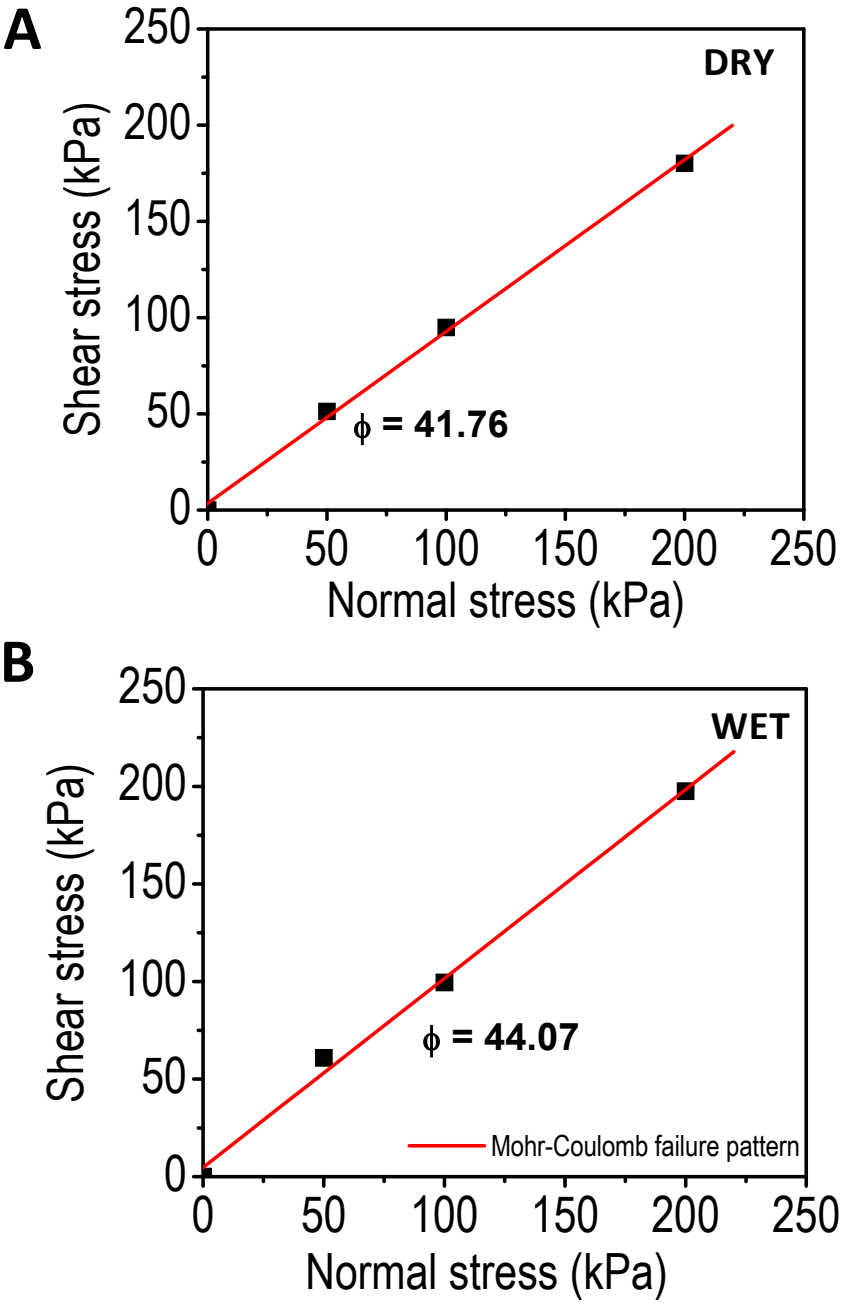

Fig. S20. Mohr-Coulomb failure pattern (Shear stress vs. Normal stress). Plot of shear stress vs. normal stress of loosely packed media showing the straight-line approximation of the Mohr-Coulomb failure pattern: **(*A*)** measured at dry condition and **(*B*)** measured at wet condition.

SUPPORTING TABLE

Table S1. Physicochemical characteristics of influent natural drinking water

(Note: All parameters are expressed in mg L^{-1}, except for pH and conductivity)

Parameters	Value
Total coliforms (CFU/mL)	1-2 x 10^3
p H @25°C	7.8
Conductivity (µS/cm)	640.000
Fluoride	0.573
Chloride	86.340
Nitrate	1.837
Sulphate	32.410
Silicate	15.870
Lithium	ND
Sodium	53.740
Ammonium	ND
Potassium	2.330
Magnesium	14.340
Calcium	28.720

ND-not detected

Natural drinking water (without treatment so that there is a residual bacterial count in it) was used for testing to ensure that that the material functions in the field.

ACS Sustainable Chemistry & Engineering

Research Article

Cite This: ACS Sustainable Chem. Eng. XXXX, XXX, XXX−XXX

Species-Specific Uptake of Arsenic on Confined Metastable 2-Line Ferrihydrite: A Combined Raman-X-Ray Photoelectron Spectroscopy Investigation of the Adsorption Mechanism

Chennu Sudhakar, Avula Anil Kumar, Radha Gobinda Bhuin, Soujit Sen Gupta, Ganapati Natarajan, and Thalappil Pradeep*

DST Unit of Nanoscience (DST UNS) and Thematic Unit of Excellence (TUE), Department of Chemistry, Indian Institute of Technology Madras, Chennai 600036, India

Supporting Information

ABSTRACT: The present study is targeted toward understanding the interaction between important and technologically relevant polymorphs of iron oxides/oxyhydroxides with arsenic species at neutral pH. The existence of various arsenic (As) species in solution was verified by Raman measurements. Their species-dependent adsorption on the affordable arsenic removal media, confined metastable 2-line ferrihydrite (CM2LF) was investigated. The results were compared with common adsorption media, hematite (α-Fe_2O_3) and magnetite (Fe_3O_4). X-ray photoelectron spectroscopy was used to investigate the changes in the core levels of Fe 2p and As 3d resulting from the uptake of arsenic species. Binding of various As species with CM2LF was confirmed by FTIR studies. Raman adsorption data were found to fit a pseudo-second-order model. Results of this study show the synthesized nanocomposite of CM2LF to be very effective for the removal of As(III) and As(V) species in comparison to various materials at neutral pH. A model for the adsorption of As(III) and As(V) species in water on a ferrihydrite particle was developed. This accounted for the large uptake capacity.

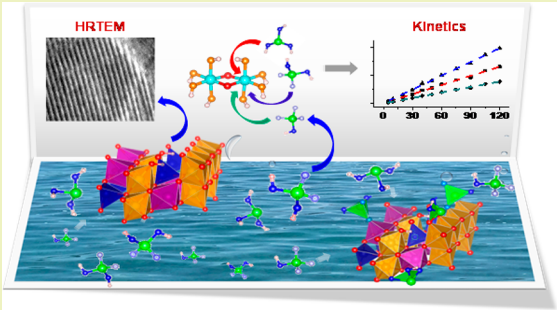

KEYWORDS: *Arsenic species, Uptake capacity, CM2LF, Hematite, Magnetite, Adsorption mechanism*

INTRODUCTION

Arsenic is one of the major contaminants in drinking water in many parts of the world. Various parts of India, Bangladesh, Cambodia, South Africa, Argentina, United States, and other countries have arsenic in the groundwater to an extent more than the permissible limit, namely 10 μg L^{-1} (10 ppb) prescribed by the World Health Organization (WHO).[1,2] Arsenic and its associated problems are still a great threat to human health, although arsenic in water was first reported by Benjamin Martin way back in 1759.[3] Arsenic occurs in natural waters as either arsenite (As(III)) or arsenate (As(V)).[4] Both forms of arsenic have strong affinity for iron oxide/oxyhydroxide surfaces near neutral pH.[5,6] The speciation of arsenic is an important aspect for understanding its mobility, bioavailability, and toxicity in groundwater.[7] A comprehensive solution for arsenic contamination was not evident as efforts made previously have faced various challenges. Arsenic in the environment has been addressed in various ways in terms of technology, and all of them have certain limitations.[8]

In this context, there is a need to explore the use of nanomaterials for arsenic mitigation due to their large surface area and enhanced surface reactivity. In the past decade, various nanostructured composites have been used to remove arsenic from water, namely, graphene oxide−$MnFe_2O_4$ nanohybrids,[9] Fe−Cu binary oxides,[10] nanocrystalline TiO_2,[3,11,12] superparamagnetic $Mg_{0.27}Fe_{2.5}O_4$,[13] GO−$ZrO(OH)_2$ nanocomposites,[14] GNP/Fe−Mg oxide,[15] etc. Recently, researchers have looked at several bioadsorbents like Eichhornia crassipes which are locally available. Powders of the roots of Eichhornia crassipes, possessing multiple functional groups (−OH, $-NH_2$, and −COOH) on the surface, were used for the potential removal of arsenic species from wastewater.[16]

However, to know the exact binding mechanism of different arsenic species on the surfaces, various spectroscopic studies are required such as Raman spectroscopy, Fourier-transform infrared spectroscopy (FTIR), and X-ray photoelectron spectroscopy (XPS). These studies too have limitations due to the difficulty in understanding adsorbed species in water and the mode of complexation onto the surfaces. To understand the complexation of arsenic onto oxides, some efforts have been made by Gustafsson et al.[17] using computational methods. Authors have used the Diffuse Layer Model (DLM)[18] and Three-Plane CD-MUSIC Model (TPCD)[19] to account for the data. It has been seen that at different pH conditions, both As(III) and As(V) exist as different species.[20,21] These species bind on different adsorbents

Received: March 17, 2018
Revised: June 4, 2018
Published: June 11, 2018

Downloaded via INDIAN INST OF TECHNOLOGY MADRAS on July 2, 2018 at 08:08:04 (UTC).
See https://pubs.acs.org/sharingguidelines for options on how to legitimately share published articles.

 © XXXX American Chemical Society

DOI: 10.1021/acssuschemeng.8b01217
ACS Sustainable Chem. Eng. XXXX, XXX, XXX−XXX

differently,[22−25] which also depend on the concentration of the species.[23,26]

Adsorption of As(III) and As(V) on amorphous aluminum and iron oxides using vibrational spectroscopy was investigated by Goldberg et al.[20] According to the report, Al−O−As stretching frequency appeared between 844 to 865 cm^{-1} for pH 5−9, while Fe−O−As frequency was observed between 817 to 824 cm^{-1} for pH 5−10.5. Arsenate forms inner sphere complexes on both amorphous Al and Fe oxides, while As(III) forms inner and outer sphere complexes on amorphous Fe oxide and only outer sphere complexes on amorphous Al oxide. Arsenic speciation in the aqueous phase was studied in detail using Raman spectroscopy by Müller et al.[21] They studied the binding mechanism of As(III) and As(V) on 2-line ferrihydrite, goethite, hematite, and feroxyhyte using Raman and diffuse reflectance infrared Fourier-transform (DRIFT) spectroscopy. In solution phase, As(III) and As(V) showed various Raman features. However, the As(III/V) adsorbed samples of ferrihydrite and feroxyhyte showed Raman feature of Fe−O−As as a broad band, centered around 840 cm^{-1} at pH 5.5 and 9. In the case of As(V), this band was more intense and better resolved than As(III). To know the oxidation state of As, extended X-ray absorption fine structure (EXAFS) spectroscopy was performed which confirmed that no change occurred in the oxidation state of As(III) and As(V) after adsorption. EXAFS and X-ray absorption near edge structure (XANES) spectroscopy studies were widely used to know the mode of complexation of arsenic species on iron oxide/oxyhydroxide.

Wang et al.[22] investigated the surface speciation of As(III) and As(V) on green rust by EXAFS and XANES spectroscopies. They found polymeric species of As(III) on the surface of green rust. Bhandari et al.[27] studied the effect of light on ferrihydrite with As(III) at pH 5 using XANES and attenuated total reflection-FTIR (ATR-FTIR) spectroscopy. They observed the oxidation of As(III) which was bound to the surface of ferrihydrite. During the adsorption process, the release of Fe(II) ions into solution from ferrihydrite was noticed. Nguema et al.[28] performed As(III) sorption with 2-line ferrihydrite, hematite, goethite and lepidocrocite using EXAFS and XANES spectroscopies. They found bidentate binuclear corner sharing (^{2}C) complexes in all cases but bidentate mononuclear edge sharing (^{2}E) complexes additionally for ferrihydrite and hematite. In the environment, the known polymorphs of iron oxides/hydroxides/oxyhydroxides are about sixteen.[29] Hematite (α-Fe_2O_3), magnetite (Fe_3O_4), goethite (α-FeOOH), and ferrihydrite ($Fe_2O_3{\cdot}0.5H_2O$) are the commonly available polymorphs and are used for various industrial and scientific applications. Hematite (HEM), magnetite (MAG), and ferrihydrite (Fh)-based materials were used extensively in water purification for the removal of heavy metal ions (Pb and As).[30−32] Higher surface area of iron oxides favors larger adsorption capacity for arsenate.[33] Iron oxide nanoparticles are also effective for the removal of other metals such as V, Cr, Co, Mn, Se, Mo, Cd, Sb, Tl, Th, and U.[34] Use of nanoadsorbents for the removal of heavy metal ions from water is particularly attractive as they can be altered suitably to achieve greater surface area and stronger binding capacity. Magnetite nanoparticles have certain advantages due to their superparamagnetic properties, ease of preparation, and biocompatibility. However, agglomeration and the loss of magnetic strength over time resulting from auto-oxidation limits the commercial application of bare iron oxide nanoparticles.[35,36] We had introduced a low cost engineered nanomaterial, named as confined metastable 2-line ferrihydrite (CM2LF), having a high adsorption capacity of 100 mg/g[37] as a solution for arsenic contamination in drinking water. Detailed characterization, comparison with other materials, batch and cartridge studies, mechanical properties, regeneration, reuse, and post adsorption characterization have been reported earlier by Kumar et al.[37] The material has been implemented in various parts of West Bengal, Uttar Pradesh, Karnataka, and Punjab states of India for arsenic removal with continuous monitoring, and the technology has reached over 600 000 people now.

Present work mainly focuses on the adsorption kinetics of common As species (H_3AsO_3, $H_2AsO_4^{1-}$, and $HAsO_4^{2-}$) which exist at pH 7. The oxidation state of iron in CM2LF, MAG, and HEM upon complexation with As species was studied using XPS. The mode of adsorption of various species on these adsorbents was studied using FTIR spectroscopy. Based on these, a mechanistic model of complexation on nanoscale materials was developed.

■ EXPERIMENTAL SECTION

Stock solutions of 100 mM As(III) and As(V) were prepared using $NaAsO_2$ and $Na_2HAsO_4{\cdot}7H_2O$, respectively. A combination of As(III) and As(V) is referred to as As(mix). A stock solution of 100 mM As(mix) solution was prepared by mixing equimolar amounts of $NaAsO_2$ and $Na_2HAsO_4{\cdot}7H_2O$. The pH of the stock solutions was adjusted to 7 by adding diluted HCl and diluted NaOH, whenever necessary.

Further, 200 mg of the material (CM2LF/MAG/HEM) was added to 150 mL of arsenic stock solution (As(III)/As(V)/As(mix)) in a 250 mL polypropylene conical flask. The flask was kept in an orbital shaker for 24 h, until an adsorption equilibrium was reached. The solution was centrifuged and the residue (i.e., the arsenic adsorbed material) was washed several times with deionized water to remove unreacted arsenic species from the surface of the material. Subsequently, the cleaned residue was dried at room temperature and a pellet was made using an IR pelletizer. The pellet was kept in a vacuum desiccator for 48 h for complete drying and also to protect it from the surrounding environment, before performing XPS and IR measurements.

To understand the adsorption kinetics of arsenic, Raman measurements were performed. For this, 3−7 g of the material (CM2LF/MAG/HEM) was added to 40−50 mM of 150 mL of arsenic (As(III)/As(V)/As(mix)) solutions in a 250 mL polypropylene conical flask. The solution was kept in an orbital shaker, and 1 mL of the solution was collected at various time intervals at 5, 10, 15, 20, 40, 60, 90, and 120 min, respectively. The solutions were subjected to centrifugation, immediately after collecting them. The material if any, separated as residue, was discarded and Raman measurements were performed using the supernatant.

In this work, each material, viz., CM2LF/MAG/HEM has been investigated thoroughly for interaction with As(III), As(V), and As(mix), respectively.

Materials. Sodium arsenite ($NaAsO_2$) and disodium hydrogen arsenate ($Na_2HAsO_4{\cdot}7H_2O$) were purchased from SD Fine Chemicals Limited. Hematite (α-Fe_2O_3) was purchased from Merck Chemicals Pvt. Ltd., India. Magnetite (Fe_3O_4) was purchased from Alfa Aesar (A Johnson Matthey Company, USA). Sodium hydroxide (NaOH) was purchased from Rankem Glasswares and Chemicals Pvt. Ltd., India. Hydrochloric acid (HCl) was purchased from Merck Life Science Pvt. Ltd., India. All chemicals were of analytical grade and were used without further purification. Deionized (DI) water was used throughout the experiments.

Instrumentation. HRTEM images of the sample were obtained with JEM 3010 (JEOL, Japan) operating at 200 kV (to reduce beam induced damage) with an ultrahigh-resolution polepiece. Samples for

DOI: 10.1021/acssuschemeng.8b01217
ACS Sustainable Chem. Eng. XXXX, XXX, XXX−XXX

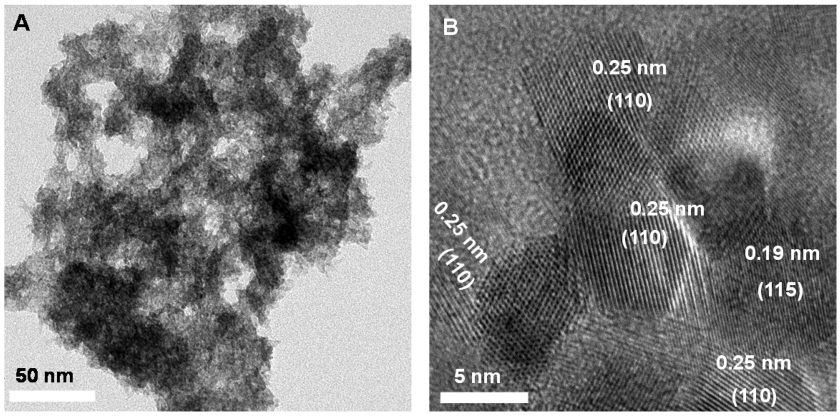

Figure 1. (A) HRTEM image of the 2-line ferrrihydrite composite (CM2LF). (B) Lattice resolved image of part A.

HRTEM studies were prepared by dropping the dispersion on amorphous carbon films supported on a copper grid and subsequent drying. XPS measurements were done using an ESCA Probe TPD spectrometer of Omicron Nanotechnology. Polychromatic Al Kα was used as the X-ray source ($h\nu$ = 1486.6 eV). Samples were mounted as pellets on a carbon tape, supported on the sample stub. Constant analyzer energy of 20 eV was used for the measurements. Binding energy was calibrated with respect to C 1s at 284.8 eV. All the XPS spectra were deconvoluted using CasaXPS software. Raman spectroscopy was performed using CRM Alpha 300 S microRaman spectrometer of WiTec GmbH (Germany). A glass slide with a cavity (which can hold 100 μL of the sample solution) was mounted on the piezoelectric scan stage of the setup. The spectra were collected at 633 nm laser excitation where a long band-pass filter, placed in the path of signal effectively cuts off the Rayleigh scattering. The signal was then dispersed using a 600 grooves per mm grating, and the dispersed light was collected by a Peltier-cooled charge coupled device. The other parameters of the instrument were kept as integration time, 70 *s* and accumulation, once. The background subtraction of spectrum was done using a second-order polynomial. All the Raman spectra were deconvoluted using OriginPro 9.0 software. A PerkinElmer FTIR spectrometer was used to measure the infrared spectra. The spectrometer resolution was kept at 4 cm^{-1}. Identification of the phase(s) of CM2LF sample was carried out by XRD (Bruker AXS, D8 Discover, USA) using the Cu Kα radiation at λ = 1.5418 Å. Various model building softwares were used to build the structures. The rectangular slab, nanosphere, and cube were built by using VESTA and Avogadro 1.2.0 software.

■ RESULTS AND DISCUSSION

Figure 1A shows a TEM image of CM2LF. It appears largely amorphous and continues to remain the same at ambient conditions even after extensive interaction with As(III) and As(V) spiked water. Upon continuous electron beam irradiation, lattice planes are seen under HRTEM due to beam induced crystallization (Figure 1B). Figure S9 shows the XRD data of CM2LF. It shows the 2-line ferrihydrite phase with characteristic features at 35.5° and 62.3° corresponding to the (110) and (115) planes. The observed lattice planes are in agreement with the Cambridge Crystallographic Database (CCD) (JCPDS, 46-1315).[37−39]

To understand the degree of protonation, polymerization, and speciation of As(III) and As(V) oxides[40] at room temperature, Raman spectra were measured at pH 7 (Figure 2Aa,Ab). As(III) in solution has two vibrational features at 703 and 656 cm^{-1} (Figure 2Aa) which correspond to the A_1 and E modes of H_3AsO_3 (C_{3v} symmetry when all OH groups are equivalent). The peak at 703 cm^{-1} corresponds to symmetric stretching (A_1) while the other peak at 656 cm^{-1} represents

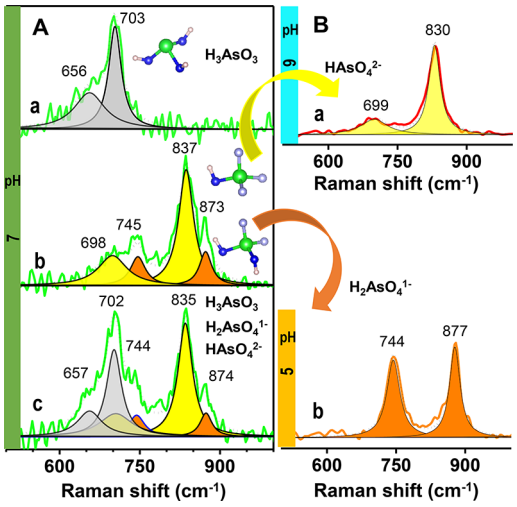

Figure 2. Raman spectra of aqueous arsenite and arsenate species. (A) Data at pH 7 for (a) As(III), (b) As(V), and (c) As(mix). Expanded view of As(V) showing different species at other pH values. (B) Most of the As(V) is in the form of (a) $HAsO_4^{2-}$ at pH 9 and as (b) $H_2AsO_4^{1-}$ at pH 5. Data have been fitted with their components.

the asymmetric stretching (E) of As−OH,[21] respectively. As(V) in solution shows four vibrational features (after deconvolution) at 873, 837, 745, and 698 cm^{-1} (Figure 2Ab). To understand the kind of speciation of As(III) and As(V) in the aqueous phase, we have performed the studies by varying pH, according to the pK_a value of their corresponding acids, and the data are shown in the Supporting Information, Figure S1. As(V) in solution exists as $H_2AsO_4^{1-}$ and $HAsO_4^{2-}$ species in the pH window of 5−9, as reported.[37,20,21] Species $H_2AsO_4^{1-}$ and $HAsO_4^{2-}$ belong to C_{2v} (when the OH groups are equivalent) and C_{3v} (when the OH group is considered as a moiety) point groups, respectively. C_{2v} has four vibrational modes, viz., A_1, A_2, B_1, and B_2 while C_{3v} has two vibrational modes, viz., A_1 and E which are Raman active. The vibrational modes of the species $H_2AsO_4^{1-}$ and $HAsO_4^{2-}$ were discussed by Müller et al.[21] As(V) solution was made at pH 5 and pH 9, separately. At pH 9, it shows two features at 830 and 699 cm^{-1} (Figure 2Ba) whereas at pH 5, they were observed at 877 and 744 cm^{-1} (Figure 2Bb). The higher frequency peaks of the spectra (at 830 and 877 cm^{-1}) correspond to the symmetric stretching of As═O, while the lower frequency peaks (699 and 744 cm^{-1}) represent the symmetric stretching of As−OH, respectively. With this explanation, we can assign the Figure

DOI: 10.1021/acssuschemeng.8b01217
ACS Sustainable Chem. Eng. XXXX, XXX, XXX−XXX

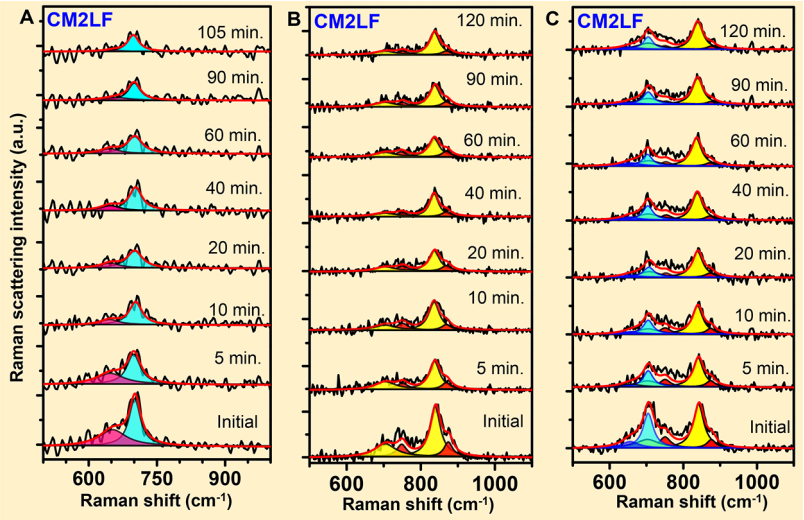

Figure 3. Time dependent Raman spectra of the interaction of CM2LF with (A) As(III), (B) As(V), and (C) As(mix).

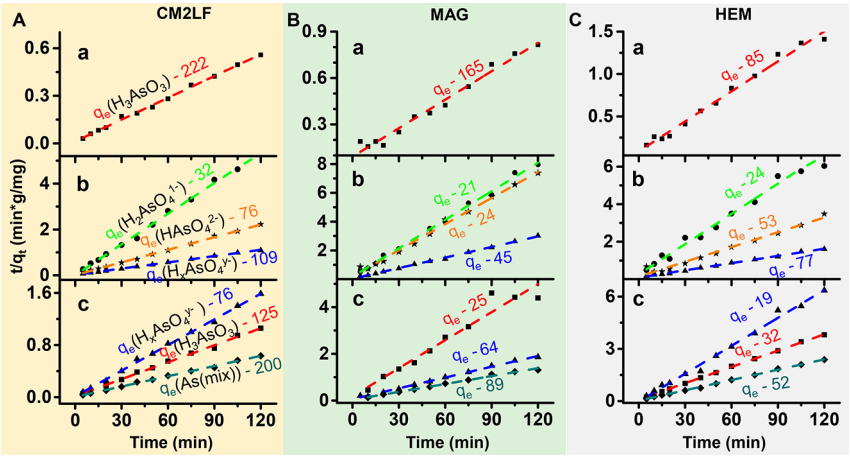

Figure 4. Pseudo-second-order kinetics graph for (A) CM2LF, (B) MAG, and (C) HEM, where plots a, b, and c represent As(III), As(V), and As(mix) removal, respectively. The unit of q_e and q_t is mg/g. The q_t of each data point was evaluated using eq 3 of Supporting Information 4.

2Ab vibrational frequencies 837, 698 and 873, 745 cm^{-1} to $HAsO_4^{2-}$ and $H_2AsO_4^{1-}$, respectively. In the case of As(mix) in solution, at pH 7, the observed six vibrational features (after deconvolution) are almost close to the vibrational frequencies of the individual As(III) and As(V) species (H_3AsO_3, $HAsO_4^{2-}$, and $H_2AsO_4^{1-}$) as discussed earlier. We did not see any additional features which also confirm that there are no adducts between As(III) and As(V) in solution as a result of mixing. Further details about As−O or As−OH stretching frequencies of arsenic oxides are discussed in Goldberg et al.[20]

The adsorption kinetics of various arsenic species in solution at pH 7 was studied for different materials, CM2LF, MAG, and HEM. The intensities of As(III), As(V), and As(mix) species decreased upon interaction with CM2LF with time, as shown in Figure 3. Similar decay in intensities of the arsenic species is seen in the case of MAG and HEM as shown in the Supporting Information, Figures S2 and S3, respectively. The data suggest that upon interaction with CM2LF, MAG, and HEM, the arsenic species in solution remained the same. Area under the peaks correspond to concentration in solution, and the data suggest that equilibrium is reached in 20 min as shown in Figure S4. The kinetic graphs in Figure S4A,B follow a pseudo-second-order expression. The similar data for MAG and HEM are shown in Figures S5 and S6, respectively. We observed that the concentration of As(III) and As(V) in solution reduced faster for CM2LF but not for MAG and HEM. Appropriate analyses of the data are presented in the Supporting Information.

Raman measurements of various concentrations of As(III) and As(V) are shown in the Supporting Information, Figure S7A,B, respectively. The correlation between the area under the peak and the concentration of As(III) and As(V) solutions are shown in Figure S7C,D, respectively. To understand the adsorption kinetics and uptake capacity, we plotted t/q_t versus t (Figure 4); the rate constants (k) and adsorption capacity (q_e) of all the materials were calculated using the slopes and intercepts of the plots. The results are tabulated in Table 1. Similar adsorption models for the uptake of arsenic have been reported earlier.[9,30,41]

The obtained rate constants for CM2LF and HEM are equal for As(III) adsorption but less for MAG (Table 1). We assume that this may due to the difference in availability of surface $-O^-/-OH$ groups on all three materials. While in the case of As(V), MAG shows faster kinetics in comparison to CM2LF and HEM, even though it shows less uptake of As(V). As we know that As(V) in solution exists as $H_2AsO_4^{1-}$ and $HAsO_4^{2-}$

DOI: 10.1021/acssuschemeng.8b01217
ACS Sustainable Chem. Eng. XXXX, XXX, XXX−XXX

Table 1. Adsorption Data in Terms of Initial Rates, Rate Constants, and Uptake of As at Equilibrium

adsorbate 150 mL	adsorbent (g)	species pH 7	q_e (mg/g) ± 5%	k (min(mg/g))$^{-1}$± 5%	initial rate $h = kq_e^2$ ± 10%	R^2
	CM2LF : 3 g	H_3AsO_3	222	1.5×10^{-3}	74	0.99
50 mM As(III)	MAG : 3 g	H_3AsO_3	165	0.4×10^{-3}	11	0.99
	HEM : 3 g	H_3AsO_3	85	1.5×10^{-3}	11	0.99
		$H_xAsO_4^{y-}$	109	5.0×10^{-3}	59	0.99
	CM2LF : 7 g	$H_2AsO_4^{1-}$	32	60.0×10^{-3}	61	0.99
		$HAsO_4^{2-}$	76	20.0×10^{-3}	115	0.99
		$H_xAsO_4^{y-}$	45	19.0×10^{-3}	38	0.98
40 mM As(V)	MAG : 7 g	$H_2AsO_4^{1-}$	21	25.0×10^{-3}	11	0.98
		$HAsO_4^{2-}$	24	17.0×10^{-3}	10	0.98
		$H_xAsO_4^{y-}$	77	2.0×10^{-3}	12	0.98
	HEM : 7 g	$H_2AsO_4^{1-}$	24	12.0×10^{-3}	7	0.98
		$HAsO_4^{2-}$	53	4.5×10^{-3}	13	0.98
		As(mix)	200	3.0×10^{-3}	120	0.99
	CM2LF : 5 g	H_3AsO_3	125	7.0×10^{-3}	109	0.99
		$H_xAsO_4^{y-}$	76	8.5×10^{-3}	49	0.99
		As(mix)	89	4.0×10^{-3}	32	0.99
50 mM As(mix)	MAG : 5 g	H_3AsO_3	25	5.0×10^{-3}	31	0.95
		$H_xAsO_4^{y-}$	64	12.0×10^{-3}	49	0.99
		As(mix)	52	13.0×10^{-3}	35	0.99
	HEM : 5 g	H_3AsO_3	32	13.0×10^{-3}	13	0.99
		$H_xAsO_4^{y-}$	20	40.0×10^{-3}	16	0.97

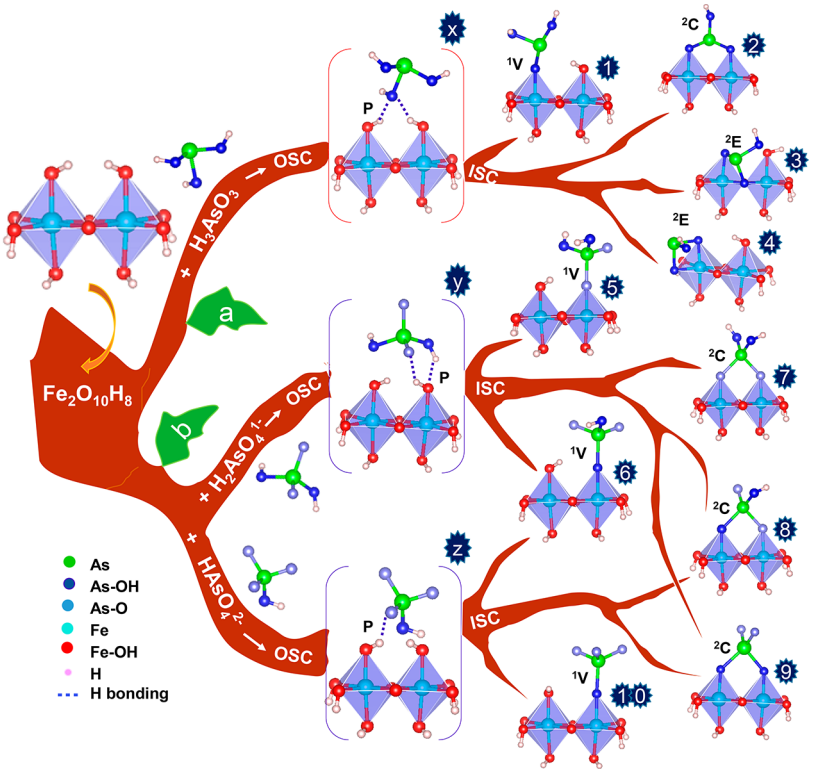

Figure 5. A model of As complexes with $Fe_2O_{10}H_8$ cluster. Path a, As(III) complexes and path b, As(V) complexes. OSC, outer sphere complexes (x, y, and z). ISC, inner sphere complexes (1 to 10). Transformation of OSC to ISC by ligand exchange is shown.

at pH 7, we were interested to know which species will have faster kinetics toward iron oxides/oxyhydroxides. Data of Table 1 reveal that $H_2AsO_4^{1-}$ shows higher rate constant than $HAsO_4^{2-}$ for CM2LF, MAG, and HEM at pH 7 irrespective of their different surface structures. Further studies were conducted using As(mix) and As(V), which showed higher rate constant than As(III). Thus, As(V) interaction with all the materials is faster in comparison to As(III) due to the difference in the species in the solution phase. As(V) shows faster adsorption kinetics as compared to As(III). It is due to As(V) ($H_2AsO_4^{1-}$/$HAsO_4^{2-}$) possessing more polarizable hydration sphere than As(III) (H_3AsO_3). Nucleophilicity

DOI: 10.1021/acssuschemeng.8b01217
ACS Sustainable Chem. Eng. XXXX, XXX, XXX−XXX

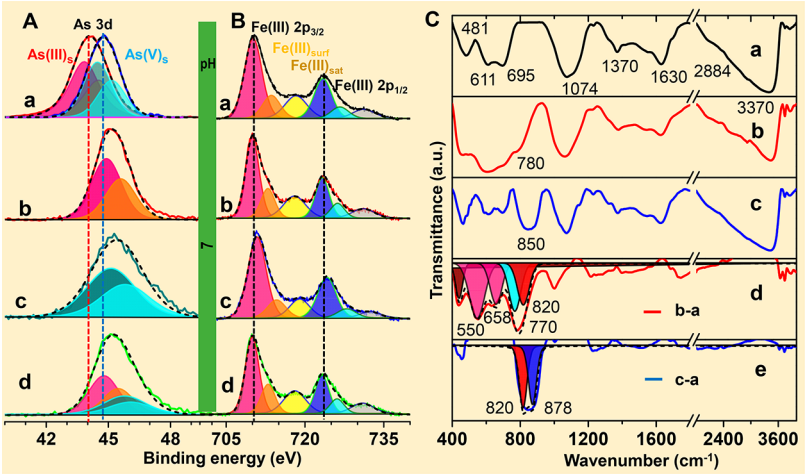

Figure 6. XPS spectrum of (A) As 3d and (B) Fe 2p. As 3d region of (A) (a) $NaAsO_2$ (red trace) and $Na_2HAsO_4{\cdot}7H_2O$ (blue trace). Comparison of the positions may be noted. (b) As(III), (c) As(V), and (d) As(mix) adsorbed on CM2LF. Spectra are fitted for the $3d_{5/2}$ and $3d_{3/2}$ features. (B) (a) CM2LF before adsorption, (b−d) Fe 2p after adsorption, as before. (C) FTIR spectra (a) CM2LF before adsorption. Spectra of (b) As(III) and (c) As(V) adsorbed materials. (d) Spectra after subtraction (curve b-a). (e) Spectra after subtraction (curve c-a).

plays an important role in the inner sphere complexation process (ligand exchange mechanism). More nucleophilic ligands ($-O^-$ > $-OH$) can easily replace the labile groups ($-OH/H_2O^+-$). In acidic pH, most of the singly coordinated oxygens are present on the surface of adsorbent in the form of $H_2O^+-/-OH$ groups. As the pH becomes basic, the singly coordinated oxygens change to $-OH/-O^-$. Thus, at pH 7, the surface of adsorbent can be composed of $H_2O^+-/-O^-/-OH$ groups. Repulsions existing between Fe−$\underline{O}^-$ (adsorbent) and As−$\underline{O}^-$ (adsorbate) groups are the cause of reduced adsorption of As(V) than As(III). As(V) has more nucleophilic ligands (−As−O^-) as compared to As(III) (−As−OH). Thus, we can conclude that nucleophilicity is one of the key factors leading to faster adsorption kinetics for As(V) than As(III) at pH 7. The effect of nuclophilicity of ligands and the difference in molecular basis of the adsorption process for As(III) and As(V) are shown in Figure S10.

Adsorption at equilibrium has shown that As(III) uptake is higher than As(V) for CM2LF and HEM (Table 1) and not for MAG. We believe that decrease in availability of adsorption sites for As(III) due to the initial occupation of them by As(V) and also pH of the solution are the major reasons for reduced uptake by MAG. Among the adsorbents studied, the rate constant is highest for MAG for As(V) uptake. It also shows the lowest rate constant for As(III) uptake (Table 1).

Effect of Competing Ions. We further studied the influence of competing ions on arsenic adsorption for CM2LF, MAG, and HEM to improve the application of materials for point-of-use water purification. We have considered the ions which are generally present in natural water: NO_3^-, CO_3^{2-}, PO_4^{3-}, SO_4^{2-}, Cl^-, and HCO_3^- and performed experiments for As(III) and As(V), separately. As(III) adsorption was more than that of As(V) for all the materials. The corresponding data are shown in Figure S11. CM2LF removes As(III) and As(V) effectively as compared to MAG and HEM even in the presence of competing ions. The data show that the influence of PO_4^{3-} ion was considerably higher than that of other ions for all the materials.

In the following, we present a model for the adsorption of arsenic species on CM2LF based on the data available. For this model, a unit of the substrate is considered. For FeOOH based materials, the $Fe_2O_{10}H_8$ unit, an edge share hydroxyl terminated bioctahedron is taken as the model system. Possible complexes that can be formed via ligand exchange mechanism upon the adsorption of As(III) and As(V) on this model cluster at pH 7 are shown in Figure 5. We may recall that the Fe_2O_{10} cluster is the common unit (two octahedra present in edge sharing fashion) of 2-line ferrihydrite, MAG and HEM. The oxide upon exposure to water will have hydroxylated surfaces making this model realistic. There are two kinds of adsorption geometries (physical and chemical) possible in the case of As species. Physical adsorption leads to outer sphere (physically bonded species (P) through hydrogen bonding) complexes while chemical adsorption result in inner sphere (chemically bonded) complexes. Most of the outer sphere complexes can transform to inner sphere complexes through ligand exchange mechanism as indicated by the pathways ("path a" and "path b"). In Figure 5, x, y and z represent the outer sphere complexes formed through hydrogen bonding between As species and iron oxides/oxyhydroxides as reported.[26,42] The inner sphere complexes are (1) monodentate mononuclear (^{1}V), (2) bidentate binuclear corner sharing (^{2}C), and (3) bidentate mononuclear/binuclear edge sharing (^{2}E). The ratio of outer to inner sphere complexes depend on the pH of the solution.[23,26] Complex 2 from Figure 5 ("path a") and complexes 7, 8, and 9 from Figure 5 ("path b") represent the ^{2}C complexes. The complexes 7, 8, and 9 are structurally similar and differ in the degree of protonation of As(V) species. As(III) and As(V) have more tendency to form ^{2}C complexes (thermodynamically favorable) than other possible structures[28,43,44] for all the adsorbents used in this work. Bidentate mononuclear edge sharing (^{2}E) complexes were found in the case of As(III) with ferrihydrite and HEM.[28] Complex 1 from Figure 5 ("path a") and complexes 5, 6, and 10 from Figure 5 ("path b") show monodentate mononuclear (^{1}V) complexes. These are found to increase in intensity noticeably at pH 7−10[23,22] in the case of As(III) and at pH 5−10[26,42] in the case of As(V) with iron oxides/oxyhydroxides.

The XPS analysis of arsenic standards in the solid form ($As(III)_s$ and $As(V)_s$, subscript "s" refers to solid state) are shown in Figure 6Aa, 7Aa, and Figure S8Aa. The measurements were done using standard arsenic compounds viz.,

DOI: 10.1021/acssuschemeng.8b01217
ACS Sustainable Chem. Eng. XXXX, XXX, XXX−XXX

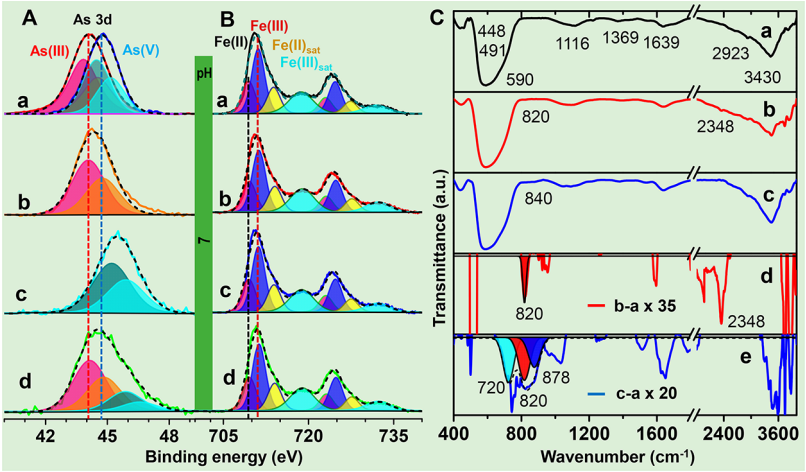

Figure 7. XPS spectrum of (A) As 3d and (B) Fe 2p. As 3d region of (A) (a) $NaAsO_2$ (red trace) and $Na_2HAsO_4{\cdot}7H_2O$ (blue trace). Comparison of the positions may be noted. (b) As(III), (c) As(V), and (d) As(mix) adsorbed on MAG. Spectra are fitted for the $3d_{5/2}$ and $3d_{3/2}$ features. (B) (a) MAG before adsorption, (b, c, and d) Fe 2p after adsorption, as before. (C) FTIR spectra (a) MAG before adsorption. Spectra of (b) As(III) and (c) As(V) adsorbed materials. (d) Spectra after subtraction (curve b-a). (e) Spectra after subtraction (curve c-a).

$NaAsO_2$ for As(III) and Na_2HAsO_4 for As(V). The As 3d peak appears at 44.2 and 44.8 eV for $As(III)_s$ and $As(V)_s$, respectively.[45] The As 3d peak was deconvoluted into $3d_{5/2}$ and $3d_{3/2}$, while Fe 2p was fitted with three pairs of peaks for CM2LF and HEM as reported.[46,47] The lower binding energy peak corresponds to −Fe−O−Fe− groups, the next higher one refers to surface >Fe−OH groups ($Fe(III)_{surf}$) followed by a satellite peak ($Fe(III)_{sat}$).[46] XPS data of each peak before and after arsenic (As(III), As(V), and As(mix)) interaction with all three materials used in this work are shown in Table S1. The standard As 3d peak was redshifted from 44.2 to 45.1 and 44.7 eV upon As(III) interaction with CM2LF (Figure 6Ab) and HEM (Supporting Information, Figure S8Ab), respectively. The observed results suggest that most of the H_3AsO_3 species on the surface of CM2LF and HEM are chemically bonded or may have got converted to As(V). In the case of As(V) adsorption on CM2LF and HEM, the As 3d peak redshifts from a value of 44.8 to 45.3 and 46.5 eV for CM2LF (Figure 6Ac) and HEM (Supporting Information, Figure S8Ac), respectively. The redshift of As 3d peak was higher in the case of HEM and lower for CM2LF (broaden to higher binding energy side). Lower redshift can refer to physically adsorbed and higher redshift can suggest chemically adsorbed species. The FTIR characteristic features of CM2LF before arsenic adsorption (Figure 6Ca) shows Fe−O stretching frequencies of 2-line ferrihydrite at 481, 611, and 695 cm^{-1}, respectively. Peaks at 1074, 1370, and 3370 cm^{-1} are due to asymmetric C−O−C stretching, N−H deformation, and N−H stretching of chitosan (the polymer used to make CM2LF), respectively. The C═O stretching of amide and C−H stretching of the polymer were noticed at 1630 and 2884 cm^{-1}, respectively, as reported by Kumar et al.[37] The peak at 3370 cm^{-1} suggest the stretching vibrations of adsorbed water and hydroxyl groups of CM2LF. The free H_3AsO_3 molecules in water show stretching vibrations of As−OH at 703 and 656 cm^{-1} (Figure 2Aa), which gives a new peak at 780 cm^{-1} upon interaction with CM2LF[26,28] due to which enhancement of Fe−O peaks of CM2LF was observed in the 600−700 cm^{-1} region. The enhancement may be due to the overlap of H_3AsO_3 (As−OH) stretching vibrations and Fe−O vibrations of CM2LF. This effect can be noticed from the subtracted spectrum, curve b-a of Figure 6Cd. The fitted curve b-a shows the adsorbed H_3AsO_3 features at 550, 658, and 770 cm^{-1}. The 770 cm^{-1} is due to chemically adsorbed species and the other two, 550 and 658 cm^{-1} suggest physically adsorbed (hydrogen bonded) H_3AsO_3 (As−OH stretching) on CM2LF. The results were supported by the work of Sverjensky et al.[23] and Fukushi et al.[26] These authors studied arsenic speciation on ferrihydrite surface using IR and extended X-ray adsorption fine structure (EXAFS) spectroscopies and applied the extended triple layer model (ETLM). The ^2C complexes dominate than the ^1V and P complexes for As(III) and As(V). In the present study, the ratio of physical to chemical adsorption is more for As(V) than for As(III) due to difference in the extent of deprotonation of arsenic species and increase of $-O^-$ groups on the surface of the adsorbent. The results suggest that the effect of pH is more on As(V) than As(III).

In the case of MAG, the Fe $2p_{3/2}$ was deconvoluted into four peaks which correspond to Fe(II), Fe(III) and two separate shakeup peaks for Fe(II) ($Fe(II)_{sat}$) and Fe(III) ($Fe(III)_{sat}$), respectively.[46,48] Similarly, the deconvolution was done for Fe $2p_{1/2}$. Upon As(III) interaction with MAG, no considerable change was observed in As 3d. The peak shifted from 44.2 to 44.3 eV (Figure 7Ab) while in the case of As(V), it redshifted from 44.8 to 45.5 eV (Figure 7Ac). Thus, we can conclude that most of the H_3AsO_3 species are physically adsorbed and $H_xAsO_4^{y-}$ species are chemically adsorbed on MAG. In both the cases, there was no considerable change in peak positions, intensity ratio, and fwhm of Fe(II) and Fe(III). These suggest that there was no conversion of Fe(II) to Fe(III) and vice versa. The characteristic features of MAG in FTIR before arsenic exposure (Figure 7Ca) shows the Fe−O stretching frequencies at 448, 491, and 590 cm^{-1}, respectively. Peaks at 1639 and 3430 cm^{-1} are due to bending and stretching vibrations of adsorbed water on MAG. Peak at 2348 cm^{-1} is due to free CO_2 in the spectrometer.

A peak at 820 cm^{-1} was found upon interaction of As(III) and As(V) with CM2LF and MAG. This feature due to Fe−O−As stretching vibrations of the bidentate binuclear (^2C) complex[49] occurs in the range of pH 7 to 9, which confirms that the arsenic species (H_3AsO_3 and $H_2AsO_4^{1-}$ and $HAsO_4^{2-}$) are forming the inner sphere complexes on the surface of these

DOI: 10.1021/acssuschemeng.8b01217
ACS Sustainable Chem. Eng. XXXX, XXX, XXX−XXX

Table 2. Correlation of Adsorption Models and Spectroscopic Data

adsorbate pH 7	adsorbent	As 3d shift (eV)	Fe $2p_{3/2}$ shift (eV)	IR features (cm^{-1})	suggested complexes[a]
As(III) (H_3AsO_3)	CM2LF	+ 0.9	0.1	820	complex 2
				550, 658	complex x
	MAG	+ 0.1	0		complex x
				820	complex 2/1
	HEM	+ 0.5	− 0.2		may be complex 2
As(V) ($HAsO_4^{2-}$/ $H_2AsO_4^{1-}$)	CM2LF	+ 0.5	+ 0.1	820	complex (7/8/9)
	MAG	+ 0.7	+ 0.3	820	complex (7/8/9)
				720	complex (y and z)
	HEM	+ 1.5	− 0.2		complex (7/8/9)

[a]Complexes refer to those in Figure 5, assigned on the basis of FTIR features and As 3d peak shift values.

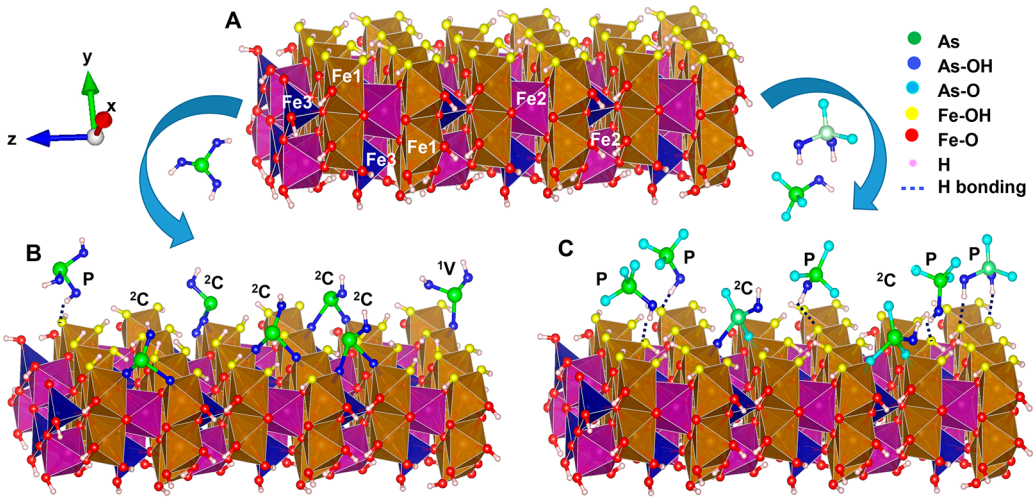

Figure 8. Schematic of a 110 plane of ferrihydrite at pH 7 (A) before adsorption, (B) after As(III) adsorption, and (C) after As(V) adsorption.

materials. CM2LF and MAG show a special feature at 878 cm^{-1} after As(V) adsorption which represents the As═O stretching vibrations[49] of $H_xAsO_4^{y-}$. Figures 6Ad, 7Ad, and Figure S8Ad show that As(III) is more interactive than As(V) at pH 7, in the case of As(mix). The results were supported by Raman data (Table 1). The correlation of adsorption models (Figure 5) and spectroscopic data (XPS and IR) based on the present work is summarized in Table 2.

The XPS data (Table 2) suggest that there is no considerable change in Fe 2p upon interaction with arsenic (As(III)/As(V)), which implies that the Fe atoms involved in the complexation did not undergo any chemical change for all the materials reported in this work. We assume that formation of the complexes follows the ligand exchange mechanism. The stability of the complexation of arsenic species with ferric hydroxides was reported by Farrell et al.[42] The stability of the complexes is in the order: bidentate binuclear (>$(FeO)_2AsOH$ ≈ ^2C) > monodentate mononuclear (>(FeO)−$As(OH)_2$ ≈ ^1V) > physical adsorption (P).

In the following, we discuss an understanding of the adsorption of arsenic species on CM2LF. In Figure 8, we used the unit cell parameters of 2-line ferrihydrite as reported in Michel et al.[39,50] to construct a rectangular slab having top and bottom surfaces parallel to the (110) plane of FeOOH (Figure 8A). The top surface contains oxygen atoms (in yellow). In general, the ferrihydrite structure has three symmetry-distinct Fe atoms. Here, we represented them as octahedra Fe1 center (dark yellow), octahedra Fe2 center (indigo), and tetrahedra Fe3 center (blue) as reported by Pinney et al.[50] The CM2LF $-O^-/-OH$ groups were shown in yellow/red, while arsenic attached $-O^-$ and −OH groups are marked in sky blue and blue, respectively. XPS and FTIR results suggest that arsenic species bind the surface Fe atoms through a ligand exchange mechanism, at pH 7. The results are supported by the literature.[23,21,24,25,20,26] In the ligand exchange mechanism, As$-O^-/-OH$ groups replace the Fe$-O^-/-OH$ groups. The formation of possible stable complexes of As(III) and As(V) with 2-line ferrihydrite are shown in Figure 8B,C, respectively. As(III) forms ^2C (major) and ^1V (minor) complexes while As(V) forms ^2C, ^1V (minor) and P (major) complexes.

We generated a 2-line ferrihydrite nanosphere of 2.6 nm in diameter (Figure 9A) and constructed a cube (Figure 9B) such that the surface area of the cube equals the surface area of the nanosphere ($6a^2 = 4\pi r^2$). The diameter chosen was to simulate the experiment. Possible sites for adsorption were counted as the number of singly coordinated oxy/hydroxy (Fe$-O^-/-$OH) groups from Fe1 (octahedral, blue color) and Fe2 (octahedral, yellow color) centers available on the surface of the nanosphere and cube. Only one site was counted if more than one site was present on the same center due to possible steric hindrance of the complexed species. Ideally, 86 sites were counted for the nanosphere and 54 sites were possible for the cube. We applied two constraints to get maximum arsenic uptake capacity of 2-line ferrihydrite. (1) All the particles (nanosphere or cube) were assumed to be well separated to make all the sites available for adsorption and (2) all the

DOI: 10.1021/acssuschemeng.8b01217
ACS Sustainable Chem. Eng. XXXX, XXX, XXX−XXX

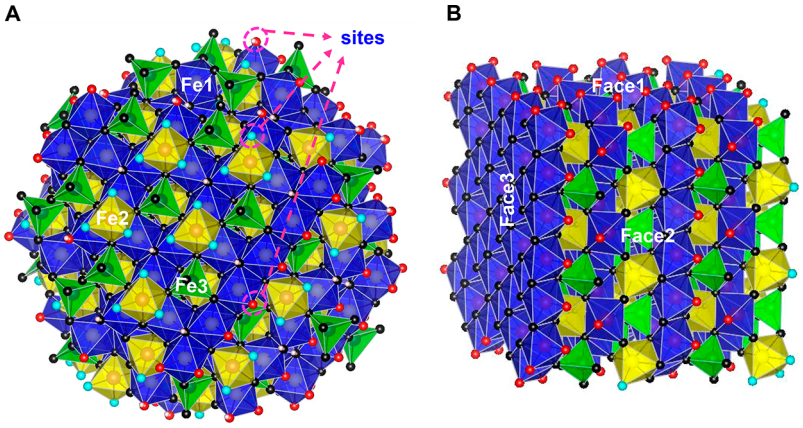

Figure 9. A generated nanosphere model of 2.6 nm diameter by using the unit cell parameters of 2-line ferrihydrite. Singly coordinated oxygens attached to the Fe1 and Fe2 centers are represented with red and sky blue colors, respectively. (B) A cube of the same sample using the information presented. We developed a model of a cubic particle of FeOOH with arsenic adsorption, such that its surface area is equal to the surface area of a 2.6 nm sphere.

arsenic species were attached to the surface Fe atoms as monodentate mononuclear (^{1}V) or bidentate mononuclear in an edge sharing (^{2}E) fashion assuming that one arsenic species should occupy one site and the other possible complexes (bidentate binuclear (^{2}C) and physical adsorption (P)) were excluded. The density of 2.6 nm particle is 3.5 g/cm^3 as reported.[51] Correspondingly, 32.21×10^{-21} g and 23.25×10^{-21} g are the masses of a single nanosphere and a cube, respectively, which are calculated using density and volume of the specific geometry (here the density of nanosphere and cube were assumed as equal). Further, 3.1×10^{19} nanospheres or 4.3×10^{19} cubes are needed to make 1 g of 2-line ferrihydrite. The total number of sites available on nanospheres ($3.1 \times 10^{19} \times 86 = 2.666 \times 10^{21} = 4.426 \times 10^{-3}$ moles of sites) or cubes ($4.3 \times 10^{19} \times 54 = 2.322 \times 10^{21} = 3.856 \times 10^{-3}$ moles of sites) for 1 g of 2-line ferrihydrite were calculated. In the case of nanospheres, ideally, the maximum adsorption capacities for As(III) and As(V) were about 557 and 620 mg/g (where all the sites fully occupied by H_3AsO_3 or $H_xAsO_4^{y-}$ species), respectively, while in the case of cubes, they were about 485 and 543 mg/g for As(III) and As(V), respectively. The theoretical calculations suggest that the shape and geometry of nanoparticle present in 2-line ferrihydrite can profoundly affect its uptake capacity. The experimental uptake capacity could reach almost half of the theoretical value.

CONCLUSIONS

Species-dependent arsenic adsorption on iron oxides/oxyhydroxides was investigated by Raman spectroscopy. Time dependent Raman measurements allowed us to understand an effective material for better arsenic uptake for various species, $H_2AsO_4^{1-}$ and $HAsO_4^{2-}$, at neutral pH. The studies suggested that their complexation with iron oxides/oxyhydroxides was driven by the ligand exchange mechanism which could lead to the formation of Fe−O−As bonds at neutral pH. Complementary data were obtained from vibrational spectroscopy. CM2LF showed the highest arsenic adsorption capacity than the commonly available polymorphs of iron oxides (MAG and HEM) at neutral pH. CM2LF showed effective removal of As(III) and As(V) in natural waters which supported its use in point-of-use water purification applications. Using the adsorption kinetics, understanding of the species present on the surfaces and speciation of arsenite and arsenate ions known previously, a model of an arsenic adsorbed nanoparticle of FeOOH was arrived at. This model explains observed results accurately.

ASSOCIATED CONTENT

Supporting Information

The Supporting Information is available free of charge on the ACS Publications website at DOI: 10.1021/acssuschemeng.8b01217.

Aqueous Raman spectra of arsenic speciation under various pH conditions; time dependent Raman spectra for the interaction of MAG and HEM with As species; representation of data in terms of area under the peak and concentration of species with time; XPS spectra of As 3d and Fe 2p before and after arsenic adsorption; XRD pattern of CM2LF; molecular basis model of the adsorption process; effect of competing ions on arsenic adsorption (PDF)

AUTHOR INFORMATION

Corresponding Author

*E-mail: pradeep@iitm.ac.in. Phone: +91-44 2257 4208. Fax: +91-44 2257 0545/0509.

ORCID

Avula Anil Kumar: 0000-0001-6878-8736

Thalappil Pradeep: 0000-0003-3174-534X

Notes

The authors declare no competing financial interest.

ACKNOWLEDGMENTS

The authors thank Mohd. Azhardin Ganayee and Tripti Ahuja for their technical support in conducting the Raman measurements. The authors also thank Ganesan Paramasivam for his help in constructing a 2.6 nm sphere of 2-line ferrihydrite. Radha Gobinda Bhuin who is currently working at University Erlangen-Nürnberg, Egerlandstrasse, Germany, Sophisticated Analytical Instrument Facility at IIT Madras is thanked for the FTIR measurements. The authors thank the Department of Science and Technology (Government of India) for constantly supporting our research program on nanomaterials.

DOI: 10.1021/acssuschemeng.8b01217
ACS Sustainable Chem. Eng. XXXX, XXX, XXX−XXX

REFERENCES

(1) *Guidelines for Drinking-Water Quality*; WHO Press, World Health Organization: Switzerland, 2011.

(2) Amini, M.; Abbaspour, K. C.; Berg, M.; Winkel, L.; Hug, S. J.; Hoehn, E.; Yang, H.; Johnson, C. A. Statistical modeling of global geogenic arsenic contamination in groundwater. *Environ. Sci. Technol.* **2008**, *42* (10), 3669.

(3) Bhattacharya, P., Polya, D., Jovanovic, D., Eds. *Best Practice Guide on the Control of Arsenic in Drinking Water*; IWA Publishing: London, 2017; DOI: 10.2166/9781780404929.

(4) Mahler, J.; Persson, I.; Herbert, R. B. Hydration of arsenic oxyacid species. *Dalton Transactions* **2013**, *42* (5), 1364.

(5) Yan, W.; Vasic, R.; Frenkel, A. I.; Koel, B. E. Intraparticle reduction of arsenite (As(III)) by nanoscale zerovalent iron (nZVI) investigated with in situ X-ray absorption spectroscopy. *Environ. Sci. Technol.* **2012**, *46* (13), 7018.

(6) Raven, K. P.; Jain, A.; Loeppert, R. H. Arsenite and arsenate adsorption on ferrihydrite: Kinetics, equilibrium, and adsorption envelopes. *Environ. Sci. Technol.* **1998**, *32* (3), 344.

(7) Mota, A. M.; Pinheiro, J. P.; Simões Gonçalves, M. L. Electrochemical methods for speciation of trace elements in marine waters. Dynamic Aspects. *J. Phys. Chem. A* **2012**, *116* (25), 6433.

(8) Ahmad, A.; et al. Arsenic Remediation of Drinking Water: An Overview. In *Best Practice Guide on the Control of Arsenic in Drinking Water*; Bhattacharya, P., Polya, D., Jovanovic, D., Eds.; IWA Publishing: London, 2017; DOI: 10.2166/9781780404929_079.

(9) Kumar, S.; Nair, R. R.; Pillai, P. B.; Gupta, S. N.; Iyengar, M. A. R.; Sood, A. K. Graphene oxide−MnFe2O4 magnetic nanohybrids for efficient removal of lead and arsenic from water. *ACS Appl. Mater. Interfaces* **2014**, *6* (20), 17426.

(10) Habuda-Stanić, M.; Nujić, M. Arsenic removal by nanoparticles: a review. *Environ. Sci. Pollut. Res.* **2015**, *22* (11), 8094.

(11) Pena, M.; Meng, X.; Korfiatis, G. P.; Jing, C. Adsorption mechanism of arsenic on nanocrystalline titanium dioxide. *Environ. Sci. Technol.* **2006**, *40* (4), 1257.

(12) Litter, M. I. Last advances on TiO2-photocatalytic removal of chromium, uranium and arsenic. *Current Opinion in Green and Sustainable Chemistry* **2017**, *6*, 150.

(13) Tang, W.; Su, Y.; Li, Q.; Gao, S.; Shang, J. K. Superparamagnetic magnesium ferrite nanoadsorbent for effective arsenic (III, V) removal and easy magnetic separation. *Water Res.* **2013**, *47* (11), 3624.

(14) Luo, X.; Wang, C.; Wang, L.; Deng, F.; Luo, S.; Tu, X.; Au, C. Nanocomposites of graphene oxide-hydrated zirconium oxide for simultaneous removal of As(III) and As(V) from water. *Chem. Eng. J.* **2013**, *220* (Supplement C), 98.

(15) La, D. D.; Patwari, J. M.; Jones, L. A.; Antolasic, F.; Bhosale, S. V. Fabrication of a GNP/Fe−Mg binary oxide composite for effective removal of arsenic from aqueous solution. *ACS Omega* **2017**, *2* (1), 218.

(16) Lin, S.; Yang, H.; Na, Z.; Lin, K. A novel biodegradable arsenic adsorbent by immobilization of iron oxyhydroxide (FeOOH) on the root powder of long-root Eichhornia crassipes. *Chemosphere* **2018**, *192*, 258.

(17) Gustafsson, J. P.; Bhattacharya, P. Geochemical modelling of arsenic adsorption to oxide surfaces. *Trace Metals and other Contaminants in the Environment* **2007**, *9*, 159.

(18) Dzombak, D. A.; Morel, F. M. M. *Surface Complexation Modeling: Hydrous Ferric Oxide*; John Wiley and Sons: New York, 1990.

(19) Hiemstra, T.; Van Riemsdijk, W. H. A surface structural approach to ion adsorption: The charge distribution (CD) model. *J. Colloid Interface Sci.* **1996**, *179* (2), 488.

(20) Goldberg, S.; Johnston, C. T. Mechanisms of arsenic adsorption on amorphous oxides evaluated using macroscopic measurements, vibrational spectroscopy, and surface complexation modeling. *J. Colloid Interface Sci.* **2001**, *234* (1), 204.

(21) Müller, K.; Ciminelli, V. S. T.; Dantas, M. S. S.; Willscher, S. A comparative study of As(III) and As(V) in aqueous solutions and adsorbed on iron oxy-hydroxides by Raman spectroscopy. *Water Res.* **2010**, *44* (19), 5660.

(22) Wang, Y.; Morin, G.; Ona-Nguema, G.; Juillot, F.; Guyot, F.; Calas, G.; Brown, G. E. Evidence for different surface speciation of arsenite and arsenate on green rust: An EXAFS and XANES study. *Environ. Sci. Technol.* **2010**, *44* (1), 109.

(23) Sverjensky, D. A.; Fukushi, K. A predictive model (ETLM) for As(III) adsorption and surface speciation on oxides consistent with spectroscopic data. *Geochim. Cosmochim. Acta* **2006**, *70* (15), 3778.

(24) Arts, D.; Abdus Sabur, M.; Al-Abadleh, H. A. Surface interactions of aromatic organoarsenical compounds with hematite nanoparticles using ATR-FTIR: Kinetic studies. *J. Phys. Chem. A* **2013**, *117* (10), 2195.

(25) ThomasArrigo, L. K.; Mikutta, C.; Byrne, J.; Barmettler, K.; Kappler, A.; Kretzschmar, R. Iron and arsenic speciation and distribution in organic flocs from streambeds of an arsenic-enriched peatland. *Environ. Sci. Technol.* **2014**, *48* (22), 13218.

(26) Fukushi, K.; Sverjensky, D. A. A predictive model (ETLM) for arsenate adsorption and surface speciation on oxides consistent with spectroscopic and theoretical molecular evidence. *Geochim. Cosmochim. Acta* **2007**, *71* (15), 3717.

(27) Bhandari, N.; Reeder, R. J.; Strongin, D. R. Photoinduced oxidation of arsenite to arsenate on ferrihydrite. *Environ. Sci. Technol.* **2011**, *45* (7), 2783.

(28) Ona-Nguema, G.; Morin, G.; Juillot, F.; Calas, G.; Brown, G. E. EXAFS analysis of arsenite adsorption onto two-line ferrihydrite, hematite, goethite, and lepidocrocite. *Environ. Sci. Technol.* **2005**, *39* (23), 9147.

(29) Jubb, A. M.; Allen, H. C. Vibrational spectroscopic characterization of hematite, maghemite, and magnetite thin films produced by vapor deposition. *ACS Appl. Mater. Interfaces* **2010**, *2* (10), 2804.

(30) Chandra, V.; Park, J.; Chun, Y.; Lee, J. W.; Hwang, I.-C.; Kim, K. S. Water-dispersible magnetite-reduced graphene oxide composites for arsenic removal. *ACS Nano* **2010**, *4* (7), 3979.

(31) Rout, K.; Mohapatra, M.; Anand, S. 2-Line ferrihydrite: synthesis, characterization and its adsorption behaviour for removal of Pb(ii), Cd(ii), Cu(ii) and Zn(ii) from aqueous solutions. *Dalton Trans.* **2012**, *41* (11), 3302.

(32) Sengupta, A.; Mallick, S.; Bahadur, D. Tetragonal nanostructured zirconia modified hematite mesoporous composite for efficient adsorption of toxic cations from wastewater. *J. Environ. Chem. Eng.* **2017**, *5* (5), 5285.

(33) Carabante, I.; Mouzon, J.; Kumpiene, J.; Gran, M.; Fredriksson, A.; Hedlund, J. Reutilization of porous sintered hematite bodies as effective adsorbents for arsenic(V) removal from water. *Ind. Eng. Chem. Res.* **2014**, *53* (32), 12689.

(34) Shipley, H. J.; Engates, K. E.; Guettner, A. M. Study of iron oxide nanoparticles in soil for remediation of arsenic. *J. Nanopart. Res.* **2011**, *13* (6), 2387.

(35) Alijani, H.; Shariatinia, Z. Effective aqueous arsenic removal using zero valent iron doped MWCNT synthesized by in situ CVD method using natural α-Fe2O3 as a precursor. *Chemosphere* **2017**, *171* (Supplement C), 502.

(36) Rashid, M.; Sterbinsky, G. E.; Pinilla, M. Á. G.; Cai, Y.; O'Shea, K. E. Kinetic and mechanistic evaluation of inorganic arsenic species adsorption onto humic acid grafted magnetite nanoparticles. *J. Phys. Chem. C* **2018**, ASAP, DOI: 10.1021/acs.jpcc.7b12438.

(37) Kumar, A. A.; Som, A.; Longo, P.; Sudhakar, C.; Bhuin, R. G.; Gupta, S. S.; Anshup; Sankar, M. U.; Chaudhary, A.; Kumar, R.; Pradeep, T. Confined metastable 2-line ferrihydrite for affordable point-of-use arsenic-free drinking water. *Adv. Mater.* **2017**, *29* (7), 1604260.

(38) Towe, K. M.; Bradley, W. F. Mineralogical constitution of colloidal "hydrous ferric oxides. *J. Colloid Interface Sci.* **1967**, *24* (3), 384.

(39) Michel, F. M.; Ehm, L.; Antao, S. M.; Lee, P. L.; Chupas, P. J.; Liu, G.; Strongin, D. R.; Schoonen, M. A. A.; Phillips, B. L.; Parise, J. B. The structure of ferrihydrite, a nanocrystalline material. *Science* **2007**, *316* (5832), 1726.

DOI: 10.1021/acssuschemeng.8b01217
ACS Sustainable Chem. Eng. XXXX, XXX, XXX−XXX

(40) Gout, R.; Pokrovski, G.; Schott, J.; Zwick, A. Raman spectroscopic study of arsenic speciation in aqueous solutions up to 275°C. *J. Raman Spectrosc.* **1997**, *28* (9), 725.
(41) Yang, J.-C.; Yin, X.-B. CoFe2O4@MIL-100(Fe) hybrid magnetic nanoparticles exhibit fast and selective adsorption of arsenic with high adsorption capacity. *Sci. Rep.* **2017**, *7*, 40955.
(42) Farrell, J.; Chaudhary, B. K. Understanding arsenate reaction kinetics with ferric hydroxides. *Environ. Sci. Technol.* **2013**, *47* (15), 8342.
(43) Liu, C.-H.; Chuang, Y.-H.; Chen, T.-Y.; Tian, Y.; Li, H.; Wang, M.-K.; Zhang, W. Mechanism of arsenic adsorption on magnetite nanoparticles from water: Thermodynamic and spectroscopic studies. *Environ. Sci. Technol.* **2015**, *49* (13), 7726.
(44) Catalano, J. G.; Zhang, Z.; Park, C.; Fenter, P.; Bedzyk, M. J. Bridging arsenate surface complexes on the hematite (012) surface. *Geochim. Cosmochim. Acta* **2007**, *71* (8), 1883.
(45) Wagner, C. D.; Riggs, W. M.; Davis, L. E.; Moulder, J. F.; Mullenberg, G. E. *Handbook of X-ray Photoelectron Spectroscopy*; Physical Electronics Division, Perkin-Elmer Corporation: Minnesota, 1979.
(46) Grosvenor, A. P.; Kobe, B. A.; Biesinger, M. C.; McIntyre, N. S. Investigation of multiplet splitting of Fe 2p XPS spectra and bonding in iron compounds. *Surf. Interface Anal.* **2004**, *36* (12), 1564.
(47) Gupta, R. P.; Sen, S. K. Calculation of multiplet structure of core p -vacancy levels. II. *Phys. Rev. B* **1975**, *12* (1), 15.
(48) Beji, Z.; Sun, M.; Smiri, L. S.; Herbst, F.; Mangeney, C.; Ammar, S. Polyol synthesis of non-stoichiometric Mn-Zn ferrite nanocrystals: structural /microstructural characterization and catalytic application. *RSC Adv.* **2015**, *5* (80), 65010.
(49) Jia, Y.; Xu, L.; Wang, X.; Demopoulos, G. P. Infrared spectroscopic and X-ray diffraction characterization of the nature of adsorbed arsenate on ferrihydrite. *Geochim. Cosmochim. Acta* **2007**, *71* (7), 1643.
(50) Pinney, N.; Kubicki, J. D.; Middlemiss, D. S.; Grey, C. P.; Morgan, D. Density functional theory study of ferrihydrite and related Fe-oxyhydroxides. *Chem. Mater.* **2009**, *21* (24), 5727.
(51) Hiemstra, T.; Van Riemsdijk, W. H. A surface structural model for ferrihydrite I: Sites related to primary charge, molar mass, and mass density. *Geochim. Cosmochim. Acta* **2009**, *73* (15), 4423.

DOI: 10.1021/acssuschemeng.8b01217
ACS Sustainable Chem. Eng. XXXX, XXX, XXX−XXX

Supporting Information

Species-specific uptake of arsenic on confined metastable 2-line ferrihydrite: A combined Raman-XPS investigation of the adsorption mechanism

Chennu Sudhakar,[†] Avula Anil Kumar,[†] Radha Gobinda Bhuin,[†] Soujit Sen Gupta,[†] Ganapati Natarajan[†] and Thalappil Pradeep[,†]*

[†] DST Unit of Nanoscience (DST UNS) and Thematic Unit of Excellence (TUE), Department of Chemistry, Indian Institute of Technology Madras, Chennai 600036, India.

* Corresponding author

Thalappil Pradeep: pradeep@iitm.ac.in

Thalappil Pradeep, DST Unit of Nanoscience (DST UNS) and Thematic Unit of Excellence (TUE), Department of Chemistry, Indian Institute of Technology Madras, Chennai 600036, India.

Tel.: +91-44 2257 4208; Fax: +91-44 2257 0545/0509

SUPPORTING INFORMATION CONTENT

Total number of pages: 17

Total number of figures: 11

Total number of tables: 1

TABLE OF CONTENTS

Sl. No.	Items	Description	Page No.
1	Supporting Information 1	Aqueous Raman spectra of arsenic species at various pH	3
2	Supporting Information 2	Time dependent Raman spectra for the interaction of MAG with As	4
3	Supporting Information 3	Time dependent Raman spectra for the interaction of HEM with As	5
4	Supporting Information 4	Reflection of Figure 3 data expressed in terms of area under the peak and concentration of species with time	6
5	Supporting Information 5	Reflection of Figure S2 data expressed in terms of area under the peak and concentration of species with time	8
6	Supporting Information 6	Reflection of Figure S3 data expressed in terms of area under the peak and concentration of species with time	9
7	Supporting Information 7	The correlation between area under the peak and concentration of species present in solution	10
8	Supporting Information 8	XPS spectra of As 3d and Fe 2p of HEM before and after arsenic adsorption	12
9	Supporting Information 9	The XRD pattern of CM2LF	13
10	Supporting Information 10	The molecular basis model of the adsorption process	14
11	Supporting Information 11	The effect of competing ions on arsenic adsorption	16

12	Supporting Table 1	XPS data of before and after arsenic adsorption	17

Supporting Information 1

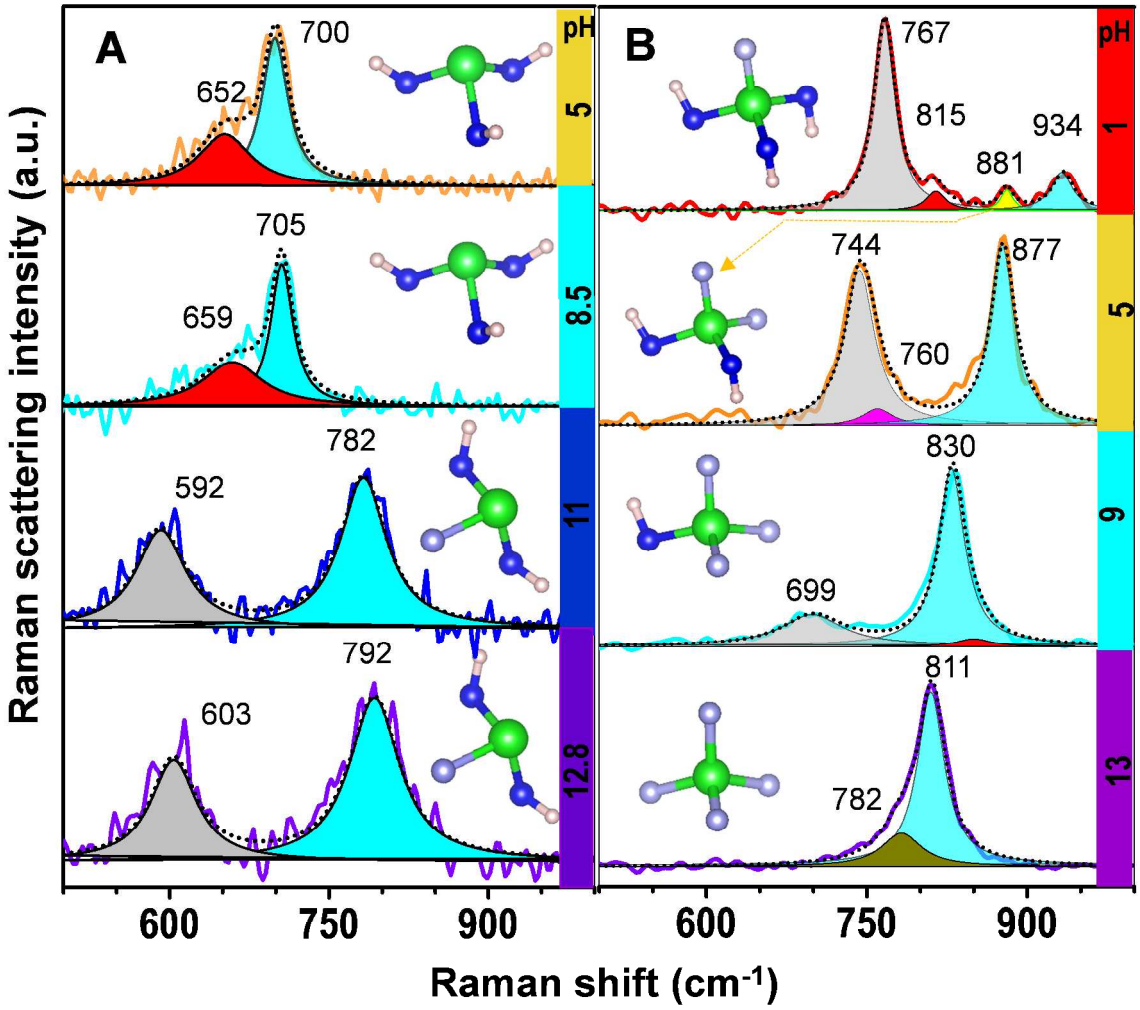

Figure S1. Aqueous Raman spectra. A) As(III)), B) As(V) speciation under various pH conditions. pH values are indicated on the right.

Supporting Information 2

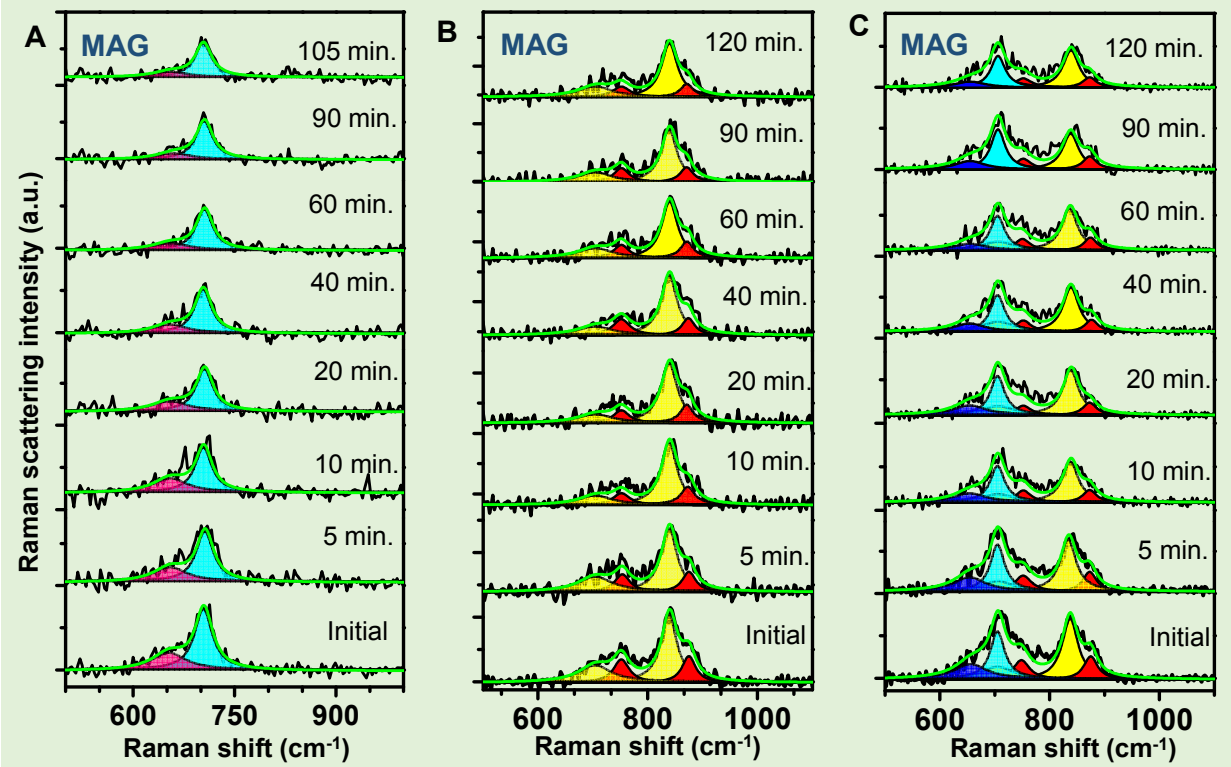

Figure S2. Time dependent Raman spectra for the interaction of MAG with A) As(III), B) As(V) and C) As(mix). Peaks have been fitted with their components.

Supporting Information 3

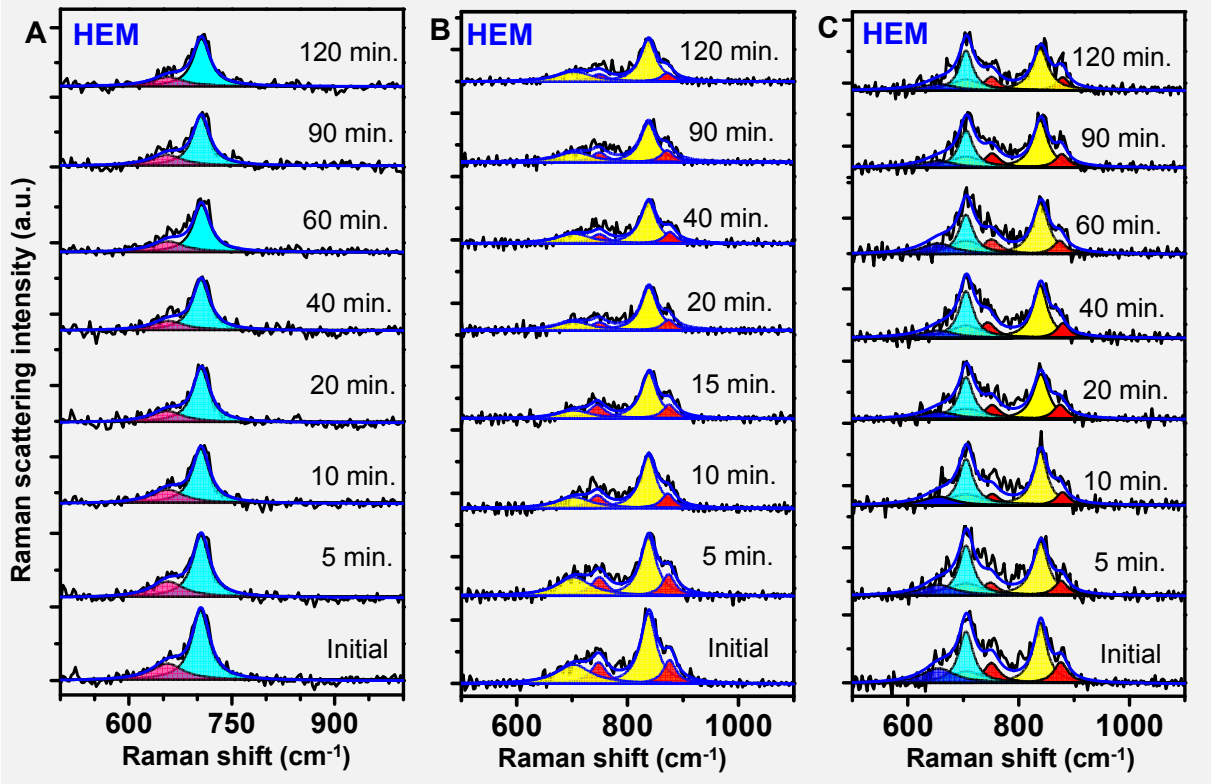

Figure S3. Time dependent Raman spectra for the interaction of HEM with A) As(III), B) As(V) and C) As(mix). Peaks have been fitted with their components.

Supporting Information 4

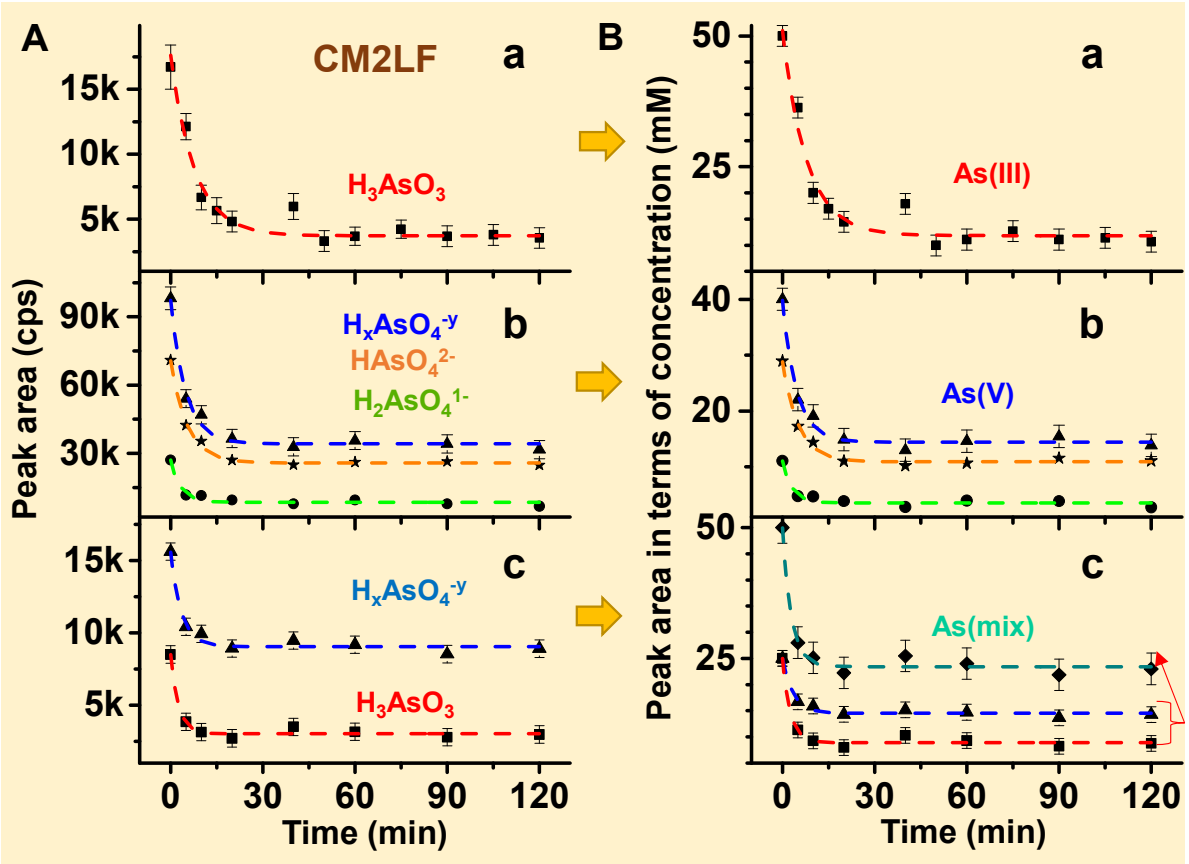

Figure S4. Representation of data presented in Figure 3 in terms of area under the peak (A) and concentration of species (B).

Adsorption kinetics can be expressed by using pseudo-second-order equation:

$$\frac{dq_t}{dt} = k(q_e - q_t)^2 \qquad \text{Equation (1)}$$

Where, q_t is the adsorption capacity of given material at time t, q_e is the adsorption capacity of the material at equilibrium and k is the pseudo-second-order rate constant, where initial rate is h = k${q_e}^2$. Integration of equation (1) with limits t = 0 to t and applying boundary conditions q_t = 0 at t = 0 gives,

$$\frac{t}{q_t} = (\frac{1}{q_e})t + \frac{1}{k{q_e}^2} \qquad \text{Equation (2)}$$

The values of k and q_e can be calculated by plotting t/q_t versus t.

Conversion of concentration of solution (mM) into q_t:

Concentration of solution (x) → $xM_{wt} \approx C_t$

M_{wt} is the molecular weight of arsenic species present in solution.

$$q_t = \left(\frac{C_0 - C_t}{m}\right)V \qquad \text{Equation (3)}$$

Where, C_0 (mg/g) is the concentration of solution at time t = 0, C_t (mg/g) is the concentration of solution at time t, V is the volume of solution in liters (L) and m is the mass of material used in grams (g).

Supporting Information 5

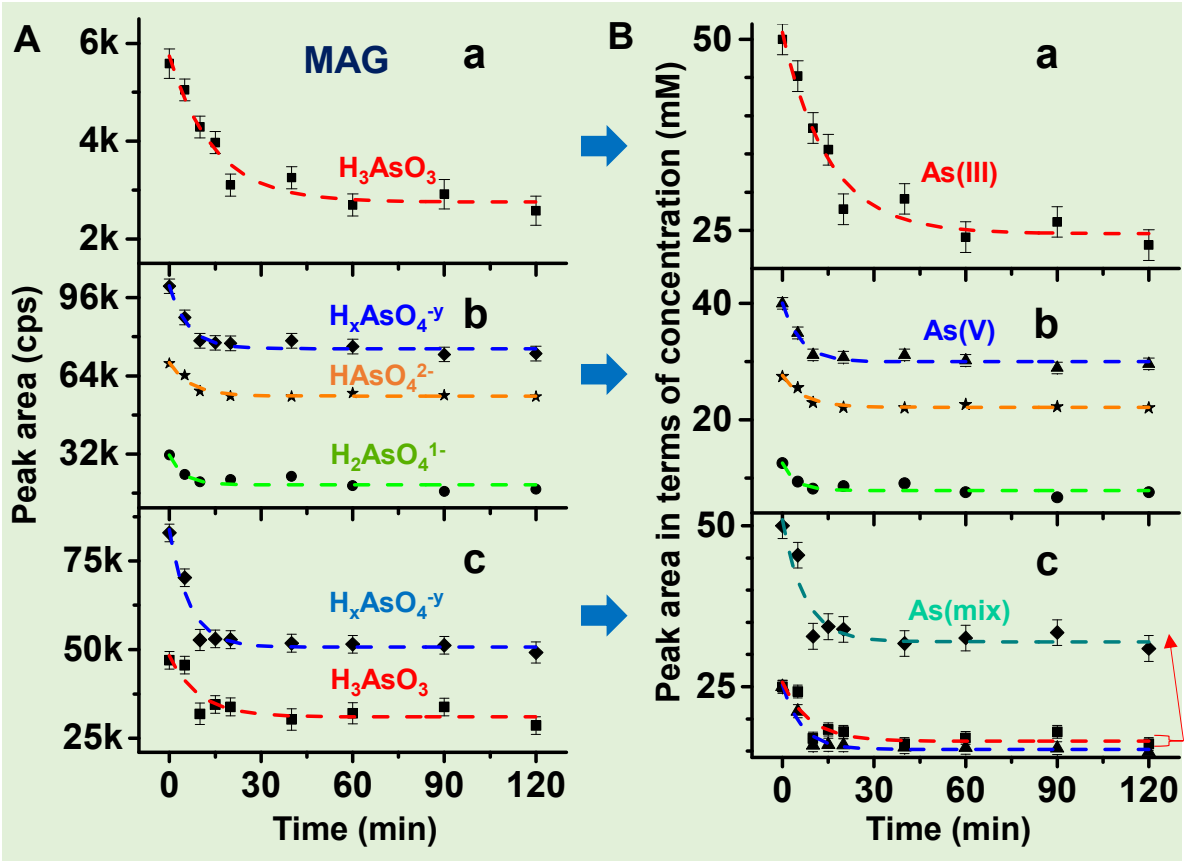

Figure S5. Representation of data presented in Figure S2 in terms of area under the peak (A) and concentration of species (B).

Supporting Information 6

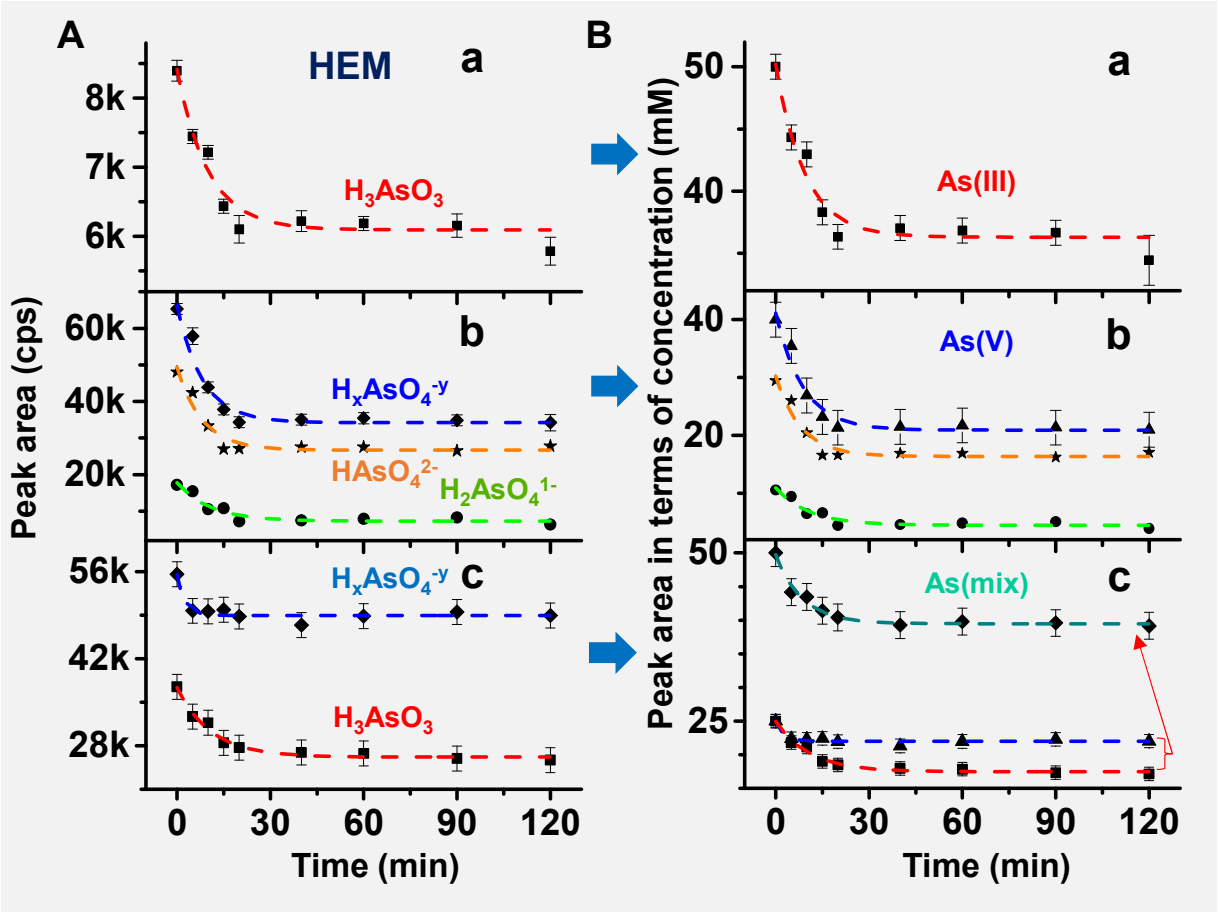

Figure S6. Representation of data presented in Figure S3 in terms of area under the peak (A) and concentration of species (B).

Supporting Information 7

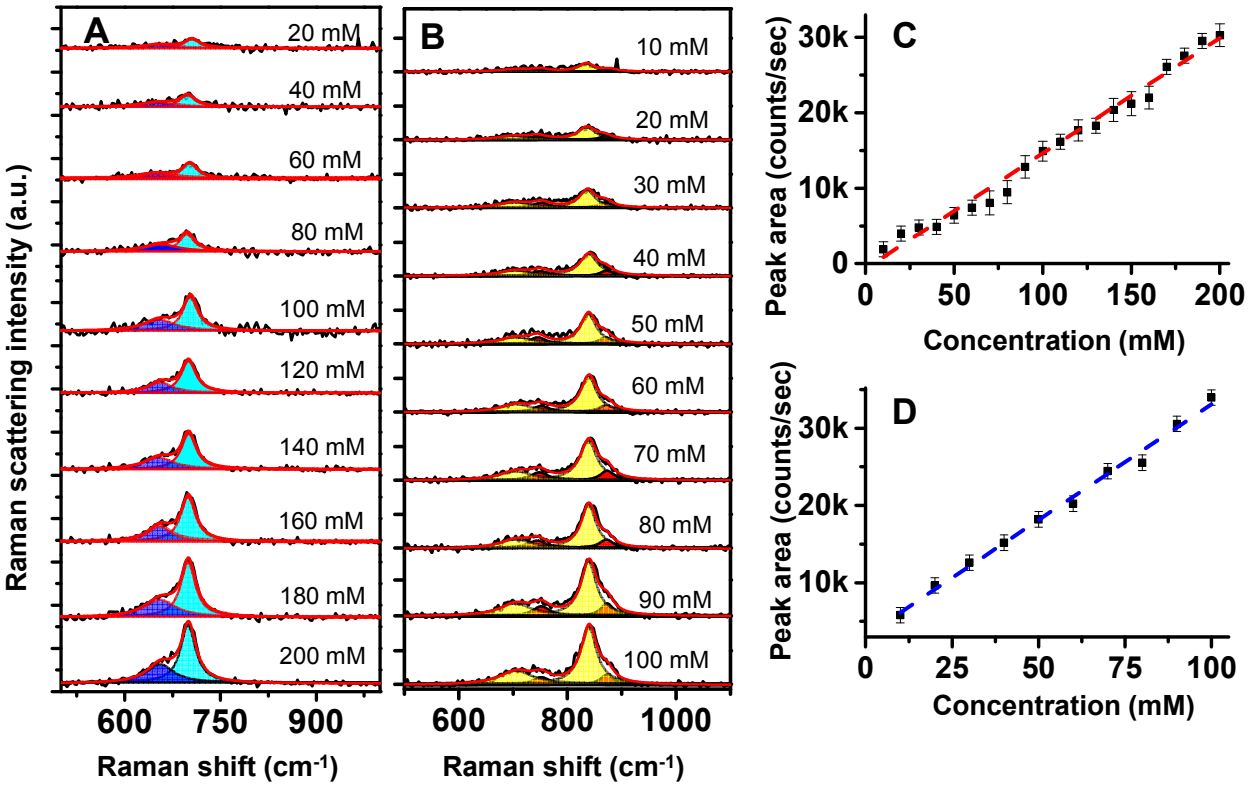

Figure S7. A) and B) Raman spectra for the various concentrations of pure As(III) and As(V) solutions at pH 7. C) Representation of data presented in A and D) Representation of data presented in B in terms of area under the peak Vs concentration of the species. Peaks have been fitted with their components.

The correlation between area under the peak and concentration of solution:

$$y = mx + c \qquad \text{Equation (4)}$$

Equation 4 can be applied for both As(III) and As(V) solutions.

Where, y is area under the peak, x is concentration of the solution (mM), c is the y intercept and m is slope of line of the plot of y versus x. For calculating the unknown concentrations of solution, the (x, y) data points of line in Figure S7C and FigureS7D were taken as reference for As(III) and As(V), respectively.

To find unknown concentration of solution (x_u):

$$x_u = \left(\frac{y_m - C}{m}\right) \qquad \text{Equation (5)}$$

y_m is area under the peak of unknown solution multiplied with laser intensity correction factor (K). K values vary with Raman measurement parameters during experiment. The each set of experimental data have different K value. K defined based on reference (x, y) data and the initial concentration of solution data (x_0, y_0).

Supporting Information 8

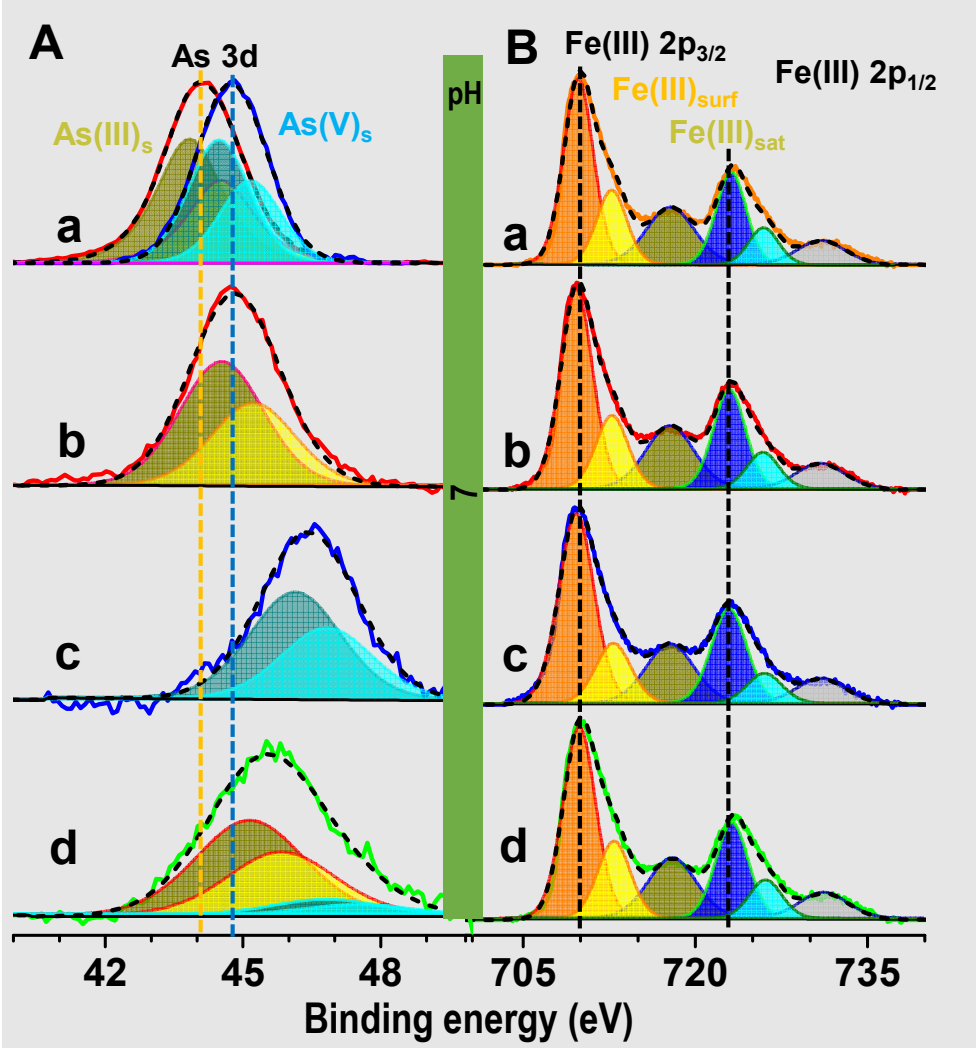

Figure S8. XPS spectrum of A) As 3d and B) Fe 2p. As 3d region of Aa) $NaAsO_2$ (red trace) and $Na_2HAsO_4.7H_2O$ (blue trace). Comparison of the positions may be noted. b) As(III), c) As(V) and d) As(mix) adsorbed on HEM. Spectra are fitted for the $3d_{5/2}$ and $3d_{3/2}$ features. Ba) HEM before adsorption, b), c) and d) are Fe 2p after adsorption, as before. Peaks have been fitted with their components.

Supporting information 9

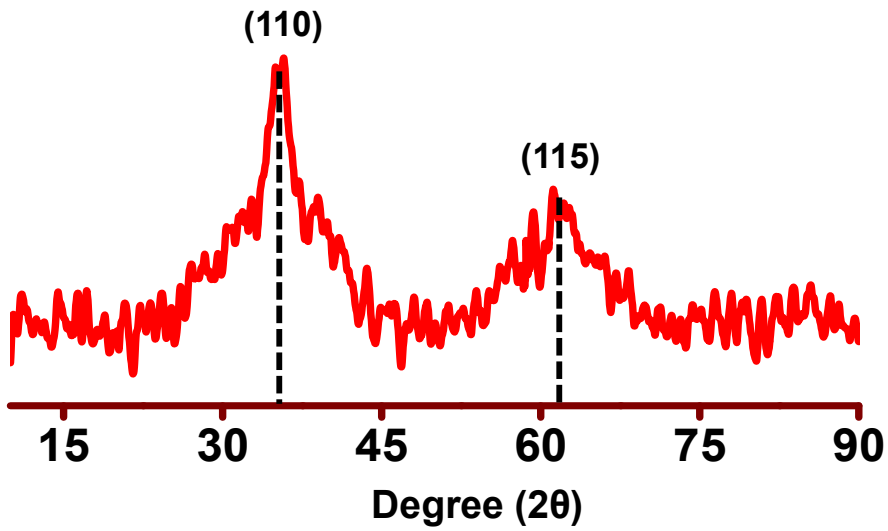

Figure S9. XRD pattern of CM2LF. Specific lines are labeled.

Supporting information 10

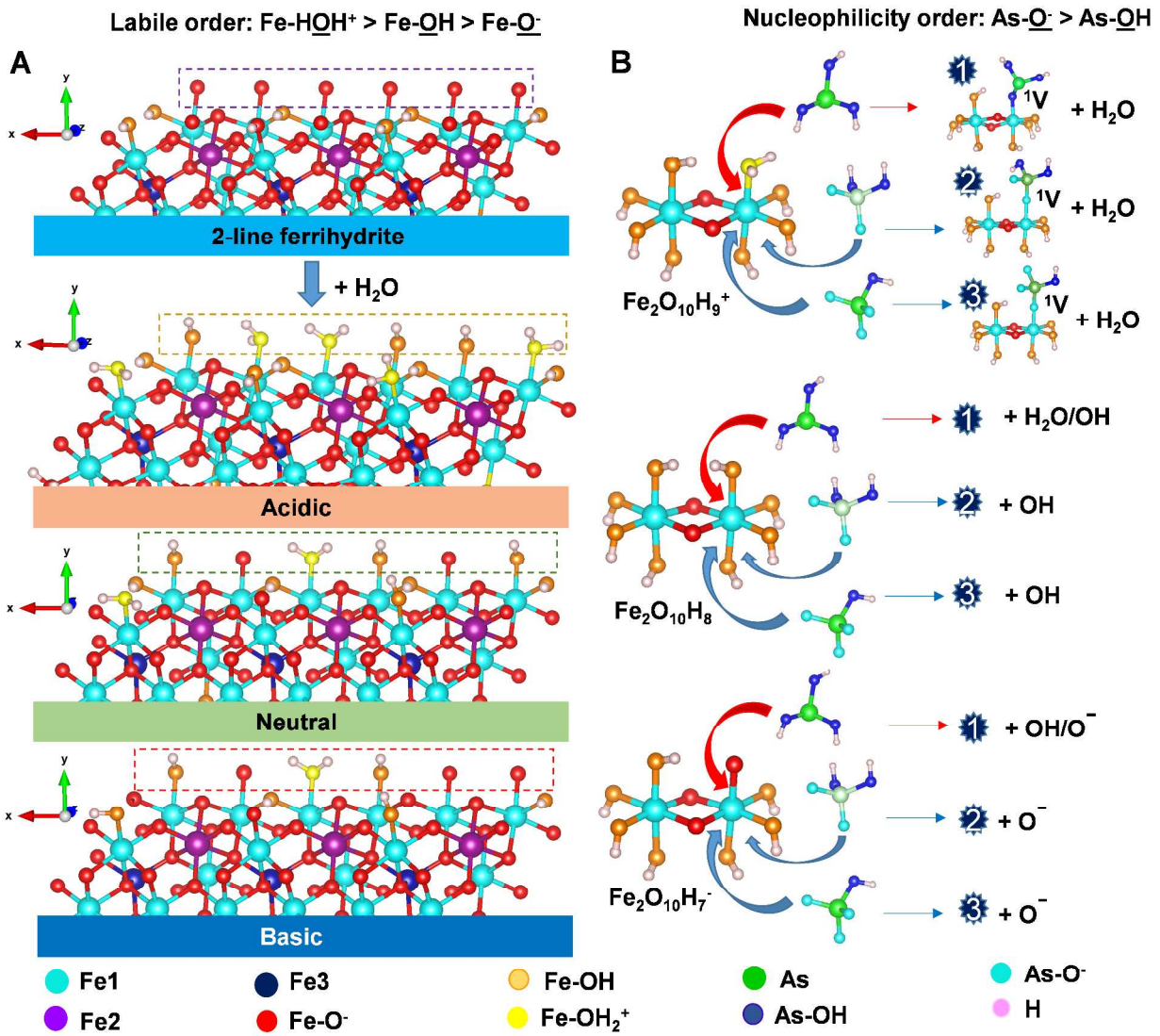

Figure S10. Schematic representation of the (010) plane of 2-line ferrihydrite surface under different conditions. A) Singly/doubly coordinated oxygens involving in protonation or deprotonation according to the solution pH. The singly coordinated surface oxygens (H_2O^+-/-O^-/-OH) are shown in dotted rectangular boxes. B) The labile nature of singly coordinated oxygens of the cluster, $Fe_2O_{10}Hy$ (y = 9/8/7) involved in the ligand exchange mechanism with As(III) and As(V) under different conditions. In each case, the preference of complexation is in the order, 3

> 2 > 1. As(III) gives complex 1 (^{1}V), while As(V) results in complex 2 (^{1}V) and complex 3 (^{1}V), respectively (^{1}V: Monodentate mononuclear complex). The 2-line ferrihydrite is composed of Fe1 and Fe2 centers which differ in the octahedral environment (FeO_6) but, Fe3 center is in tetrahedral environment (FeO_4) as shown in Figure 8A.

Supporting information 11

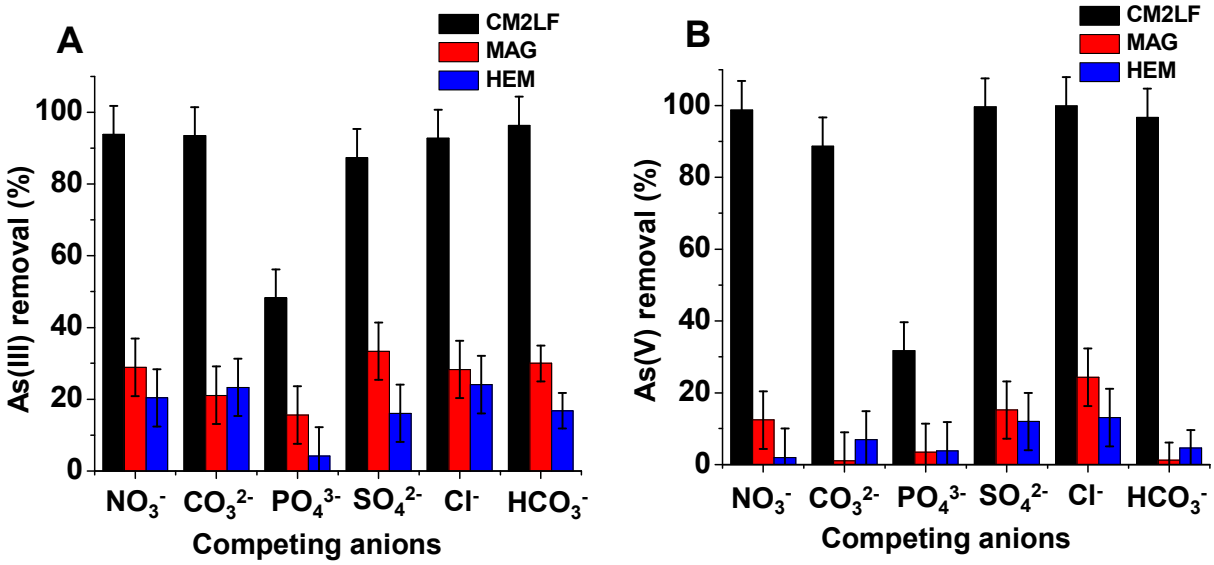

Figure S11. The influence of competing ions on arsenic adsorption for CM2LF, MAG and HEM with an input concentration of 1.0 mg L^{-1} for both A) As(III) and B) As(V), separately. 100 mL arsenic contaminated deionized water was taken with 25 mg of CM2LF/MAG/HEM and the incubation time was kept as 150 min. The individual ion concentration taken was 1 mM, before spiking arsenic in water.

Supporting Table 1

Table S1. XPS data of before and after arsenic adsorption.

Energy levels (eV)	CM2LF	MAG	HEM
Before As treatment			
As 3d	$NaAsO_2$: 44.2	$Na_2HAsO_4.7H_2O$: 44.8	
	----	---	----
Fe $2p_{3/2}$	710.1	Main peak : 710.4 Fe(II) : 709.5 Fe(III) : 711.2	710
Fe $2p_{1/2}$	723.2	Main peak : 724.0 Fe(II) : 723.1 Fe(III) : 724.8	723.1
After As(III) treatment			
As 3d	45.1	44.3	44.7
Fe $2p_{3/2}$	710.0	Main peak : 710.4 Fe(II) : 709.6 Fe(III) : 711.3	709.8
Fe $2p_{1/2}$	723.1	Main peak : 724.0 Fe(II) : 723.2 Fe(III) : 724.9	722.9
After As(V) treatment			
As 3d	45.3	45.5	46.5
Fe $2p_{3/2}$	712.2	Main peak : 710.7 Fe(II) : 709.5 Fe(III) : 711.2	709.8
Fe $2p_{1/2}$	725.3	Main peak : 724.3 Fe(II) : 723.1 Fe(III) : 724.8	722.9

SUPPORTING DOCUMENTS

“12. PRE-TREATMENT PROTOCOL”

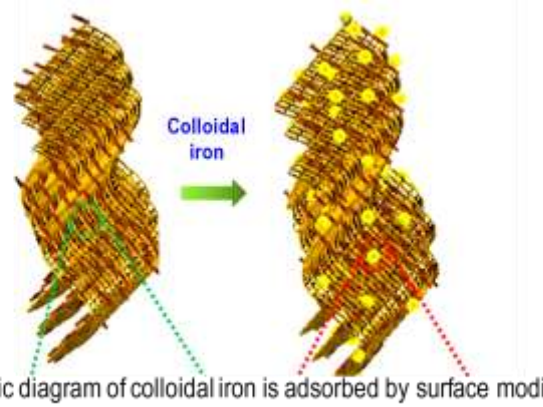

Schematic diagram of colloidal iron is adsorbed by surface modified nanomaterial composition

REMOVAL OF COLLOIDAL IRON

PRE-TREATMENT PROTOCOL: ABOUT IRON REMOVAL UNIT

Iron being a major component of earth's constituent involves incredibly complex chemical transformations in water. Iron present in water is usually in dissolved form which forms colloidal particles on exposure to air.
Presence of iron in drinking water is a major water quality problem owing to loss of transparent nature of water and staining of cloths caused by iron in water.

Amongst various practiced methods for iron removal, filtration is the most commonly practiced. Filtration is typically carried out through trapping of colloidal particles in granular bed of activated carbon, sand gravels or such particles. However, this method has huge disadvantage: nearly daily backwash required to clean the filtration bed and treatment of sludge containing backwash water. Maintenance of such plants becomes extremely difficult for local communities.

With advent of nanotechnology, it is possible to effectively remove colloidal iron in a very effective approach, requiring nearly no backwash. Colloidal iron is removed through adsorption on a nanomaterial adsorbent. This method of iron removal is first-of-its-kind in the world and near zero maintenance system. Unit has in-built mechanism for life indicator.

What it means in terms of performance and affordability? IRON composition can handle any concentration of colloidal iron, even reaching up to 50 ppm. And bring the output below the detection limit (<100 ppb). There is no similar example of composition across the world which can remove iron from water without requiring any backwash. Composition offers extremely high adsorption kinetics, thereby requiring minimal contact time for iron removal. This helps from several aspects: treatment cost reduces, filtration unit becomes smaller, filtration unit can be operated with minimum pressure and nearly zero maintenance.

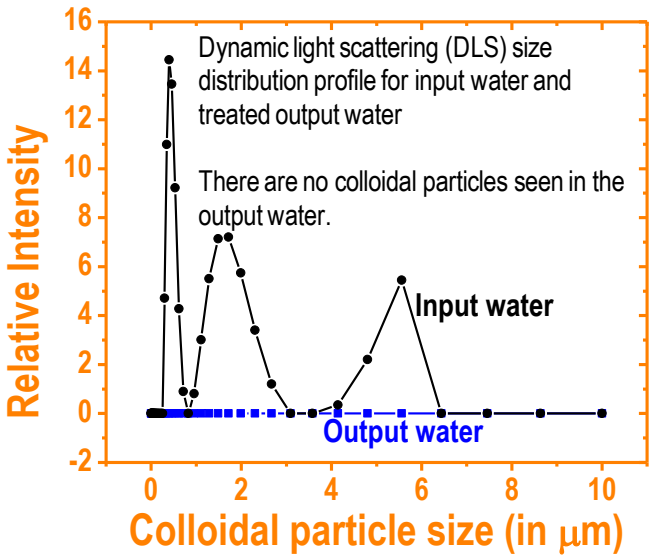

Efficiency of the unit can be measured by checking the input and output water in dynamic light scattering instrument (Horiba NanoZS). It can be seen that while in input water, there are particles of various size ranges (going from nanometer to micron size), there are no colloidal particles observed in the output water. This clearly shows the efficiency of iron adsorbent in effectively removing colloidal iron from drinking water.

STANDARD OPERATING PROCEDURE FOR THE UNIT IS AS FOLLOWS:

1. Conversion of dissolved iron to colloidal iron using aeration or chlorinator or oxidation media
2. Colloidal iron is passed through the filter element using water pump

SUPPORTING DOCUMENTS

"16. OPERATIONS AND MAINTENANCE COST AND PROTOCOL"

STANDARD OPERATING PROCEDURE

STANDARD OPERATING PROCEDURE

SLUICE VALVE POSITIONS (VALVES OUTSIDE THE FILTRATION UNIT)

Supply of filtered water to distribution line	Supply of filtered water to overhead tank
4” metal sluice valve - closed	4” metal sluice valve - closed
3” metal sluice valve (filter input) – open	3” metal sluice valve (filter input) – open
3” metal sluice valve (filter output) – open	3” metal sluice valve (filter output) – open
Overhead tank metal sluice valve – closed	Overhead tank metal sluice valve – open
Distribution line metal sluice valve – open	Distribution line metal sluice valve – closed
Supply of direct water to distribution line	**Supply of direct water to overhead tank**
4” metal sluice valve - open	4” metal sluice valve - open
3” metal sluice valve (filter input) – closed	3” metal sluice valve (filter input) – closed
3” metal sluice valve (filter output) – closed	3” metal sluice valve (filter output) – closed
Overhead tank metal sluice valve – closed	Overhead tank metal sluice valve – open
Distribution line metal sluice valve – open	Distribution line metal sluice valve – closed

MULTIPORT POSITION EXPLANATION

MULTIPORT NUMBER 1

Position 6: Run the filter
Position 12: Backwash the filter

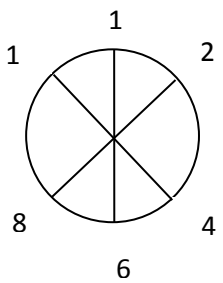

MULTIPORT NUMBER 2

Position 6: Run the filter
Position 12: Backwash the filter

STEPS FOR RUNNING THE FILTRATION UNIT

1. Check the pressure in pressure gauge no. 1. It should be 0 kg/cm^2. If it is not 0, allow it to reduce to 0 before going to step 2. If pressure is not reducing, open the sluice valves located outside the filtration unit. Once the pressure has reduced to 0, again go back to sluice valves and close/open as per the requirement explained in table above.
2. 15000 mg/20000 L prepare the chlorine dosing tank. Chlorine dosing system is part of existing structure of rural water supply scheme. For every run, chlorine dosing tank should be washed with fresh water and freshly filled. Dosing quantity: 250 g calcium hypochlorite is added per 50 L of fresh water in chlorine dosing tank. This shall last around 4 h of pump run. To fill the chlorine dosing tank, open 4” sluice valve and close 3” sluice valves and open the ball valve for chlorine tank filling.

3. Put the multiport no. 1 in backwash mode (**POSITION 12** as marked in figure above). Open ball valves number 5, 6 and close the ball valve numbers 2 and 3.
4. Run the pump along with chlorinator for 3 minutes. This will backwash the iron filter unit. Record the pressure in pressure gauge no. 1. Pressure should be between >0.15 kg/cm^2. Else continue the run for 3 more minutes.
5. Switch off the pump and chlorinator. Allow the pressure in pressure gauge no. 1 to reduce to 0 kg/cm^2.
6. Put the multiport no. 1 in rinse mode (**POSITION 4** as marked in figure above).
7. Put the multiport no. 1 in run mode (**POSITION 6** as marked in figure above). Close ball valves number 5, 6 and open the ball valve numbers 2 and 3.
8. Check the position for UPVC ball valves: 1 (closed), 2 (open), 3 (open), 4 (closed), 5 (closed), 6 (closed), 7 (closed), 8 (open), 9 (open).
9. Run the pump along with chlorinator for obtaining the purified drinking water. Continuously monitor the pressure in pressure gauges. Pressure in pressure gauge number 1 should not cross 4 kg/cm^2, pressure in pressure gauge number 2 should not cross 3 kg/cm^2, pressure in pressure gauge number 3 should not cross 2.5 kg/cm^2, pressure in pressure gauge number 4 should not cross 2.5 kg/cm^2.

SUPPORTING DOCUMENTS

"18. REJECT MANAGEMENT COST AND PROTOCOL"

TOXICITY CHARACTERISTIC LEACHING PROCEDURE (TCLP) RESULTS

ADVANCED MATERIALS
www.advmat.de

ADVANCED SCIENCE NEWS
www.advancedsciencenews.com

Confined Metastable 2-Line Ferrihydrite for Affordable Point-of-Use Arsenic-Free Drinking Water

*Avula Anil Kumar, Anirban Som, Paolo Longo, Chennu Sudhakar, Radha Gobinda Bhuin, Soujit Sen Gupta, Anshup, Mohan Udhaya Sankar, Amrita Chaudhary, Ramesh Kumar, and Thalappil Pradeep**

HIGHLIGHTED TEXT FROM PAGE 5, PARAGRAPH 2 OF THE PUBLISHED ARTICLE.

porting Information) for As(III) and As(V), respectively. The toxicity characteristic leaching protocol (TCLP, https://www.epa.gov/sites/production/files/2015-12/documents/1311.pdf) studies were conducted using the saturated composites to know the leaching of adsorbed arsenic and iron. The tests showed a leaching of 1 μg L^{-1} (total As), 2 μg L^{-1} (total As) and 24 μg L^{-1} (total Fe) for As(III), As(V) and iron, respectively.

SUPPORTING DOCUMENTS

"20. CERTIFICATION OF PRODUCT"

A. MDWS APPROVAL

B. ARSENIC TASK FORCE APPROVAL

C. INDIAN INSTITUTE OF SCIENTIFIC EDUCATION & RESEARCH APPROVAL

WQ-11015/13/2015-O/o JS (W&A)
Government of India
Ministry of Drinking Water & Sanitation
(Water Quality Section)

4th Floor, Paryavarn Bhawan,
CGO Complex, Lodhi Road,
New Delhi – 110003.

Dated, the 23rd September, 2015.

Subject: Report on Field Visit of Joint Secretary (Water) to Nadia district of West Bengal to Review Arsenic Mitigation Measures – 11th and 12th September, 2015.

This is to inform you that during the Field Visit of Joint Secretary (Water), Ministry of Water Supply and Sanitation on 11th and 12th September, 2015 to Nadia district of West Bengal to review the short-term and long-term measures undertaken by the State Government to mitigate the arsenic problem in the district, it was found that some of the interventions are based on nano-technology which is good to use in view of the fact that there is no reject management issue. A detailed report in this regard is attached herewith.

All the States having arsenic affected habitations are requested to depute State Government officials to visit West Bengal and replicate the best practices in their State taking help of NRDWP fund, State resources, 14th Finance Commission or any other funding.

Yours faithfully,
23/9/15
(D. Rajasekhar)
Dy. Adviser (WQ)
Tel No: 011-24361656

To:
Principal Secretaries in-charge of rural drinking water in Assam, Bihar, Karnataka, Punjab & Uttar Pradesh.

For information:
Principal Secretary in-charge of rural drinking water in West Bengal.
PS to Hon'ble Minister RD, PR & DWS.

Report on Field Visit of Joint Secretary (Water) to Nadia district of West Bengal to Review Arsenic Mitigation Measures – 11th and 12th September, 2015

Report on Field Visit of Joint Secretary (Water) to Nadia district of West Bengal to Review Arsenic Mitigation Measures – 11th and 12th September, 2015.

Background:

It was in the 80's when Arsenic contamination in groundwater was detected for the first time in West Bengal. Soon after the detection of geogenic arsenic contamination of ground water, various short term measures like i) installation of hand pump tube wells at deeper aquifer ii) installation of arsenic removal units attached to the hand pumps iii) construction of new dug wells etc. were taken up. However, most of those shot term measures failed because of complicated operation and maintenance issues and non-acceptance by the society. Afterwards it was felt that a comprehensive action plan has to be taken to combat the Arsenic menace and therefore a **Master Plan for Arsenic Mitigation** was conceived in the year **2006-07** to cover **6623 habitations**, at a cost of Rs. 2831 **Crores** (revised) under **Water Quality Submission** with a cost sharing of **75:25** between the **Centre** and the **State**. However this Water Quality Sub Mission was made an integral component of **National Rural Drinking Water Programme** (NRDWP) since 1.4.2009. The Master Plan comprising of **338 nos.** of new **Groundwater based Piped Water Supply Schemes, 12 nos.** of new **Surface Water based Piped Water Supply Schemes** & **165 nos.** of **Arsenic Removal Plants** (ARP) in existing Groundwater based Schemes, is still under implementation under the NRDWP. Apart from the aforesaid Master Plan, arsenic mitigation programmes are also being implemented by the State under other programmes like, **Minority Sector Development Programme (MSDP), under the Ministry of Minority Affairs, Border Outpost Programme under the Ministry of Home Affairs** etc.

Field visit was made to see different types of interventions, both short-term and long-term, undertaken by the State Government which is narrated below:

A) Mega Piped Water Supply Scheme based on River Water

Arsenic contamination of ground water in West Bengal is largely spread over the Gangetic Alluvium of West Bengal and therefore the State Government has taken up 12 (twelve) Mega Piped Water Supply Scheme based on River Ganges. One such scheme is named as **"Haringhata and Chakdah (Part)" in the Nadia District** which has been declared as the first ODF district in the State, very recently.

The Salient feature of this Surface Water Based Piped Water Supply Scheme is tabulated below:

- Name of the Scheme — Surface Water Based Piped Water Supply Scheme for Arsenic Affected Areas of Haringhata and Chakdah (Part) Block of Nadia District
- Name of the Blocks Covered — Haringhata & Chakdah (Part)
- Number of Villages covered — RURAL: 129 Nos. Census Town: 1 Nos.
- Number of Rural Habitations — 266 Nos. (Arsenic affected 155 habitations)

• Design Population (2028)	Total: 4,86,904 [Rural: 4,68,376 and CT: 18,528]
• Command Area	24,379.42 Hectares
• Number of Zones	13 (Thirteen) Nos.
• Per Capita Service Level	Rural- 49 lpcd (considering 30% population to be served through house connection @ 70 lpcd and 70% population to be served through street hydrants @ 40 lpcd)
• Daily Water Demand	Raw Water: 33.39 MLD, Clear Water: 31.72 MLD, Net Water: 28.55 MLD
• Source of Water	Surface water of River Hooghly
• Treatment Plant Capacity	33.39 MLD [7.35 MGD]
• Treatment Methodology	Conventional Treatment (Coagulation and Flocculation, Clarification, Rapid Gravity Filtration and Disinfection)
• Over Head Reservoir (OHR)	12 (twelve) nos. new to be provided in each zone over and above existing 02 (two) nos.
• Sanctioned Estimated Cost	Rs. 118.98 Crores (under NRDWP)
• Date of Commencement	24.12.2009
• Date of Commissioning	June 2012.
• Cost of production of water	Rs. 7/Kl

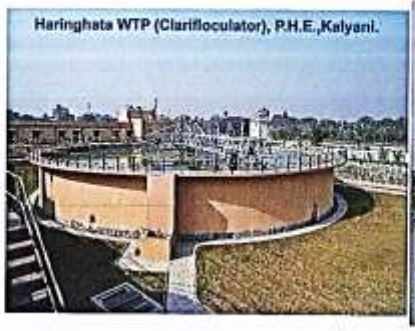

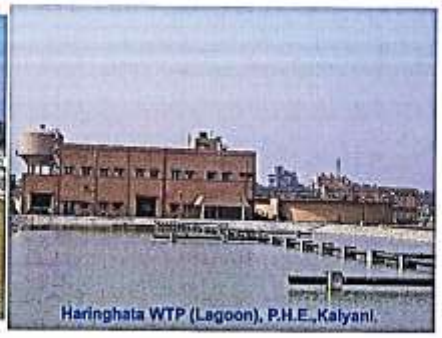

B) Multi Village Piped Water Supply Scheme based on Ground Water with Arsenic Removal Plants

The State is implementing **338** Ground Water based Piped Water Supply Schemes in arsenic affected areas, wherever Surface Water based schemes are not techno-economically feasible. A number of technologies have been adopted to treat the excess amount of Arsenic present in ground water. However, on 11.09.2015, the field visit was made to one Arsenic Removal Plant based on Nano technology as detailed below:

Arsenic Removal Plant Based on Nanotechnology - This nano-technology based Arsenic Removal Plant has been installed in **Umapur, Phulia, Block – Shantipur, District–Nadia**. The nanoparticles used in the Plant is Iron-oxy-hydroxide which reduces arsenic concentration to <10 ppb and iron to <100 ppb from influent concentration of arsenic and iron up to 500 ppb and 3000 ppb respectively. The treatment methodology is based on oxidation followed by iron and arsenic adsorption. The Arsenic present in raw water is adsorbed in the nanoparticles used as media in such a manner that there is little chance of leaching arsenic from the meager amount of sludge produced in the treatment process.

IIT Chennai has developed the technology and in order to promote this technology an incubation company was formed in which the professors, research students from IIT and others are the shareholders. This incubation company has tied up with one local company based in West Bengal who is the implementing agency engaged by the State Government or PRI.

The Salient feature of the above scheme is furnished below:

- Name of the Scheme — Ground Water based water supply scheme for Arsenic affected areas of Goalpur , Block Shantipur, District Nadia
- Number of Villages : 2 Nos.
- Number of Rural Habitations : 9 Nos. (Arsenic affected habitations = 4)
- Design Population (2032) Total: 5,693
- Command Area 300.63 Hectares

• Number of Zones	2 (Two) Nos.
• Per Capita Service Level	Rural- 61 lpcd (considering 70% population to be served through house connection @ 70 lpcd and 30% population to be served through street hydrants @ 40 lpcd)
• Daily Water Demand	387 KLD
• No. of Tube Wells	4 Nos.
• Discharge of each Tube Well	2 nos. @ 13,750 liters/hour 2 nos. @ 10,437 liters/hour
• Over Head Reservoir (OHR)	2 (Two) nos.
• Sanctioned Estimated Cost	Rs. 2.09 Crores (NRDWP)
• Year of Commencement	2009
• Year of Commissioning	2014
• Capacity of the Arsenic removal plant	17,000 litre/hr.
• Cost of production of water	Rs. 4/Kl

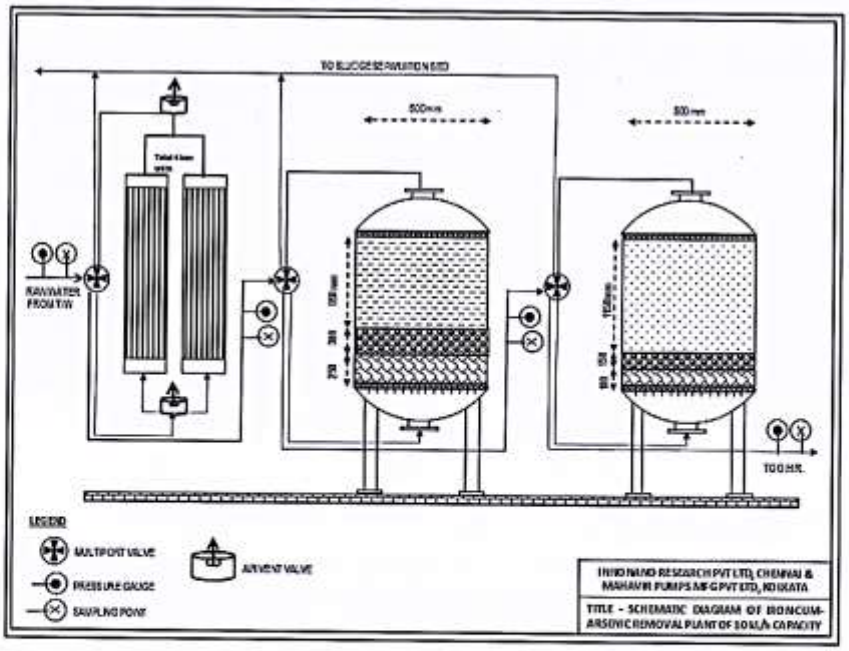

Sectional view of Iron and arsenic removal plant based on Nano-technology

4

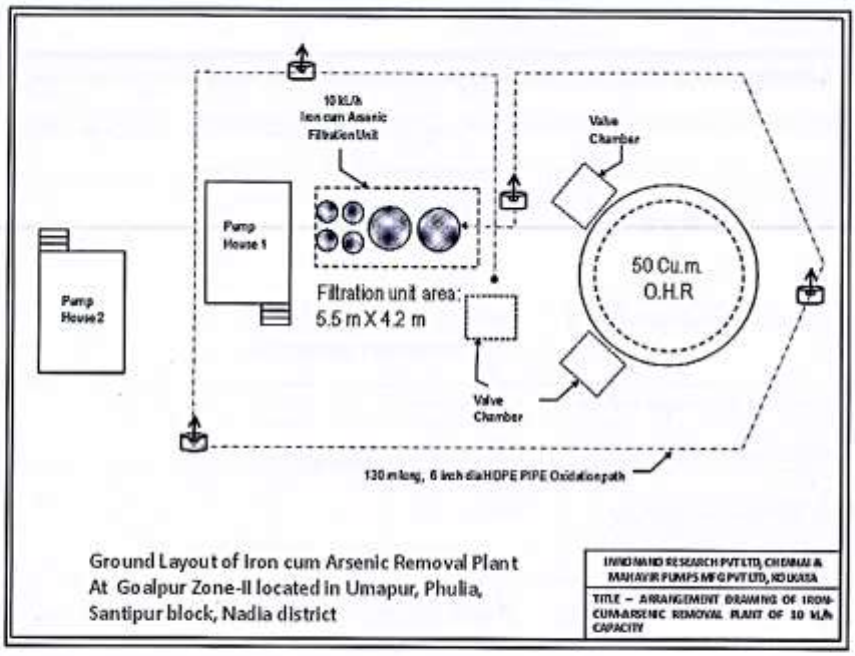

Ground layout of Iron and arsenic removal plant based on Nano-technology

Arsenic Removal Plant, installed in Umapur, Phulia, Block – Shantipur, District – Nadia

Other Technologies used for removal of Arsenic in Ground Water is also furnished below:

a) Modified Sujapur–Sadipur Model - This technology is based on oxidation followed by co-participation through coagulation, flocculation, clarification, filtration and finally adsorption through activated Alumina chamber and solid/ liquid separation of sludge as mortar block. The capacities of these plants may vary be from 20m^3/hr. to 100 m^3/hr.

b) Gobordanga Model – This model has also been adopted by the State which is for smaller capacities in the range of 5 to 20 m3/hr. This technology is based on oxidation

by chlorination in a designed path, adsorption through naturally available Red Hematite, Green Sand and polishing through Activated Alumina. Entire system is made in a closed pressurized system to reduce cost of land and installation time.

c) Few other technologies based on Granular Ferric Hydroxide, Resins, In-situ remediation etc. has also been successfully adopted/ being adopted, to treat contaminated ground water.

C) Community Based Arsenic Removal Plant

Implementation of multi-village piped water supply schemes are time taking and of high cost. Therefore, the State has also taken up about 400 Community Purification Plants based on the technologies which are already functioning successfully for more than 2 years. These plants would cater to the drinking water needs @ 8 litres per capita for about 1000 persons. The cost of such plants is Rs.10.00 lakhs (approx.). VWSC or users' committee also collects fund from the users. One such plant based on Nano technology was visited at Nabadwip, District Nadia on 11.09.2015.

The Salient feature of this Community purification plant is -

- Location: Block Development Office Nabadwip, District- Nadia, West Bengal
- Runs on GRID powered can also be attached solar power based Submersible Pumping.
- Iron Removal: Based on Oxidation by MnO_2 & Green Sand and through filter sand.
- Arsenic Removal: Based on Nano scale Iron-oxy-hydroxide absorbent technology by IIT Madras.
- Bacteriological Removal: UV Filter.
- Treatment Capacity: 8,000 liter per day.

(Interaction of JS (Water) with Nabadwip villagers and PRI representatives)

(D) **Hand Pump Attached Arsenic Removal Plant**

Arsenic removal plants, comparatively on a smaller scale, have also been installed under other programmes like Border Aea Development Programme, Minority Sector Development Prgramme etc. These plants are genrally attached to the existing hand pump tubewells, yielding arsenic beyond permissible level and generally they cater to the drinking water need of school, madrasah, health centre etc. The technology is again based on nano adsorbent, developed by IIT, Chennai. Salient feature of 2 such models is detailed below:

Model 1:

- **Location:** Swami Vivekananda School Chapra Block – District Nadia.
- **User:** School Students & Local Community, approx 200 person.
- **Design:** Bamboo shaped which attracts people and especially the children.
- **Cost of Each Unit:** ` 72,000.00
- **Iron Removal:** Based on Oxidation by Resins (ISR) & Green Sand and other filter media.
- **Arsenic Removal:** Based on nanoscale iron oxyhydroxide absorbent technology by IIT Madras.
- **Output:** 1000 liter per day.
- **Operation:** It is quite easy as with every stroke it delivers clean drinking water free of iron and arsenic through its lift & force option. It has option of drawing water for other purpose such as washing, bathing by using the normal mode of the handpump.

- **Maintenance/Backwash:** By turn of few valves the system can be backwashed for few minutes and the system is recouped back for normal use. After each back wash the system is rinsed before drawing of clean water. This periodic cleaning/backwash will depend on turbidity level/iron content in the input water. The Arsenic Absorbent Unit doesn't require any backwash as it simply needs to replace with new cartridge after the same is exhausted.

Total 330 such Units have been installed in the schools and some habitations, in the district of Nadia, Murshidabad

Model 2

- **Location:** Sealmara Madhyamik Siksha Kendra - Berhampore Block – District Murshidabad.
- **Design:** Coconut shaped which attracts people and especially the children.
- **Cost of Each Unit:** ` 95,000.00
- **User:** School Students & Local Community, approx 250 person.
- **Iron Removal:** Based on Terafil Filters.
- **Arsenic Removal:** Based on nanoscale iron oxyhydroxide absorbent technology by IIT Madras.
- **Output:** 1200 liter per day.
- **Operation:** Easy to operate the system works on gravity flow principal. Only daily filling of water through a lift & force (it also has option of drawing water from other purpose such as washing, bathing) or through a electric mono block pump.
- **Maintenance:** The Upper Tank of the systems storing raw water requires periodic cleaning depending on turbidity level/iron content in the input water. The filtrates clog the top surface of the Terafil over time hence flow rate drops. This requires cleaning/scrubbing the surface of the cake rigidity with a soft nylon brush / coir / or spay of water with the sprayer provided with the system. This will remove the sediments and open new pores for rejuvenation of filtration process. The Arsenic Absorbent media doesn't require any maintenance it simply needs to replace with new cartridge after specific interval.

Total 1000 such units are being installed in Schools/ Anganwadis/ Madrasah/ Health Centres/ Mosque/ Habitation etc. in the district of Murshidabad, West Bengal

Way Forward:

The total no. of identified arsenic affected habitations in the State was about **6586** considering the permissible limit of arsenic in groundwater as **0.05 mg/ltr**. Out of the above habitations about **645 nos**. are yet to be covered. Of late, there is a debate on reducing the limit of arsenic to **0.01 mg/lt,** which will result in the addition of affected habitations by **3610 nos** habitations. However, the State Government is poised to cover all the affected habitations by either of the above measures/ technologies as mentioned above by March, 2017. A majority of the affected habitations, lying within the range of 0.01 to 0.05 mg/lt, are already covered by the mega surface water or ground water based multi village piped water supply projects and some of the affected habitations (in the range 0.01 to 0.05 mg/lt) may also be covered by simply extending of distribution pipelines. However, the State Govt. is yet to take some action for providing house connection from piped water supply schemes. Therefore, in many areas where there is a piped water supply, rural people continue to drink contaminated water from private tubewells due to lack of awareness or reluctance. On this score, the Sate Government has taken up a slew of measures like red marking of tubewells, extensive awareness, training, water quality monitoring involving the GPs etc. State Government officials were advised to intensify the awareness programme involving the local PRIs and grassroot level ASHA and Anganwadi workers.

******

Dated: 10/07/2012

The Report on the Presentation of technologies for Arsenic removal before the Technical Committee of the Arsenic Task Force (ATF) held on 27th June. 2012 at 2.30 PM in the Conference Hall of PHED, 7th Floor, New Secretariat Building, 1, K.S. Roy Road, Kolkata 700 001

The meeting was chaired by Prof. K.J. Nath, Chairman, Arsenic Task Force. The following members were present in the meeting.

1. Sri Kamal Mazumdar, Technical Advisor, PHED
2. Sri Satyadeb Bhattacharya, Chief Engineer, Planning & WQM, PHE Dte
3. Sri S. Sengupta, Deputy Secretary (Technical), PHED
4. Sri Gautam Roy Chowdhury, SE, North 24 Parganas, W/S Circle, PHED
5. Sri B.K. Dutta, SE, PC-I, PHED
6. Sri Tapan Sen, SE, PC-II, PHED
7. Dr. S.P. Sinha Ray, Convenor, Core Committee on Water Quality, Safety and Security & Member, ATF
8. Dr. Anirban Gupta, Professor, Dept. of Civil Engineering, BESU, Shibpur, Howrah & Member, ATF
9. Dr. Debashish Chatterjee, Professor, Dept. of Chemistry, Kalyani University & Member, ATF
10. Prof. A. Majumder, Member, Arsenic Task Force& Emeritus Professor, SOWS, JU
11. Sri T.K. Das, O.S.D. (Mon. Cell). PHE Dte.

The following organizations/experts made presentation on their technologies

Sl. No.	Name of the Presenter	Name of the Organization
i	Prof. Sanjeev Chaudhari	Centre for Environmental Science & Engineering, Indian Institute of Technology, Bombay.
ii	Mr. Anshup & Mr. Praveen Poddar on behalf of Prof. T. Pradeep	Dept. of Chemistry, Indian Institute of Technology, Madras
iii	Ms. Sonja Hahn Tomer and Dr. Konrad Siegfried	Helmholtz-Zentrum für Umweltforschung GmbH - UFZ, Centre for Environmental Research, Leipzig, Germany
iv	Mr. S. Ganguly	S.S. Enterprise, Sodepur, Kolkata

Presentation 1

Presentation was made by Prof. Sanjeev Chaudhari of Centre for Environmental Science & Engineering, Indian Institute of Technology, Bombay.

Prof. Chaudhari made a presentation on the development of hand pump attached indigenous arsenic removal filter based on Zero Valent Iron (ZVI). The process achieves almost complete oxidation of As_3 to

As_5 and subsequent arsenic removal by ZVI without the addition of any chemical. Presentation was based on laboratory findings and their pilot studies in Sonakhali, Shikaripara, Kalyani, Ghanguria and Palashi in West Bengal. IIT-B, arsenic filter is able to achieve arsenic label of less than 10 ppb in treated water from an initial arsenic concentration ranging to 60 to 500 mg/litre most of the time. The cost of producing 1 m^3 of water varies from 10 paise to Re. 1.00. Volume of sludge produced is low, 35 kg/year for a plant meant for 200-300 families.

General Comments & Recommendations

The Technical Committee felt that the technology is indigenous and cost effective and has the potential for scaling up. It is recommended that the PHED should consider having a pilot project with IIT, Bombay for scaling up the technology and evaluating the efficacy of the same.

Presentation 2

Presentation was made on behalf of Prof. T. Pradeep, Dept. of Chemistry, Indian Institute of Technology, Madras by Mr. Anshup & Mr. Praveen_Poddar of M/s Mahavir Pumps Pvt. Ltd. Kolkata

The presentation included the basic concept of using nanotechnology (nano material based composition) for the removal of pesticides, arsenic and micro-organisms. Presently two unit based on this technology are undergoing field trials in Baugachi Kashibala Vidhyapith, Habra and Daskhin Nanga IB School, Kumra, Habra, North 24 Parganas. The performance of the units claimed in the presentation indicates reduction of arsenic concentration from 150 ppb to below detection level. The presentation also depicted the design of the proposed community level anti-microbial and arsenic removal filter to treat 3000 litres/hour. Approximate cost 2-3 paise/litre of water treated.

General Comments & Recommendations

The Technical Committee strongly recommends, considering that nanotechnology is emerging as a tool with lot of potential for comprehensive water purification for both microbial and chemical contaminants, PHED should consider collaboration with IIT, Madras for pilot studies and scaling up of the technology.

Presentation 3

Presentation was made by Ms. Sonja Hahn Tomer and Dr. Konrad Siegfried of Helmholtz-Zentrum für Umweltforschung GmbH - UFZ, Centre for Environmental Research, Leipzig, Germany

They presented the technology of Arsenic Bio Sensor and they also demonstrated the use of the field kit. In this field kit, the arsenic resistance of the applied bacteria is used as a "bacterial switch". The patented bio sensor emits light when brought into contact with arsenic dissolved in water. The bio luminescence of the genetically modified non-pathogenic bio reporter bacteria E-Coli K12 is detected by a potable luminometer. The quantifiable light intensity directly correlates with the concentration of arsenic. The field kit is easy to

perform and could be used by non-skilled rural workers if trained properly and it is very sensitive and accurate. The kit has been field tested in Germany, Bangladesh and Nepal.

General Comments & Recommendations

The Technical Committee is of the opinion that a few of such field kits could be procured for the State / District level regional laboratories for emergency use. However, as the kit uses genetically modified bacteria, permission would be required from the Ministry of Environment, Govt. of India, prior to its use.

Presentation 4

Presentation by Mr. S. Ganguly of S.S. Enterprise, Sodepur, Kolkata

Presentation was made by Mr. S. Ganguly of S.S. Enterprise, Sodepur, Kolkata. The presenter being a non-technical person could not throw much light on the technology. However, they submitted a report on the performance evaluation of their water filter by the School of Water Resource, Jadavpur University. The report shows that at the rate of filtration of 10 litres /hour, the filter is capable of bringing down arsenic in raw water of 0.23 mg/litre to less than 0.01 mg/litre in the treated water. However, the arsenic concentration in filtered water is found to be more than 0.01 mg/litre after filtering more than 500 litres. The arsenic in treated water also increases when rate of filtration is more. The technology has not been scaled up. The efficacy of the filter in removing bacteria and other microbial contaminants is also questionable.

General Comments & Recommendations

On the whole, the Technical Committee on the strength of the presentation, does not recommend the technology for use by the PHED. Moreover, the organization appears to have no technical expertise on water purification.

(Prof. K.J. Nath)
Chairman, Technical Committee of the Arsenic Task Force

3

भारतीय विज्ञान शिक्षा एवं अनुसंधान संस्थान कोलकाता
(भारत सरकार के मानव संसाधन विकास मंत्रालय द्वारा स्थापित एक स्वायत्तशासी संस्थान)
INDIAN INSTITUTE OF SCIENCE EDUCATION AND RESEARCH KOLKATA
IISER KOLKATA (An autonomous Institute established by Ministry of Human Resource Development, Government of India)

TO WHOMSOEVER IT MAY CONCERN

Subject: Report about arsenic media quality

We have studied the media for arsenic removal developed in Prof. T. Pradeep's laboratory at IIT Madras. Results of scientific studies are as follows:

Adsorbent	Iron hydroxide/oxyhydroxide
Particle size	0.5 to 2 mm
Moisture content	Less than 5%
Density	1 to 1.1 g/mL
Active adsorbent content	Min 85%
Adsorption capacity @ 200ppb input conc (As^{3+}:As^{5+} = 1:1)	15 mg/g
EBCT	Minimum 90 mins
Hydraulic loading rate	15 $m^3/m^2/h$
Flow direction	Anti-gravity

In case any further clarification is required, undersigned may be contacted.

Signed on 06/08/17

Dr. Venkataramanan Mahalingam
Associate Professor, Department of Chemical Sciences
Indian Institute of Science Education and Research, Kolkata

SUPPORTING DOCUMENTS

"24. TEST TRAILED: WHETHER TEST TRAILED/IMPLEMENTED"

TEST REPORT

May 23, 2018

Government of West Bengal
Public Health Engineering Directorate
Nadia Divisional Laboratory, S.T.P. Kalyani, Nadia.
Water Quality test Report

Sample send by: The Executive Engineer, Nadia Arsenic Division I, Kalyani, Nadia

SL.No	Name of the Scheme	Date of collection	Date of Testing	[As] in mg/l	Fe] in mg/l
1.	Goalpur ZoneII,H.W site(Raw)	21.02.14	22.02.14	0.112	1.67
2.	Goalpur Zone II, 2nd site(Raw)	21.02.14	22.02.14	0.069	1.33
3.	Goalpur Zone II,(Treated)	21.02.14	22.02.14	<0.01	0.11
IS:10500:2nd revision (2012)	Requirement acceptable limits			0.01	0.3
	In absence of alternative source Permissible limits			0.05	No relaxation

24-02-14
Chemist
Nadia Divisional Laboratory
P.H.Engineering Dte.

24/02/14
Assistant Engineer
Kalyani sub-Division –I
P.H.Engineering Dte

Government of West Bengal
Public Health Engineering Directorate
Nadia Divisional Laboratory, S.T.P. Kalyani, Nadia.
Water Quality test Report
Sample send by: The Executive Engineer, Nadia Arsenic Division I, Kalyani, Nadia

Sl. No.	Name of scheme	Date of collection	Date of testing	[As] mg/l	[Fe] mg/l
1.	Umapur Phulia IAAP (RW), (Post Chlorination)	15.03.15	23.03.15	0.119	1.37
2.	Umapur Phulia IAAP , Post Iron Removal	15.03.15	23.03.15	0.083	0.92
3.	Umapur Phulia IAAP , Post Arsenic Removal	15.03.15	23.03.15	BDL	0.28
4.	Umapur Phulia IAAP , Stand Post	15.03.15	23.03.15	BDL	0.19
IS:10500:2nd revision (2012)	Requirement acceptable limits			0.01	0.3
	In absence of alternative source Permissible limits			0.05	No relaxation

24-03-15
Chemist
Nadia Divisional Laboratory
P.H.Engineering Dte.

Assistant Engineer
Kalyani sub-Division –I
P.H.Engineering Dte

Copy Recieved by me
31/3/15

Our workplace